Dissertations, Master's Theses and Master's Reports

2017

DESIGN OF ROBUST HYDROGEL BASED ON MUSSEL-INSPIRED CHEMISTRY

Yuan Liu
Michigan Technological University, yliu23@mtu.edu

DESIGN OF ROBUST HYDROGEL BASED ON MUSSEL-INSPIRED CHEMISTRY

By

Yuan Liu

A DISSERTATION

Submitted in partial fulfillment of the requirements for the degree of

DOCTOR OF PHILOSOPHY

In Biomedical Engineering

MICHIGAN TECHNOLOGICAL UNIVERSITY

2017

This dissertation has been approved in partial fulfillment of the requirements for the Degree of DOCTOR OF PHILOSOPHY in Biomedical Engineering.

Department of Biomedical Engineering

Dissertation Advisor: *Bruce P. Lee*

Committee Member: *Jingfeng Jiang*

Committee Member: *Megan C. Frost*

Committee Member: *Qingli Dai*

Department Chair: *Sean J. Kirkpatrick*

To DQX

Table of Contents

Preface

The material used in Chapter 1 of this dissertation was excerpted from book chapter *Biomimetic Adhesives and Coatings Based on Mussel Adhesive Proteins, Biological Adhesives, Second Edition* 2016, doi: 10.1007/978-3-540-31049-5_13" [1] with permission from Springer International Publishing. The material used in Chapter 2 of this dissertation was previously published in *Journal of Materials Chemistry B* 2016, doi: 10.1039/C6TB01828A [2]. This article was reproduced in its entirety as a chapter in this dissertation with permission from RSC publishing. The material used in Chapter 3 of this dissertation previously published in *ACS Applied Materials & Interfaces* 2014, doi: 10.1021/am504566v [3]. This article was reproduced in its entirety as a chapter in this dissertation with permission from ACS Publications. The material used in Chapter 4 of this dissertation was previously published in *Angewandte Chemie International Edition* 2017, doi: 10.1002/anie.201700628 [4]. This article was reproduced in its entirety as a chapter in this dissertation with permission from John Wiley & Sons.

I am the first author of the publications mentioned above, my contribution includes collecting the data, analyzing the results, and writing the papers. Dr. Bruce P Lee is the corresponding author of the publications, he has been supporting my research work with his grants. The book chapter's content used in Chapter 1 was written by me, the content in this book chapter contributed by other co-authors (i.e., Hao Meng, Phillip B. Messersmith, and Jeffrey L. Dalsin) was not included. In Chapter 3, the biocompatibility testing was contributed by Dr. Hao Meng and Dr. Rupak Rajachar. PEG-D was synthesized by Shari Konst. Rheometry testing was conducted with help from Ryan Sarmiento. In Chapter 4, the SEM imaging was conducted by Dr. Hao Meng. Cell attachment was contributed by Zichen Qian and Dr. Feng Zhao. MS characterization was conducted by Dr. Ni Fan. EWC was contributed by Wonyoung Choi.

Acknowledgement

I would like to express my deepest gratitude to Dr. Bruce Lee for accepting me to pursue my research in his laboratory, as well as his guidance and encouragement towards my doctoral studies. I am very much grateful for his support and patience which helped me through many hard situations during these years of research. I am sincerely grateful to my committee members Dr. Jingfeng Jiang, Dr. Megan Frost, and Dr. Jeremy Goldman for their support to finish my doctoral studies. I would also like to thank my lab mates, especially Hao Meng, who provided indispensable assistance to help me carry out my research work. Furthermore, this research was conducted with the support of Doctoral Finishing Fellowship awarded by the Graduate School of Michigan Technological University.

Most importantly, thank my friends and family who are always there for me, you know you much I appreciate and cherish that.

Abstract

The structure of catechol is found in mussel adhesive proteins and contributed to both wet-resistant adhesion and cohesive curing of these proteins. A synthetic nano-silicate, Laponite was incorporated into catechol-containing hydrogels and the hydrogel network-bound catechol formed strong reversible interfacial interaction with Laponite. The contribution of incorporated catechol-Laponite reversible interfacial interactions to the mechanics of hydrogels constructed by different strategies was studied. In the first strategy, Laponite and catechol were introduced into the double network hydrogel (DN) via the free radical co-polymerization of a catechol-containing monomer, backbone monomer, and crosslinker. The introduction of catechol-Laponite interactions significantly improved the compressive strength and toughness of DN without compromising the compliance of the hydrogel and enabled the DN's ability to recover its mechanical properties during successive loading cycles. In the second strategy, Laponite was combined with an catechol-modified 4-armed poly(ethylene glycol)-based adhesive, which cured in the present of an oxidative catalyst, sodium periodate, to form an injectable naoncomposite tissue adhesive hydrogel. The addition of up to 2 wt% Laponite significantly reduced the cure time, enhanced the bulk mechanical and adhesive properties of the adhesive due to strong catechol-Laponite interfacial binding. Additionally, subcutaneous implantation result showed that incorporation of Laponite effectively promote cell infiltration into the nanocomposite hydrogel, providing a simple way to improve the bioactivity of a bio-inert, synthetic poly(ethylene glycol)-based adhesive. On the basis of the second strategy, higher

concentration of Laponite was combined with catechol-modified 6- and 8-armed PEG-based adhesive to form a nanocomposite hydrogel without introducing additional oxidative catalyst in the third strategy. This hydrogel underwent unique dynamic crosslinking process. At early stage it recovered to its original stiffness immediately after failure induced by shear strain up to 1000% interactions and could be reshaped to adhere to the contour of tissue due to the catechol-Laponite interactions and loosely chemically crosslinked network structure, respectively. The hydrogel gradually transformed to a densely chemically crosslinked network meanwhile fixed its shape as tissue sealant. This dissertation provided an insight of exploiting mussel-inspired chemistry in designing a hydrogel with specific materials property.

Chapter 1 Background and introduction[1]

1.1   Mussel adhesive proteins and catechol

The attachment apparatus of mussels is called the byssus, which is a bundle of threads extending from within the shell of the mussel, each of which terminates in an adhesive plaque attached to a substrate (**Figure 1.1**) [5, 6]. An entire byssal thread and adhesive plaque is formed by secretion of liquid protein from within glands of the mussel foot in a process that resembles polymer injection molding. Solidification of the liquid occurs rapidly to provide a stable attachment, and the process is sequentially repeated many times to deposit each byssal thread and plaque. The proteins of the byssal threads resemble collagen and elastin and will not be further discussed [5]. The adhesive plaque located at the distal end of each thread will be emphasized here, because this is where adhesion to the substrate is enforced.
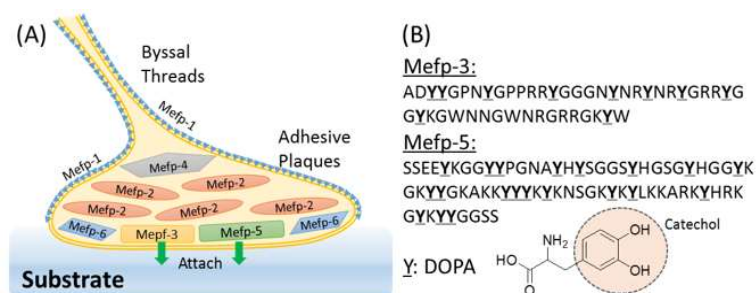
Figure 1.1 Schematic illustration of a byssal thread and adhesive plaque (A). The sequences of the interfacial proteins Mefp-3 and Mefp-5 are shown along with the chemical structure of DOPA (B).

At least six *Mytilus edulis* foot proteins (Mefps) have been identified [6-8]. Mefp-1 is the key protein of the byssal cuticle while Mefp-2 through 6 are found within the adhesive plaque. These proteins all share a common distinguishing feature: the presence of 3,4-dihydroxyphenylalanine (DOPA), a residue formed by post-transitional hydroxylation of tyrosine. It is the 3,4-dihydroxyphenyl (catechol) side chain that gives DOPA its unique properties related to adhesion. The DOPA content of Mefps range from a few percent to well above 20% [9]. Mefp-3 and Mefp-5 are predominately found near the interface between the adhesive plaque and substratum [6, 10], and may function as mediators of adhesion at the interface between the plaque and the foreign surface.

Mefp-3 and Mefp-5 have the highest DOPA contents of the foot proteins at 20 and 27 mol %, respectively, and also contain a large number of basic residues (arginine in Mefp-3 and lysine in Mefp-5) [10, 11]. Mefp-5 also contains phosphoserine residues in a *N*-terminal sequence reminiscent of acidic mineral-binding motifs that appear in statherin and osteopontin [10]. Little is known about the role of phosphoserine residues, although it is interesting to note that phosphoserines are known to bind to calcareous mineral surfaces, which are common substrates of mussels in the marine environment [12, 13].

1.2 Catechol chemistry

The DOPA residues found in the mussel adhesive proteins are widely believed to fulfill two important roles: cohesion and adhesion. Cohesion, as we use the term here, refers to the bulk elastic properties of the adhesive, whereas adhesion refers very

specifically to those physicochemical interactions occurring at the interface between adhesive pad and substrate. Both cohesive and adhesive properties of MAPs are important in achieving the final outcome of secure, water-resistant attachment to surfaces. The catechol side chain of DOPA is capable of various catechol-catechol and catechol-surface interactions, leading to the curing of the catechol-containing adhesive and strong interfacial binding (**Figure 1.2**). Additionally, catechol is a unique molecule capable of forming strong bonds to both inorganic and organic substrates while utilizing either reversible physical or irreversible covalent crosslinks.
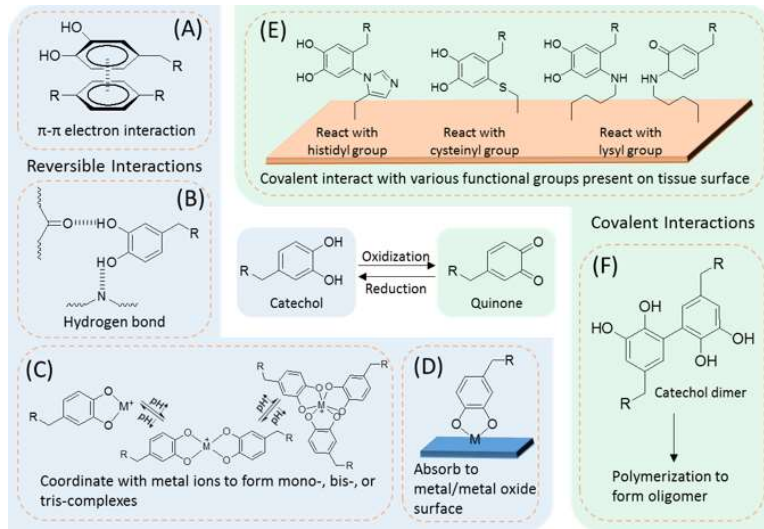
Figure 1.2 Catechol side chain chemistry. Center: the catechol-quinone equilibrium is affected by pH and the presence of redox-active species. (A) Catechol forms π-π electron interactions with benzene rings. (B) Catechol forms hydrogen bonds through phenol hydroxyl groups. (C) Catechol chelates metal ions to form complexes with different stoichiometry depending on the solution pH. (D) Catechol forms coordination bonds with metal and metal oxide surface. (E) Quinone covalently react with neucleophilic groups present on tissue surface through Michael addition or Schiff base substitution resulting in adhesion to tissue substrates. (F) Catechol and quinone polymerize to form oligomers.

1.2.1 Reversible interactions

The benzene ring of catechol can form π-π interaction with another benzyl moiety (**Figure 1.2A**), allowing the catechol-containing material to be able to bind to surfaces rich in aromatic compounds such as polystyrene [14]. The hydroxyl groups of catechol forms extensive hydrogen bonds (**Figure 1.2B**), which allows catechol to compete with water for hydrogen bonding sites and absorb onto mucosal tissues [15-18]. These interaction also contributes to the cohesive properties of the catechol-containing materials [6, 19].

Catechol is capable of forming strong complexes with metal ions (Fe^{3+}, Ca^{2+}, Cu^{2+}, Ti^{3+}, Ti^{4+}, Mn^{2+}, Mn^{3+}, Zn^{2+}) with different stoichiometry (i.e., mono-, bis-, and tris-complexes; **Figure 1.2C**) [20-23]. Strong and reversible catecholate-metal ion complexation is responsible for the wear resistance properties, high extensibility and elevated hardness of mussel byssal cuticles [24, 25]. Metal ions account for as much as 1% by weight in Mefp-1 and its removal resulted in a 50% reduction in cuticle hardness. Similarly, catechol forms reversible complex with boronic acid [26, 27]. The formation of catechol-boronate complexation have been utilized as a temporary protecting group for the synthesis of catechol modified monomers and polymers [28].

The affinity of catechol for metal is not limited to soluble metal ions but is also extended to metal and metal oxide surfaces (**Figure 1.2D**). Catechol can be absorbed onto various metal (i.e., Ti alloys and stainless steel) and metal oxides (i.e., Au_2O_3, Al_2O_3, Fe_3O_4, SiO_2, TiO_2, ZnO) [29-40]. Single molecule pull-off tests have demonstrated that the force required to break a metal-catechol bond (0.8 nN) averaged

around 40% that of a covalent bond (2 nN) [41]. This interaction is reversible and is one of the strongest reversible bond involving a biological molecule reported to date.

1.2.2 Oxidization-induced covalent interactions

In the presence of oxidizing reagent (i.e., IO_4^-, H_2O_2, enzyme etc.), catechol is oxidized to its quinone form [42, 43]. Catechol can also auto-oxidize in a slightly basic aqueous solution [44-46]. Quinone is highly reactive and can form covalent crosslinks with various neucleophilic functional groups present on tissue surface (i.e., $-NH_2$, $-SH$, imidazole from lysine, cysteine, and histidine residues, respectively) through either Michael addition or Schiff base substitution (**Figure 1.2E**), contributing to forming interfacial bonds with tissue substrates [47, 48]. Additionally, quinone can polymerize to form oligomers consisting of up to 6 DOPA residues (**Figure 1.2F**), leading to the rapid hardening of catechol-containing adhesives [49].

Crosslinking of catechol is highly dependent on pH. Under mild acidic conditions (pH=5.7-6.7), catechol crosslinks at a slower rate as a result of increased stability of transient oxidation intermediates (i.e., quinone methide), which reduce the rate of subsequent crosslinking reactions [50, 51]. On the other hand, a fast crosslinking rate was observed at a neutral to basic pH (pH=7.4-8). Interfacial covalent binding to tissue substrates is also limited at a lower pH due to the protonation of nucleophilic functional groups (e.g., pKa of ε-lysine ~10) [50]. These reported results provide guides for bioadhesive design due to variable physiological pH levels (pH = 4–6 for skin [52], pH = 6.7–7.1 for subcutaneous tissue [53], pH = 7 for dysoxic tissue due to extensive hemorrhage or ischemia [54]).

15

Catechol that contains a free amine group (i.e., dopamine) undergoes intramolecular cyclization between the catechol side chain and the amine group to form a leukochrome, which can continue to polymerize in a process similar to melanin formation [49, 55]. Application of polydopamine as versatile coating and grafting platform is introduced in a later section.

1.3 Mussel-inspired polymers and hydrogels design based on catechol chemistry

The ability for catechols to participate in various types of chemical interactions has inspired the development of polymers and hydrogels with new and improved properties. Deming and coworkers synthesized MAP mimetic polypeptides (**Figure 1.3A**) by polymerization of N-carboxyanhydride monomers of lysine and DOPA to form DOPA-containing peptide [56, 57] and tested adhesion to steel, aluminum, glass and several synthetic polymer surfaces [46, 57]. Copolypeptides containing 10 mol% DOPA were crosslinked via oxidation and adhered approximately ten times stronger to aluminum than a polylysine control polymer. Although suggestive of an adhesive role for DOPA, the results are difficult to interpret in view of the potential effects of DOPA crosslinking on cohesive strength of the polymer adhesive. A subsequent study of metal substrate adhesion by the same group using model peptide compounds and similar polypeptides further defined the role of non-oxidized DOPA as adhesive, and that of oxidized DOPA species as contributing primarily to cohesion [46]. Another example of DOPA-containing adhesive polymer is DOPA/styrene copolymer system (**Figure 1.3B**) [58-60]. The incorporation of styrene has demonstrated extremely high adhesive strength, up to 11 MPa adhesive strength was achieved in aluminum surface lap shear

adhesion testing. And co-polymerization of DOPA with the cationic composition exhibited enhanced binding property to rock surface in wet environment (**Figure 1.3C**) [46, 61].
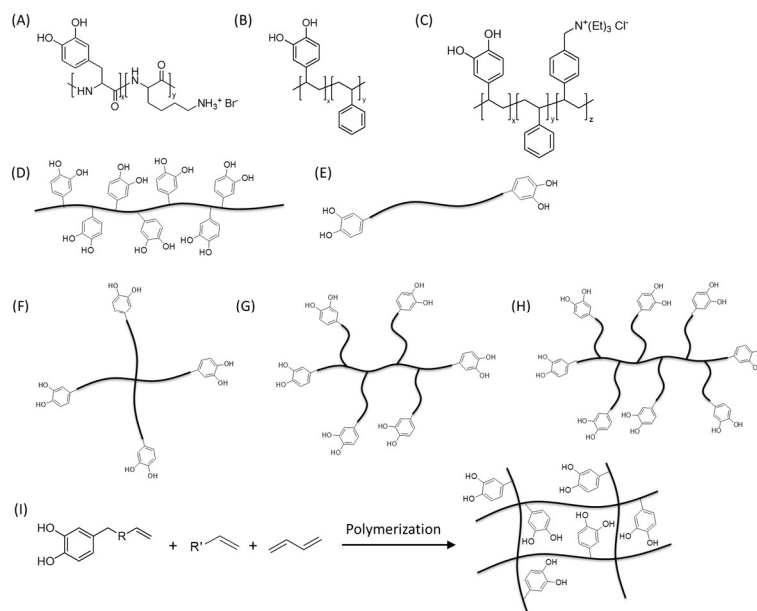
Figure 1.3 Chemical structures of mussel-inspired polymers. (A) Co-polymer of DOPA and lysine. (B) Co-polymer of catechol and styrene. (C) Co-polymer containing catechol, styrene, and cationic side chains. (D) Macromolecule with side chain modification of catechol. (E-H) Linear and 4-, 6-, 8-armed PEG end-modified with catechol. (I) Schematic of catechol-containing polymer network preparation via free radical polymerization.

Incorporation of catechol groups into polymer side chain (**Figure 1.3D**) usually aims for promoting the adhesion to tissue and substrate [28, 62-64], or providing the functional groups for cohesive crosslinking based on reversible/irreversible catechol interactions [65-68]. Catechol–modified polyacrylamide main chain was blended with a nano-silicate to construct nanocomposite hydrogel with enhanced materials properties through strong interfacial interactions between the catechol and the incorporated nanoparticles [69]. A small amount of incorporated catechol (~0.1 wt%

in swollen hydrogel) could significantly increase the network crosslinking density over a wide pH range (pH=3.0–9.0). Similarly, increased stability was observed in calcium crosslinked catechol-modified alginate gel through catechol-catechol dimer formation [70]. Additionally, this catechol modification strategy has been widely applied to biopolymers which have desirable degradation rate and bioactivity. Polysaccharides-based bioadhesive polymers have been created by direct coupling of either amine or acid-functionalized catechols onto alginate [71, 72], chitosan [73, 74], dextran [75, 76], gelatin [77, 78], and hyaluronic acid [79, 80].

Linear (**Figure 1.3E**) and multi-armed (**Figure 1.3F-H**) poly(ethylene glycol) (PEG) end-capped with catechol have been employed to prepare fast curing, injectable tissue adhesive and sealant [49, 81]. PEG is a hydrophilic and biocompatible polymer that widely used for biomedical application [82]. Crosslinking of catechol at polymer end chain through oxidation reaction or catechol-metal ion coordination gives rise to the formation of 3D polymeric network *in situ*. Adhesive fabricated with PEG-catechol have demonstrated cytocompatibility, comparable adhesive properties with commercial fibrin glue [83], and have successfully sealed human fetal membrane defects [81, 84]. The adhesive and degradation properties of PEG-catechol adhesive can be controlled by PEG architecture (i.e., linear, 4-, 6-, 8- arm), molecular weight (2-20 kDa), and PEG-catechol linkage (i.e., ester, urethane, amide) [82, 85, 86].

Another advance in enhancing the mussel-inspired adhesives property is the modification of amphiphilic multiblock copolymer films with the adhesive catechol [87-90]. This type of adhesive polymer contains PEG segments which allows the

polymer to maintain good "wetting" with the tissue substrates, and hydrophobic polyester segments such as polycaprolactone (PCL) to increase cohesive strength due to its ability to self-assemble in the presence of water. This PEG-PCL-catechol polymer can be casted as a thin film (50-120 μm) on biologic scaffolds (i.e, small intestinal submucosa, dermal tissues, and pericardium) [90] or synthetic meshes [88, 89]. These adhesive-coated constructs exhibited 20-fold increase in adhesive strength compared to fibrin glue, reached almost 60% that of cyanoacrylate-based adhesive, and demonstrated the ability of augmenting primary suture repair of transected porcine Achilles tendons.[47]

Preparation of an oxidation-free crosslinking of catechol-containing hydrogel relies on free radical co-polymerization of a catechol-containing monomer, backbone monomer, and crosslinker (**Figure 1.3I**) [91]. The effect of catechol containing monomers on gelation time, gel conversion, and elastic modulus of the photocured hydrogels was investigated. While the presence of catechol-containing monomers did not prevent polymerization, longer irradiation time was needed to achieve gelation. Gel conversion, extent of catechol incorporation, and elastic modulus also decreased with increasing catechol concentration, suggesting a retarding effect on free radical polymerization. Despite this effect, catechol was successfully incorporated into hydrogels with elastic moduli (ca. 50 kPa) suitable for many biomedical applications. To counter act the retardation effect of catechol on free radical initiated polymerization, catechol modified triblock copolymers consisting of polylactic acid (PLA) and PEG have been used to segregate catechol from polymerizable methacrylate group to

achieve rapid photo-initiated curing [83]. Similarly, removal of molecular oxygen have been used to create hydrogel networks with minimal reduction in mechanical properties [92, 93].

Hydrogels that can change their shapes and physical properties in respond to environmental stimuli (i.e., temperature, pH, electricity) have found applications as soft robotic components, biosensors, artificial muscle tissues, and drug carriers [94-96]. Recently, Lee et al. [97] reported a hydrogel actuator that based on catechol-metal ion coordination chemistry. Hydrogels modified with catechol were locally printed with ferric (Fe^{3+}) ions by applying electric potential (2.5-25 V) using an iron electrode as the anode and an aluminum foil as the cathode electrode. Locally deposited metal ions were captured by the network-bound catechol. When the hydrogels were submerged in a basic solution (pH 9.5), the formation of the tris-catechol-Fe^{3+} complex increased local crosslinking density at the site of ionoprinting and resulted in hydrogel bending. When the hydrogels were subsequently submerged in an acidic solution (12 mM HCl), catechol formed mono-complex with the imprinted ion, resulting in reduced crosslinking density and allowing the hydrogel to return to its original shape [97-99]. Fe^{3+} ions in hydrogel can be removed by ethylenediaminetetraacetic acid (EDTA) treatment and reintroduced in a new pattern, so that the hydrogel can be designed to bend to a different shape [97]. The rate and extent of hydrogel actuation can be effectively tuned by catechol and metal ion content, pH, hydrogel thickness, and metal ion type [98, 100].

Strong physical and chemical interactions of catechol have been used to design self-healing hydrogels (**Figure 1.4**). The ability of catechol to coordinate with various types of metal ions (i.e., Fe^{3+}, Zn^{2+}, Al^{3+} Ga^{3+}, In^{3+}) under basic condition have been used to create self-healing hydrogels by combining catechol-containing polymer with metal ions and metal oxide nanoparticles [101-106]. The modulus of the self-healing hydrogel composed by 4-armed PEG end-modified with catechol and Fe^{3+} ions approached those of covalently crosslinked hydrogels [104]. Similarly, pH-responsive self-healing hydrogels based on catechol-boronate complexation were reported [107, 108]. Under basic condition (pH~9), a tetrahedral boronate ester was established between 1,3-benzenediboronic acid or sodium tetrahydroborate with polymer-bound catechol to form 3-dimentional polymer networks with viscoelastic behavior. Recently, a mussel-inspired polymer self-healed in acidic environment was reported [109]. Polyacrylates and polymethacrylates functionalized with triethylsilyl-protecting catechol were cut and rejoined together through slight compression in acidic solution (pH = 3). The triethylsilyl-protecting group was removed under acidic aqueous environment and the exposed catechol groups formed hydrogen bonds, facilitating the polymer healing.
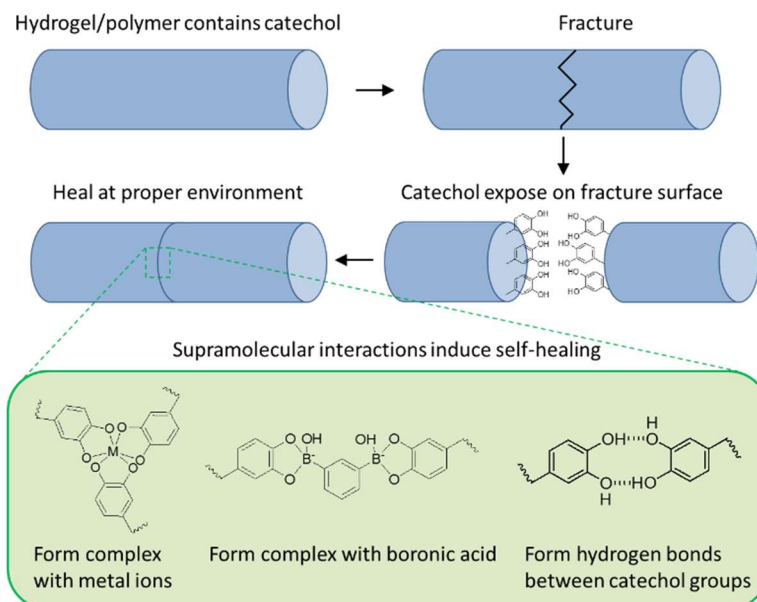
Figure 1.4 Scheme of catechol-containing polymer self-healing process based on catechol chemistry

In this dissertation we utilized the reversible interaction between catechol and a synthetic nano-silicate, Laponite to introduce this particular interactions into hydrogels fabricated by different chemical strategies. The contribution of the catechol-Laponite interactions to the hydrogels performance was investigated.

Chapter 2 Recovery property of double-network hydrogel containing mussel-inspired adhesive moiety and nanosilicate[2]

2.1 Abstract

Although double network (DN) hydrogels are extremely tough, they are irreversibly softened during large strain deformation. We incorporated mussel-inspired adhesive moiety, catechol, and a synthetic nano-silicate, Laponite, into DN to examine the effect of strong, reversible crosslinks on the DN's ability to recover its mechanical properties during successive loading cycles. The introduction of catechol and Laponite drastically increased the compressive strength and toughness of DN without compromising the compliance of the hydrogel. After 2 hours of recovery at room temperature, the nanocomposite DN hydrogel recovered over 95 and 82 % of its strain energy and hysteresis, respectively, during successive compressive loading to a strain of 0.5. Both equilibrium swelling and oscillatory rheometry data confirmed that there were minimal changes to the network crosslinking density and stiffness after large strain compressive deformation, indicating that mechanical loading did not result in irreversible structural damage. Strong catechol-Laponite interactions can be repeatedly broken and reform to dissipate fracture energy and enable the recovery of DN hydrogel.

2.2 Introduction

Hydrogel is a widely used biomaterial due to its excellent biocompatibility, diversity of functionality, and tunable material and physical properties. Hydrogels have been utilized as tissue engineering scaffolds [110-113], tissue adhesives [90, 114], biosensors [115, 116], and soft actuators [97, 100, 117]. For many applications (e.g. repair of soft connective tissue), hydrogels are required to maintain their structural integrity while resisting large and repeated mechanical loading [118, 119]. Designing mechanically strong hydrogels with exceptional recovery properties remains a challenge.

Gong and co-workers [120, 121] developed a new type of interpenetrating network hydrogel, the so-called double network (DN) hydrogel, which exhibited remarkable high strength (10^6-10^7 Pa) and fracture toughness (10^2 to 10^3 J/m^2). Despite having high water contents (65-95 wt%), DN hydrogels exhibited fracture toughness similar to those of solvent free rubbers and connective tissues [121, 122]. DN is composed of a stiff, densely crosslinked first network, interpenetrated with a soft, loosely crosslinked second network. While these two networks are not suitable for mechanical loading in and of themselves, their unique combination yields a fracture resistant DN hydrogel that exhibits mechanical properties that are two to three orders of magnitude higher than those of the two individual networks comprising the DN [120]. However, this remarkable mechanical property is achieved at the expense of irreversible bonds breakage within the hydrogel architecture, and a large deformation (> 0.2 strain) irreversibly softened DN hydrogels [123]. The irreversible nature of DN

may hinder its usage in applications where repeated, large strain load-bearing is required.

Recently, recoverable DN hydrogels composed of a physically crosslinked first network (i.e., alginate [124] and agarose [125]) have been reported. However, heating to elevated temperatures for extensive periods of time (i.e., 80 °C for 1 day and 100 °C for 30 min for alginate and agar, respectively) were needed for recovery, which is impractical for many applications. Additionally, only less than 70 % energy recovery was reported. Other recoverable DN hydrogels have not been able to replicate the elevated mechanical properties of DN [126-128].

Marine mussels secrete adhesive proteins that enable these organisms to bind to different surfaces in a wet environment [19, 129] These proteins contain a unique amino acid, 3,4-dihydroxyphenylalanine (DOPA), with a catechol side chain that is capable of binding to both organic and inorganic surfaces through either covalent crosslinking or strong reversible bonds [130]. Hydrogels constructed by catechol-metal ions chelation [104, 131], catechol-boronate complexation [107], and catechol-inorganic nanoparticles interfacial binding [105] have been reported self-healing property. The reversible bond formed between a catechol and a metal surface averaged around 800 pN, reaching 40 % that of a covalent bond [41]. Our lab previously exploited this interaction to create nanocomposite hydrogels with improved strength and toughness by incorporating network-bound catechol and a nano-silicate, Laponite [3, 66, 69]. These nanocomposite hydrogels were capable of sustaining repeated large strain (0.8) deformation and recovery without fracturing [66].

In this work, we tested the hypothesis that the incorporation of catechol and Laponite can be used to construct recoverable DN hydrogel. Both network-bound catechol and Laponite were introduced into the first network and the influence of catechol-Laponite interaction on the recovery property of the nanocomposite DN hydrogel was evaluated.

2.3   Experimental section

2.3.1 Materials

Acrylamide (AAm) and 2-acrylamido-2-methyl-1-propanesulfonic acid (AMPS) were purchased from Sigma Aldrich (St. Louis, MO). N,N'-Methylene-bisacrylamide (MBAA) and 2,2-dimethoxy-2-phenylacetophenone (DMPA) were obtained from Acros Organics (Geel, Belgium). Dimethyl sulfoxide (DMSO) was purchased from Fisher Scientific Co. (Pittsburgh, PA). Dopamine methacrylamide (DMA), which contained the adhesive catechol and polymerizable methacrylate group, was synthesized as previously described [28]. Laponite XLG was a gift from Southern Clay Products, Inc. (Austin, TX).

2.3.2 Synthesis of hydrogel

The double network hydrogels were prepared in two steps. To prepare the first network, Laponite, AAm, and AMPS were dissolved in deionized water. DMA and MBAA were dissolved in an aqueous solution containing 50 % DMSO. DMPA was dissolved in anhydrous ethanol at 10 mg/ml. These three solutions were mixed together to give the precursor solution for the first network, and the combined monomer (AAm/AMPS/DMA) concentration was kept at 1 M in the precursor solution. The

concentration of AAm and AMPS were kept at equimolar while the concentration of DMA was kept at 0-10 mol% relative to the total concentration of the monomers. The crosslinker (MBAA) and the photoinitiator (DMPA) were kept at 4 and 0.1 mol%, respectively, relative to the monomers. Laponite was kept at 0-4 wt% in the precursor solution. The precursor solution was deoxygenated with three vacuum-nitrogen purge cycles [66] and was photo-irradiated for 2.5 h in a mould consisting of two glass plates separated by 1.5 mm thick rubber spacer using a UV crosslinker (XL-1000, Spectronics Corporation, Westbury, NY) located in a nitrogen-filled glove box (830-ABB Plas-Labs, Lansing, MI). The first network hydrogels were denoted using the notation DxLy, where x is the mol % of the DMA relative to monomer and y is the wt% of Laponite.

The first network hydrogel was submerged in degassed second network precursor solution, composed of 2 M AAm, 0.1 mol % MBAA and DMPA for 24 h. The swollen hydrogel that was infused with the second network precursor solution was photo-irradiated for 2.5 h in a nitrogen-filled glove box. DN hydrogels were denoted using the notation DxLy/DN. A second network composed of PAAm was also synthesized by photo-irradiating the precursor solution.

2.3.3 Hydrogel characterization

Fourier transform infrared (FTIR) spectra of the dried samples were obtained using a Perkin Elmer Spectrum One spectrometer. Equilibrium water content (EWC) was determined by incubating the hydrogels in mildly acidic water (pH = 3.5) and vacuum-dried for 2 days. EWC was defined as:

$$EWC = \frac{M_s - M_d}{M_s} \times 100\% \qquad (2.1)$$

27

where M_s and M_d are the mass of swollen and dried hydrogels, respectively. The mass ratio between the second network and the first network within a DN (R_{mass}) was defined as:

$$R_{mass} = \frac{M_{DN} - M_{FN}}{M_{FN}} \qquad (2.2)$$

where M_{FN} and M_{DN} denote the average dry mass of the first network and its corresponding DN hydrogel, respectively.

2.3.4 Compression testing

Unconfined, uniaxial compression testing was performed using an ElectroForce 3200 Series III Test Instrument (Bose Corporation, Eden Prairie, MN, USA). Hydrogels (n = 3) were compressed at a rate of 1.8 mm/min until the sample fractured. The dimensions of each hydrogel (diameter ~ 7 mm; thickness ~ 3 mm) were measured using a digital caliper immediately before testing. Stress was determined based on the measured load divided by the initial surface area of the sample. Stress was normalized for the amount of second network in dry sample as follows:[132]

$$\sigma_{normal} = \frac{\sigma_{original}}{r^{2/3}} \qquad (2.3)$$

where σ_{normal} and $\sigma_{original}$ are the stress of normalized and calculated. r is the mass fraction of second network in DN, which is determined by

$$r = \frac{M_{DN}}{M_s} \times \frac{R_{mass}}{R_{mass} + 1} \qquad (2.4)$$

Strain was determined by dividing the change in the position of the compressing plate by the initial thickness of the hydrogel. Toughness was determined by the integral of the stress-strain curve. The elastic modulus was taken from the slope of the stress-strain curve between a strain of 0.05 and 0.15.

For repeated cyclic loading, hydrogels were compressed to a strain of 0.5 and unloaded to 0 strain at a fixed rate of 0.85 mm/min with a wait time of 0 or 2 h between cycles. Strain energy was determined by the area under the loading portion of the stress-strain curve. The energy dissipated during each cycle was determined by finding the area of hysteresis within a cycle of the stress-strain curve. The % recovery was defined by the ratio of the values found in the 2nd loading cycle divided by those found in the 1st cycle.

2.3.5 Effect of compressive loading on hydrogel equilibrium volume

Hydrogels were subjected to compressive cyclic loading to a strain of 0.5 at a rate of 0.85 mm/min and allowed to re-equilibrate in mildly acidic water (pH = 3.5) for 24 h. The hydrogel volumetric ratio R_{volume} was determined by:

$$R_{volume} = \frac{V_{after\ compression}}{V_{virgin}} \qquad (2.5)$$

where V_{virgin} and $V_{after\ compression}$ denote the hydrogel equilibrium volume of a virgin hydrogel and a hydrogel subjected to compressive loading cycle, respectively. The equilibrium volume of hydrogel in each state was determined by:

$$V = \frac{M_p}{\rho_p} + \frac{M_{lap}}{\rho_{lap}} + \frac{M_{H_2O}}{\rho_{H_2O}} \qquad (2.6)$$

where M_p, M_{lap}, M_{H_2O} are the mass of polymer matrix, Laponite, and water, respectively. ρ_p is the density of polymer (1.3 g/cm³) [133], ρ_{lap} is the density of Laponite (2.53 g m/cm³) [134], and ρ_{H_2O} is the density of water (1 g/cm³). M_{H_2O} was determined from subtracting the dried mass of hydrogel (M_d) from its swollen mass (M_s). Both M_d and R_{mass} were used to calculate M_p and M_{lap} based on the theoretical wt% of Laponite used in the precursor solution in the first network.

2.3.6 Effect of compressive loading on rheological properties

Rheological properties of virgin hydrogels and those that were previously subjected to a compressive loading cycle (strain = 0.5, rate = 0.85 mm/min) were characterized using a HR-2 rheometer (TA Instruments, New Castile, DE, USA). A frequency sweep (0.1 - 20 Hz at 0.1 strain) experiment was performed to determine the storage (G') and loss (G") modulus. Hydrogel discs (diameter ~ 8 mm, n = 3) were tested using parallel plates at a gap distance that is set at 90 % that of the individual hydrogel thickness, as measured by a digital caliper.

2.3.7 Statistical analysis

Statistical analysis was performed using Origin Pro software. Student t-test and One-way analysis of variance (ANOVA) with Tukey HSD analysis were performed for comparing means of two and multiple groups, respectively, using a p-value of 0.05.

2.4 Results and discussion

Nanocomposite DN hydrogels containing Laponite and network-bound catechol groups were prepared. Catechol and Laponite were incorporated into the first network (FN) to introduce reversible crosslinking into the DN. Given that catechol readily undergoes auto-oxidation in a basic condition, hydrogels were equilibrated in a mildly acidic aqueous solution (pH = 3.5) to preserve the reduced and adhesive form of the catechol side chain for our experiments [69, 135].

2.4.1 Hydrogel characterization

FTIR spectra (**Figure 2.1**) confirmed the presence of catechol and Laponite in the nanocomposite DN hydrogels. The spectrum of PAAm exhibited feature bands at 1645 cm^{-1} for C=O, 3326 cm^{-1} and 3188 cm^{-1} for—NH_2, 2929 cm^{-1} and 1447 cm^{-1} for –CH_2–, confirming the presence of acrylamide. The band at 1037 cm^{-1} of D0L0 was assigned to the S=O stretching of SO_3H in AMPS. In addition to PAAm and AMPS features, D10L2/DN also exhibited characteristic peaks at 988 and 1529 cm^{-1} for the Si-O-Si stretching of Laponite and the benzene ring of catechol, respectively.
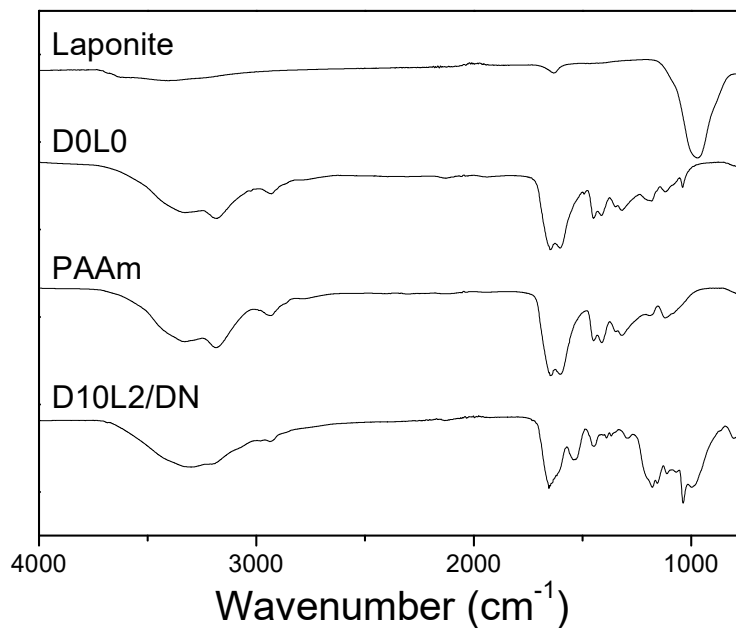
Figure 2.1 FTIR spectra of Laponite, D0L0, PAAm, and D10L2/DN

The FN hydrogel, D0L0, was highly swollen with a EWC of over 99 wt% due to the highly charged AMPS side chain (**Table 2.1**). The addition of only Laponite (D0L2) and DMA (D10L0) marginally decreased the hydrogel water content when compared to D0L0, which is attributed to the interfacial interaction between Laponite and polymer matrix [136, 137] and intermolecular interactions (i.e., π-π interaction, hydrogen bonding) [19, 138] between network-bound catechol groups, respectively. When the DMA concentration was fixed at 10 mol%, increasing the Laponite concentration from 0 to 4 wt% significantly decreased the EWC of hydrogels. A similar trend was observed when the Laponite concentration was fixed at 2 wt% and the DMA concentration was increased from 0 to 10 mol%. Strong catechol-Laponite interactions resulted in the formation of new crosslinking points within the network, causing it to deswell.

32

The EWC for DN was significantly lower when compared to values for the corresponding FN due to the infiltration of a second network. Additionally, the mass ratio between the second and first networks of DN (R_{mass}) varied proportionally with the EWC of the first network. The ability for the first network to swell allowed more of the second network monomer to infiltrate into the first network, resulting in a higher R_{mass} value. As such, incorporating both DMA and Laponite drastically reduced R_{mass} value.

Table 2.1 Equilibrium water content (EWC) of the first network (FN) and its corresponding double network (DN), and the mass ratio between the second and first network (R_{mass}).

	FN (%)	DN (%)	R_{mass}
D0L0	99.1 ± 0.0854	92.3 ± 0.140	7.7
D0L2	98.9 ± 0.0591 [a]	91.7 ± 0.126	6.6
D10L0	98.5 ± 0.155 [a]	91.0 ± 0.392	5.1
D5L2	98.6 ± 0.221 [a]	91.6 ± 0.105	5.0
D10L2	98.3 ± 0.353 [a,b]	89.2 ± 0.572 [a,b,d]	5.4
D10L4	97.4 ± 0.476 [a,b,c]	91.2 ± 0.318	2.4

[a] $p < 0.05$ when compared to D0L0.
[b] $p < 0.05$ when compared to D0L2, D10L0, and D5L2
[c] $p < 0.05$ when compared to D10L2.
[d] $p < 0.05$ when compared to D10L4.

2.4.2 Unconfined compression testing

The representative compressive stress-strain curves for the first network hydrogel containing 10 mol % DMA and 2 wt% Laponite (D10L2), the polyacrylamide second network (PAAm), and the corresponding DN hydrogel (D10L2/DN) are shown in **Figure 2.2**. The densely crosslinked D10L2 behaved as a brittle polymer network, while PAAm was loosely crosslinked and significantly more compliant. The combination of these two polymer networks resulted in a tough DN, which exhibited mechanical properties that were more than an order of magnitude higher when

compared to the individual networks used to form the DN (**Figure 2.3, Table 2.2**). For example, the toughness of D10L2/DN was measured to be 67 and 24 times higher when compared to those measured for D10L2 and PAAm, respectively. This indicated that we have successfully prepared DN containing catechol and Laponite.
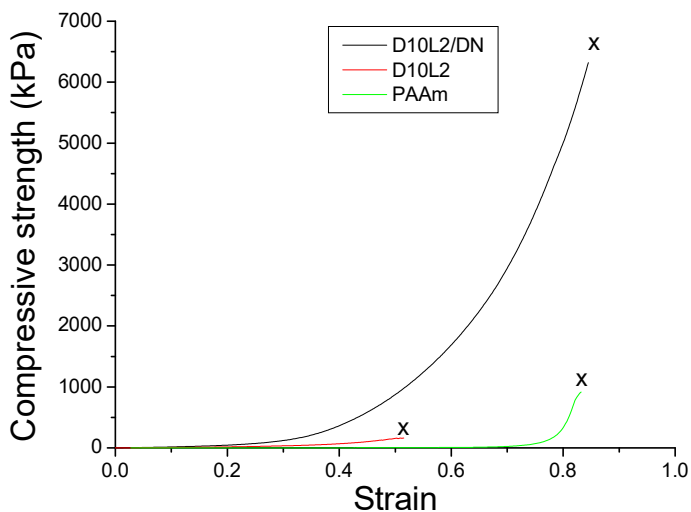
Figure 2.2 Representative stress-strain curves for the first network (D10L2), the second network (PAAm), and corresponding double network (D10L2/DN) hydrogels under unconfined uniaxial compression testing. "x" marks the indicate fracture point.

To obtain DN with elevated mechanical property, the molar concentration of the second network is required to be 20-30 times that of the first network ($R_{mass} \sim 7$-10) [120, 121]. Negative charged monomer AMPS was introduced to promote the swelling of first network in second network precursor solution which ensured the R_{mass}. Additionally, due to the existence of AMPS, the polymer chains of first network straightened during swelling to give a rigid network, which contributed to the stiffness of DN. And the stiff first network underwent fracture during deformation, which contributed to the energy dissipation of DN [139, 140].

Table 2.2 Compressive properties of the first and second network hydrogels.

	Max stress (kPa)	Max strain	Elastic modulus (kPa)	Toughness (kJ/m³)
D0L0	160 ± 12	0.53 ± 0.012	65 ± 8.7	14 ± 0.36
D0L2	160 ± 18	0.54 ± 0.014	74 ± 9.1	15 ± 2.5
D10L0	160 ± 25	0.55 ± 0.011	72 ± 8.8	15 ± 2.1
D5L2	160 ± 13	0.56 ± 0.012	120 ± 11 a	18 ± 1.3 a
D10L2	180 ± 3.9 [a]	0.62 ± 0.15 [a]	110 ± 8.0 a	18 ± 2.0 a
D10L4	210 ± 3.1 [a,b]	0.63 ±0.022 [a]	160 ± 30 [a,b]	20 ± 0.82 [a,b]
PAAm	1200 ± 290 [c]	0.78 ± 0.050 [c]	2.8 ± 0.21 [c]	50 ± 4.5 [c]

[a] $p < 0.05$ when compared to D0L0, D0L2, and D10L0.
[b] $p < 0.05$ when compared to D5L2 and D10L2.
[c] $p < 0.05$ when compared to the first network hydrogels.

Laponite interacted weakly to the hydrogel matrix [39, 137]. At the concentrations tested, incorporation of Laponite alone (D0L2/DN) did not significantly increase its mechanical properties when compared to D0L0/DN (**Figure 2.3**). On the other hand, when 10 mol% of DMA alone was introduced (D10L0/DN), max stress, elastic modulus, and toughness were moderately enhanced. This observation demonstrated that intermolecular interactions between network-bound catechol groups contributed to the mechanical properties of DN.
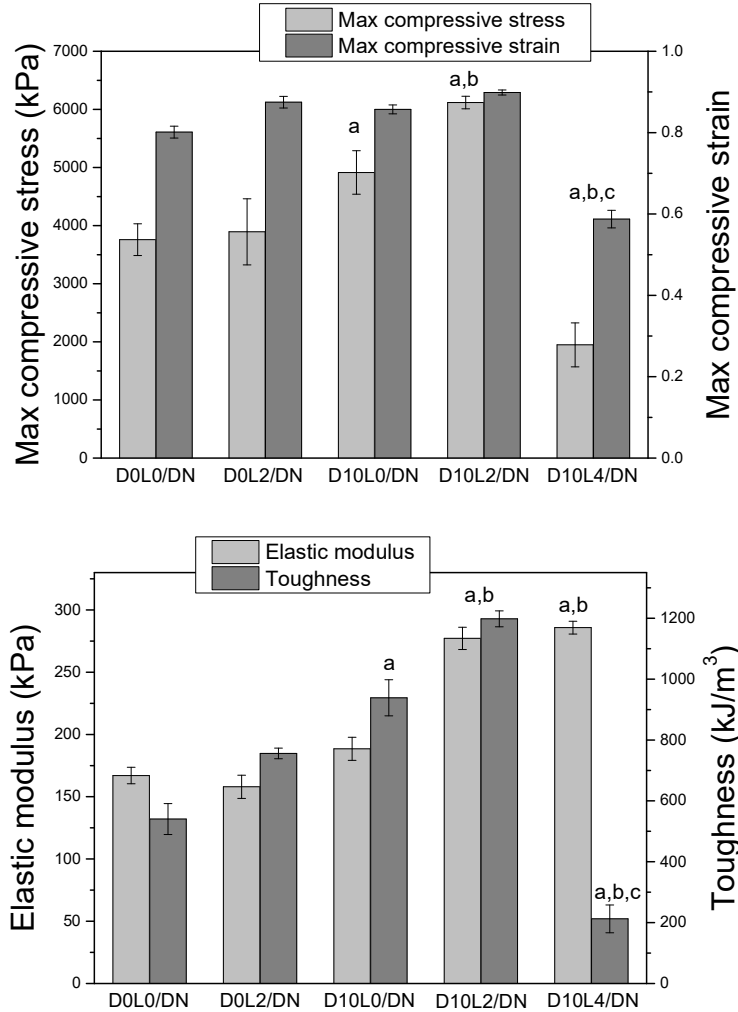
Figure 2.3 Measured compressive strength, strain, elastic modulus, and toughness of DN hydrogels. Data were presented as mean ± SD (n = 3). [a] $p < 0.05$ when compared to D0L0/DN and D0L2/DN, [b] $p < 0.05$ when compared to D10L0/DN, [c] $p < 0.05$ when compared to D10L2/DN.

When the Laponite content in first network was fixed at 2 wt%, the mechanical properties of DN was significantly enhanced when DMA concentration increase from 0 to 10 mol% (**Figure 2.4**). Among the formulations tested, D10L2/DN exhibited the highest max stress (6.1 ± 0.11 MPa) and toughness (1200 ± 26 kJ/m^3). This increase in the mechanical properties coincided with an increase in its first network hydrogel (D10L2) when compared to those without both DMA and Laponite (i.e., D0L0, D0L2,

and D10L2) and D5L2 (**Table 2.2**). Our data confirmed previously published results,

where the elastic modulus of the first network greatly influences the mechanical

properties of the corresponding DN hydrogels [140, 141]. This increase in mechanical

properties did not compromise the compliance of D10L2/DN.
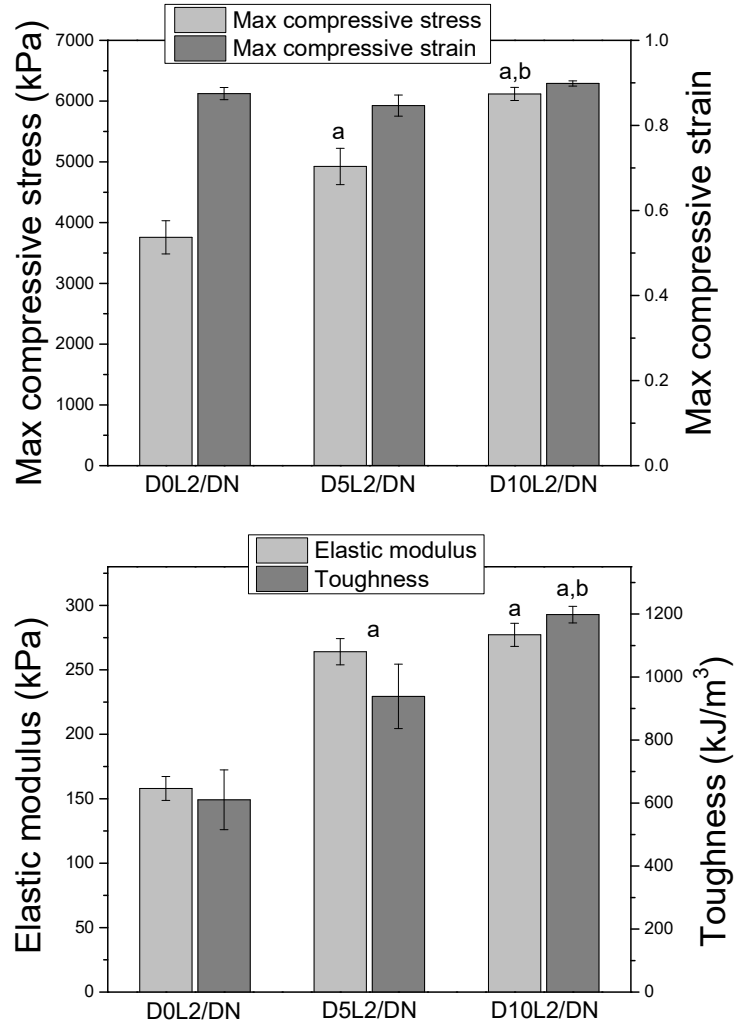

Figure 2.4 Measured compressive strength, strain, elastic modulus, and toughness of DN hydrogels. Data were presented as mean ± SD (n = 3). [a] $p < 0.05$ when compared to D0L2/DN, [b] $p < 0.05$ when compared to D5L2/DN.

Further increase in Laponite content resulted in a stiff but brittle DN (i.e., D10L4/DN). D10L4 had the lowest EWC among all the first network formulation tested due to extensive physical crosslinking between catechol and Laponite (**Table 2.1**). This prevented swelling and diffusion of monomers into D10L4, resulting in the lowest second network mass ratio (R_{mass} = 2.4). The ductile second network prevents macroscopic crack propagation through viscous dissipation [120]. Therefore, the low second network content in D10L4/DN contributed to a significantly reduced toughness.

Given the amount of second network varied in different DN formulation. The strength of DN was normalized for the second network fraction. D10L2/DN exhibited a 1.35 fold increase in normalized strength when compared to D0L0/DN (**Table 2.3**), suggesting that other factor, in this case is the formulation of first network and DMA-Laponite interactions, other than R_{mass} contributed to the elevated mechanical property of D10L2/DN.

Table 2.3 Normalized max stress for the second network content in DN

Formulation	r	Normalized max stress (kPa)	Comparative value
D0L0/DN	0.068	23000	1.00
D0L2/DN	0.072	23000	1.00
D10L0/DN	0.075	28000	1.22
D5L2/DN	0.070	29000	1.26
D10L2/DN	0.091	31000	1.35
D10L4/DN	0.062	12000	0.52

[a] $p < 0.05$ when compared to D0L0, D0L2, and D10L0.
[b] $p < 0.05$ when compared to D5L2 and D10L2.
[c] $p < 0.05$ when compared to the first network hydrogels.

2.4.3 Recovery property of DN during successive compressive loading

D0L0/DN and D10L2/DN were chosen to conduct cyclic compression cycles with or without wait time between loading cycles (**Table 2.4**). **Figure 2.5** shows the representative stress-strain curve of D10L2/DN and D0L0/DN during two successive testing cycles with 2 h wait time. D0L0/DN exhibited a significant decrease in the measured strain energy and hysteresis in the 2nd testing cycle and the % recovery of these value did not change with increasing wait time. This indicated that compressive loading irreversibly damaged D0L0/DN. On the other hand, when D10L2/DN was allowed to recover after the 1st loading cycle, there was a dramatic increase in the recovered strain energy and hysteresis (82 and 95 %, respectively) when compared to those measured without wait time (73 and 49 %, respectively).

Table 2.4 Strain energy and hysteresis measured for D0L0/DN and D10L2/DN after successive compressive cycles to a strain of 0.5. Data were presented as mean $\pm$ SD (n = 3)

		Strain Energy (kJ/m³)		
		Cycle 1	Cycle 2 No wait time	Cycle 2 2 h wait time
D0L0/DN		41 ± 1.5	27 ± 1.8	25 ± 2.1
	% recovery	-	64%	62%
		Hysteresis (kJ/m³)		
		Cycle 1	Cycle 2 No wait time	Cycle 2 2 h wait time
		20 ± 1.4	6.9 ± 0.52	6.0 ± 0.70
	% recovery	-	34%	32%

* $p < 0.05$ when compared to 2 h wait time.

		Strain Energy (kJ/m³)		
		Cycle 1	Cycle 2 No wait time	Cycle 2 2 h wait time
D10L2/DN		61 ± 5.0	43 ± 1.7*	58 ± 2.2
	% recovery	-	73%	95%
		Hysteresis (kJ/m³)		
		Cycle 1	Cycle 2 No wait time	Cycle 2 2 h wait time
		38 ± 1.5	17 ± 1.7*	32 ± 0.70
	% recovery	-	49%	82%

* p < 0.05 when compared to 2 h wait time.
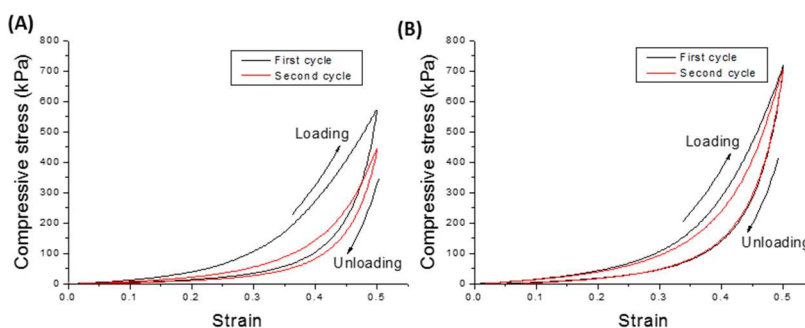
Figure 2.5 Representative stress-strain curves of the 1st (black) and 2nd (red) loading cycles in unconfined uniaxial compression for D0L0/DN (A) and D10L2/DN (B) hydrogels. The hydrogels were compressed to a strain of 0.5 and unloaded back to 0 strain. The gel samples were allowed to recover in mildly acidic water bath (pH = 3.5) for 2 hours at room temperature between cycles.

The equilibrium volumes of hydrogel before (virgin) and after compression were measured to determine the effect of deformation on the network architecture (**Figure 2.6**). For samples that do not contain both DMA and Laponite (i.e., D0L0/DN, D0L2/DN, and D10L0/DN), compressive loading resulted in structural damage and an increase in the equilibrium volume of these networks by more than 30 % (R_{volume} ~ 1.3). Although these networks did not fracture macroscopically, deformation led to irreversible covalent bond breakage in the first network, and these fractured first

network pieces were held together by the loosely crosslinked PAAm network [139, 140]. When these gels were allowed to re-equilibrate in a water bath, water diffused into the hydrogel network to cause an increase in its volume (**Figure 2.7**). Conversely, the change in the equilibrium volume of D10L2/DN was significantly lower R_{volume} (1.1±0.050, **Figure 2.6**), indicating that there was minimal structural damage to D10L2/DN as a result of compressive loading.
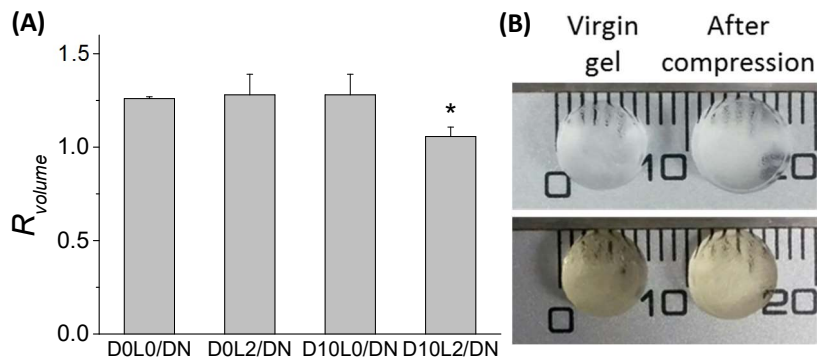

Figure 2.6 The ratio of the volume (R_{volume}) of DN after compression to a strain of 0.5 when compared to virgin DN (A). Data were presented as mean ± SD (n=3). * p<0.05 when compared to D0L0/DN, D0L2/DN, and D10L0/DN. Photographs of D0L0/DN (top) and D10L2/DN (bottom) in the virgin state and after compression (B).

Similarly, oscillatory rheometry was performed to determine the changes in the viscoelastic properties of DN before and after compression (**Figure 2.8**). D0L0/DN exhibited a nearly 3 fold reduction in the measure G' values, indicating a reduction in crosslinking density after compression. The G" of D0L0/DN exhibited the similar change to that of G'. The irreversible breakage of covalent bonds led to a decreased level of loss modulus [142, 143]. On the other hand, there was no significant difference between the measured G' and G" values between the virgin D10L2/DN and those that were compressed to a strain of 0.5. This result further confirmed that the presence of

DMA and Laponite minimized changes to the mechanical properties and the architecture of the DN hydrogel.
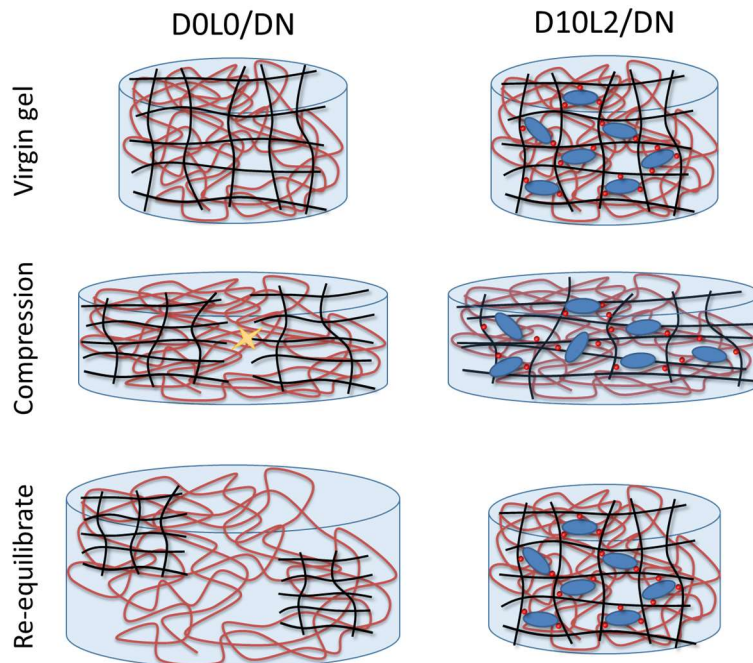
Figure 2.7 Schematic representation of DN hydrogels subjected to compression and subsequently re-equilibrated in a water bath. Compression of D0L0/DN resulted in damage to its first network and an increase in its volume after it was allowed to swell. For D10L2/DN, breaking of DMA-Laponite bonds dissipated fracture energy and the network exhibited minimal volume and structural change after the reformation of the reversible bonds. Black line: first network backbone, red line: second network backbone, red circle: catechol chemically bound to first network, blue ellipse: Laponite, yellow star mark: breaking of covalent bonds.

Collectively, our results confirmed that large strain deformation led to irreversible damage of conventional DN hydrogels [144]. Covalent bond breakage within the backbone of the first network dissipates energy, which contributed to the toughening of DN [139, 140]. However, these damages were not recoverable and

resulted in the softening of the DN. As such, these conventional DN are not suitable for repeated, large strain deformation. Conversely, incorporating DMA and Laponite into the first network, introduced strong reversible crosslinks within DN. The binding energy between catechol and silica oxide is estimated to be 33 kCal/mol [145]. Although this is significantly lower when compared to that of a carbon-carbon (C-C) covalent bond (85 kcal/mol) [146]. The interaction between catechol and Laponite is reversible. DMA-Laponite bonds were broken during the initial loading cycle, which dissipated fracture energy. These interfacial bonds reformed over time, which contributed to the recovery of the measured mechanical properties. This recovery is much faster when compared to previously reported recoverable DN and without the need for heating [124, 125].
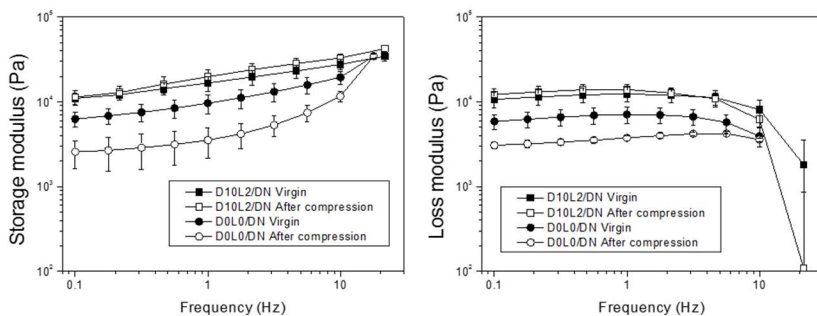
**Figure 2.8** Storage (G') and loss (G") modulus of D0L0/DN (circles) and D10L2/DN (squares) hydrogels in the virgin state (filled symbols) and after compression to a strain of 0.5 (open symbols). Data were presented as mean ± SD (n = 3).

2.5 Conclusion

In this work, we prepared DN hydrogel composed of DMA and Laponite within its first network. This nanocomposite DN hydrogel exhibited enhanced mechanical

properties when compared to DN that do not contain both DMA and Laponite. The reversible DMA-Laponite bonds were broken under compressive loading, which dissipated fracture energy. When the nanocomposite DN were allowed to recover, DMA-Laponite bonds reformed and the hydrogel recovered over 82% of energy dissipated during successive loading cycles. In addition, both the equilibrium volume and oscillatory rheological data demonstrated that these gels exhibited minimal changes to the architecture and stiffness of the network after compression.

2.6 Acknowledgement

Chapter 3 Injectable dopamine-modified poly(ethylene glycol) nanocomposite hydrogel with enhanced adhesive property and bioactivity[3]

3.1 Abstract

A synthetic mimic of mussel adhesive protein, dopamine-modified 4-armed poly(ethylene glycol) (PEG-D4), was combined with a synthetic nano-silicate, Laponite $(Na^{0.7+}(Mg_{5.5}Li_{0.3}Si_8)O_{20}(OH)_4)^{0.7-})$ to form an injectable naoncomposite tissue adhesive hydrogel. Incorporation of up to 2 wt% Laponite significantly reduced the cure time while enhancing the bulk mechanical and adhesive properties of the adhesive due to strong interfacial binding between dopamine and Laponite. The addition of Laponite did not alter the degradation rate and cytocompatibility of PEG-D4 adhesive. Based on subcutaneous implantation in rat, PEG-D4 nanocomposite hydrogels elicited minimal inflammatory response and exhibited an enhanced level of cellular infiltration as compared to Laponite-free samples. The addition of Laponite is potentially a simple and effective method to promote bioactivity in a bio-inert, synthetic PEG-based adhesive while simultaneously enhance its mechanical and adhesive properties.

3.2   Introduction

Tissue adhesives are widely used in surgery for wound closure, sealing suture lines, fixating of implants and functioning as a hemostatic agent [147-149]. Tissue adhesives can simplify complex procedures, reduce surgery time, and minimize trauma. However, there are limitations associated with existing commercial adhesives. Fibrin glue (e.g., Tisseel, Baxter, Inc.) is hampered by weak adhesive properties and the risk for transferring blood-borne diseases (i.e. HIV, hepatitis) [150-152]. Although cyanoacrylate-based adhesive (e.g., Dermabond, Ethicon, Inc.) exhibits excellent adhesive strength, it releases toxic degradation product (formaldehyde), has poor biomechanical compatibility with the repaired tissues, and degrades over an extremely long period of time (>3 years) [153, 154]. Synthetic adhesives consisting of biocompatible polyethylene glycol (PEG; e.g., CoSeal®, Baxter, Inc.) have poor mechanical properties and may swell excessively to apply pressure to surrounding tissues (e.g., nerve compression) [155, 156]. Additionally, PEG-based hydrogels act as a barrier to tissue ingrowth and wound healing [157]. Thus, there is a continued need for the development of biocompatible and biodegradable tissue adhesives with superior adhesive strengths.

Marine mussels secrete adhesive proteins that enable these organisms to attach to surfaces (rocks, boats, etc.) in a wet, saline environment [19, 158]. These proteins contain as much as 28 mol% of a catecholic amino acid, 3,4-dihydroxyphenylalanine (DOPA), which plays an important role in interfacial binding and intermolecular crosslinking [130]. The catechol is a unique and versatile adhesive molecule capable

of binding to both inorganic and organic surfaces through either reversible or covalent bonds. Catechol forms strong, reversible bonds with metal oxides with bond strength reaching 40% that of a covalent bond [41]. This is the strongest reversible bond involving a biological molecule reported to date. When catechol is oxidized to form the highly reactive quinone, it participates in intermolecular covalent crosslinking leading to the rapid curing of catechol-containing adhesives [159, 160] and reacts with nucleophile (i.e., $-NH_2$, $-SH$) found on biological substrates resulting in strong interfacial binding [41, 161]. Catechol-modified bioadhesvie materials demonstrated potential in suture-less wound repair [162], sealing of fetal membranes [81, 84], Achilles tendon repair [47], cell engineering [80, 163], and local delivery of therapeutic drug particles [72].

In this study, we combined a biomimetic PEG-based adhesive with a synthetic, biodegradable nano-silicate, Laponite ($Na^{0.7+}(Mg_{5.5}Li_{0.3}Si_8)O_{20}(OH)_4)^{0.7-}$), to create a novel nanocomposite tissue adhesive. Laponite has similar chemical composition as bioactive glass and mimics some of its biological properties [164-166]. Laponite degrades into non-toxic products (Na^+, $Si(OH)_4$, Mg^{2+}, Li^+) at neutral pH [167]. Orthosilicic acid ($Si(OH)_4$) is naturally found in numerous human tissues and organs (e.g., bone, tendon, liver, and kidney tissues) [168] and it had been demonstrated to promote synthesis of type I collagen and osteoblast differentiation in human osteosarcoma cells *in vitro* [169]. Mg^{2+} ions also play an important role in mediating cellular adhesion [170]. Incorporation of Laponite into bio-inert polymeric networks promoted cell attachment and proliferation while greatly enhanceing the mechanical

properties of these materials [171, 172]. Recently, our lab demonstrated that the strong interfacial binding between Laponite and network-bound dopamine greatly enhanced the mechanical strength and toughness of nanocomposite hydrogels [66].

Here, we combined Laponite with an injectable PEG-based adhesive that is modified with biomimetic catechol adhesive moiety (PEG-D4, **Figure 3.1**). The effect of Laponite incorporation on the curing rate, degradation rate, mechanical and adhesive properties, and biocompatibility (both in culture and in a rat subcutaneous model) of the nanocomposite bioadheisve were evaluated.
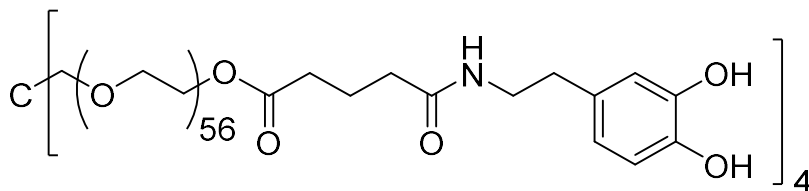
Figure 3.1 Chemical structure of PEG-D4.

3.3   Experimental section

3.3.1   Materials

Sodium periodate (NaIO$_4$, >99.8%) was obtained from Acros Organics (Fair Lawn, NJ). Bovine pericardium was purchased from Sierra for Medical Science (Whittier, California). 3-(4,5-dimethylthiazol-2-yl)-2,5-diphenyltetrazolium bromide 98% (MTT) was from Alfa Aesar (Ward Hill, MA). 1X phosphate buffer saline was from Fisher Scientific Co. (Pittsburgh, PA). Histology mounting medium polyfreeze, Trichrome Stain (Masson) Kit, bouin solution, and Weiger's iron hematoxylin solution were purchased from Sigma-Aldrich (St. Louis, MO). Anti-S100A4 antibody (ab27957), goat anti-rabbit IgG H&L (Alexa Fluor® 488) (ab150077), anti-CD68 antibody (ab125212) and goat anti-rabbit IgG H&L (Alexa

Fluor® 647) were purchased from Abcam (Cambridge, MA). 4',6-Diamidino-2-phenylindole (DAPI) was obtained from Invitrogen (Grand Island, NY). Laponite XLG (Laponite) was a gift from Southern Clay Products, Inc. (Austin, TX). PEG-D4 was prepared as previously described [85].

3.3.2 Preparation of PEG-D4 nanocomposite hydrogel and curing time testing

Hydrogels were formed by mixing equal volume of the polymer precursor solution (300 mg/mL PEG-D4 in 20 mM phosphate buffer solution at pH 7.4) and NaIO$_4$ solution (54.5 mM in deionized H$_2$O with 0-4 wt% Laponite). The concentrations of the respective constituents in the hydrogel are diluted by half after mixing, so that the concentrations of PEG-D4 and Laponite were kept at 150 mg/ml and 0-2 wt%, respectively. The final NaIO$_4$ to dopamine molar ratio ranged from 0.1-1.5. The time it took for the adhesive to cure was determined when the mixture ceased to flow in a tilted vial [49]. Unless specified otherwise, all hydrogels were allowed to cure for 24 hours and equilibrated in PBS (pH=7.4) for further characterizations.

3.3.3 Characterization of PEG-D4 nanocomposite hydrogel

Hydrogels were equilibrated in phosphate buffer saline (PBS, pH=7.4) overnight, then vacuum-dried for at least 2 days to obtain dry gels. Fourier transform infrared (FTIR) spectra of the dried samples were obtained using a Perkin Elmer Spectrum One spectrometer. Equilibrium water content (EWC) was defined as:

$$EWC = \frac{M_s - M_d}{M_s} \times 100\% \qquad (3.1)$$

where M_s and M_d denote the mass of swollen and dry hydrogels, respectively.

3.3.4 *In vitro* degradation

Hydrogel discs (diameter = 10 mm, thickness = 1.5 mm, n = 3) were transferred into vials containing 5 ml PBS (pH = 7.4) and incubated at 37 °C. The PBS solution was removed and replaced with fresh PBS every 7 days. At a specific time point, samples were dried to determine their remaining mass (M_t) at time t. The percent residual mass of hydrogels was determined by:

$$Residual\ Dry\ Mass\ \% = \frac{M_t}{M_0} \times 100\% \qquad (3.2)$$

where M_0 is the average dry mass of 3 samples that did not undergo degradation.

3.3.5 Compression testing

Unconfined, uniaxial compression testing was performed using a servohydraulic materials testing system (8872 Instron, Norwood, MA). Hydrogels (n = 3) were compressed at a rate of 1.8 mm/min until the sample fractured. The dimensions of each hydrogel (diameter ~ 10 mm; thickness ~ 5 mm) were measured using a digital caliper immediately before testing. Stress was determined based on the measured load divided by the initial surface area of the sample. Strain was determined by dividing the change in the position of the compressing plate by the initial thickness of the hydrogel. Toughness was determined by the integral of the stress-strain curve. The elastic modulus was taken from the slope of the stress-strain curve between a strain of 0.05 and 0.2.

3.3.6 Oscillatory rheometry

Rheological properties of the nanocomposite hydrogels were characterized using a Bohlin C-VOR 200 NF rheometer. Frequency sweeps (0.1–100 Hz at 0.1 strain)

were performed to determine the storage (G') and loss (G") moduli. Hydrogel discs (diameter=25 mm, thickness = 1.5 mm, n=3) were tested using parallel plates at a gap distance that is set at 87.5% of the individual hydrogel thickness, as measured by a digital caliber. Mineral oil was applied around the edge of the hydrogel to prevent dehydration.

3.3.7 Lap shear adhesion testing

Adhesive properties of hydrogels were determined by using lap shear adhesion test according to American Society for Testing and Materials (ASTM) standard F2255-05 [173]. Bovine pericardium were cut into 2.5 cm × 2.5 cm strips and hydrated in PBS. PEG-D4 nanocomposite hydrogels were cured between two partially overlapping bovine pericardium with an overlapping area of 2.5 cm × 1 cm. The adhesive joint was compressed with a 100-g weight for 10 min and further conditioned in PBS (pH=7.4) at 37 °C for overnight prior to testing. A commercial PEG-based sealant, CoSeal (Baxter, Inc.), was prepared the same way and tested for comparison. The dimensions of contact area of each adhesive joint were measured using a digital caliper immediately before testing. The adhesive joints were pulled to failure at a rate of 5 mm/min until the tissues separate using a servohydraulic materials testing system (8872 Instron, Norwood, MA). The adhesive strength and work of adhesion were determined by the max load and integral area of load vs. displacement curve divided by the initial contact area of the adhesive joint, respectively [93].

3.3.8 Cell culture and *in vitro* cytotoxicity study

Cytotoxicity was evaluated by determining the viability of cells exposed to the hydrogel extracts [50, 162], as measured using quantitative MTT assay according to

ISO 10993-5 guideline [174]. L929 mouse fibroblasts were cultured in Dulbecco's modified Eagle's medium (DMEM) containing 10% fetal bovine serum (FBS), and 10 units/ml penicillin-streptomycin at 37 °C in 5 % CO_2 humidified atmosphere. Hydrogels were cut into disc shape (5-mm diameter, 2-mm thick) and sterilized using 2 methods (ethanol [175] and sterile filtration [162]). For ethanol based sterilization, hydrogels were submerged in 70 % (v/v) ethanol for 45 min followed by washing three times with 20 ml of sterile PBS for 90 min. The hydrogels were then incubated in DMEM (10 mg/mL) for 24 hours at 37 °C to obtain hydrogel extract. To test if ethanol sterilization method may potentially remove cytotoxic leachable materials, disc-shaped hydrogels were formed using unsterile precursor solutions and incubated in DMEM (10 mg/mL) for 24 hours at 37 °C. The hydrogel extracts were then filtered through 0.22 μm sterile filter to remove biological contamination factors. L929 cells were suspended in DMEM and seeded into 96-well microculture plates at a density of 10^4 cells/100 μL/well and incubated in humidified incubator (37 °C, 5% CO2) for 24 hours to obtain a confluent monolayer of cells, then the medium was replaced by 100 μL/well of hydrogel extract. The cells cultured in DMEM were set as control. After incubation for 24 hours the medium was removed, and replaced with 50 μL of MTT solution (1 mg/ml in PBS) and incubated for another 2 hours. Finally all solution was removed and 100 μL /well DMSO was added to dissolve the crystals completely. The absorbance of each well was measured at 570 nm (reference 650 nm) using a Synergy HT Multi-Mode Microplate Reader (BioTek, USA). The relative cell viability (mean% ± SD, n = 3) was expressed as:

$$Cell\ Viability = \frac{Abs_{hydrogel}}{Abs_{control}} \times 100\% \qquad (3.3)$$

where $Abs_{hydrogel}$ and $Abs_{control}$ are the absorbance for cells cultured in hydrogel extract and DMEM, respectively. For each hydrogel formulation (PEG-D4 with 0, 1, and 2 wt% Laponite), 3 independent cultures were prepared. Samples with relative cell viability less than 70% was considered to be cytotoxic [176].

3.3.9 Subcutaneous implantation

Healthy, weight matched Sprague Dawley rats were obtained from Michigan Technological University animal facility. PEG-D4 hydrogel and PEG-D4 nanocomposite hydrogel with 2 wt% Laponite discs (diameter=10 mm, thickness=1.5 mm) were bilaterally implanted subcutaneously in the backs of Sprague Dawley rats. The subcutaneous implantations were performed following the approved protocol by the Michigan Technological University Animal Committee (IACUC). Hydrogels samples were sterilized using the same procedure (ethanol based sterilization) as in the *in vitro* cytotoxicity study [175]. Rats were anesthetized using an isofluorane-oxygen gas mixture and fur around the implantation site was removed. A pouch was formed using a pair of fine scissors and a hydrogel was placed in this pouch. 4 and 8 weeks post-surgery, the animals were sacrificed and implanted hydrogel along with surrounding skin tissues were collected and embedded in polyfreezethen flash frozen in liquid nitrogen. The frozen samples were stored in -80 °C freezer before sectioning. All tissues were cryosectioned into 10 μm thick sections and stained with Masson's trichrome staining for morphology and collagen production evaluation. Additionally, immunohistochemistry analysis was performed by staining the tissue sections with

inflammatory cell marker CD68, fibroblast cell marker S100A4 for evaluating inflammatory cells invasion and fibroblasts infiltration. DAPI was used to locate the cells via staining the nuclei of cells. All histological imaging analyses were performed on an Olympus microscope. Trichrome staining was used to separate cellular rich layers (red color) close to implant interface from collagen layer (blue color) [177]. Fluorescent staining was used to identify the main cell types (e.g. fibroblasts and macrophages) found at the implant interface. Cells infiltration and local collagen content were quantified by ImageJ.

3.3.10 Statistical analysis

Statistical analysis was performed using Origin software. One-way analysis of variance (ANOVA) with Tukey HSD analysis and student t-test were performed for comparing means of multiple groups and two groups, respectively, using a p-value of 0.05.

3.4 Results and discussion

3.4.1 Preparation of PEG-D4 nanocomposite hydrogel

A novel injectable nanocomposite adhesive was prepared by combining PEG-D4 and Laponite (**Figure 3.2**). PEG, a hydrophilic, biocompatible polymer used in numerous Food and Drug Administration (FDA) approved products [178], was employed as the major structural component for this tissue adhesive hydrogel. The 4-armed PEG (10 kDa) was end-modified with glutaric acid and dopamine. PEG and glutaric acid are linked by a hydrolysable ester linkage, and breaking of this bond results in adhesive degradation. Dopamine contains a catechol group that can be

oxidized by oxidants (e.g., NaIO$_4$) to form highly reactive quinone that is capable of intermolecular crosslinking (**Figure 3.2A**) [46, 49]. Additionally, quinone reacts with functional groups (i.e., –NH$_2$, –SH) found on biological tissue surfaces resulting in strong interfacial binding (**Figure 3.2B**) [41, 161]. Finally, catechol forms strong physical interfacial bonds with Laponite, which greatly enhances the materials properties of the nanocomposite hydrogel (**Figure 3.2C**) [66]. Although samples characterized in this report were formed by simple mixing of the precursor solutions using pipette tips, the precursor solutions can be delivered and mixed using a dual-barreled syringe (**Figure 3.3**).
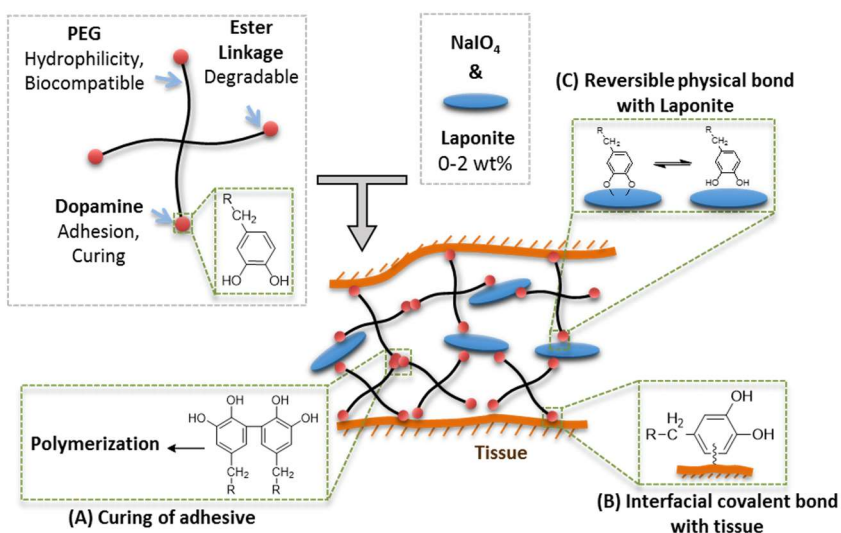

Figure 3.2 Schematic representation of applying the nanocomposite adhesive to tissue by mixing PEG-D4 with NaIO$_4$ and Laponite. Dopamine is capable of forming three types of crosslinks in this system: (A) covalent crosslinking and polymerization between dopamine moieties resulting in curing of the adhesive, (B) interfacial covalent crosslinking between dopamine and functional groups (e.g., -NH$_2$) found on tissue surface, and (C) reversible physical crosslinks between dopamine and Laponite.
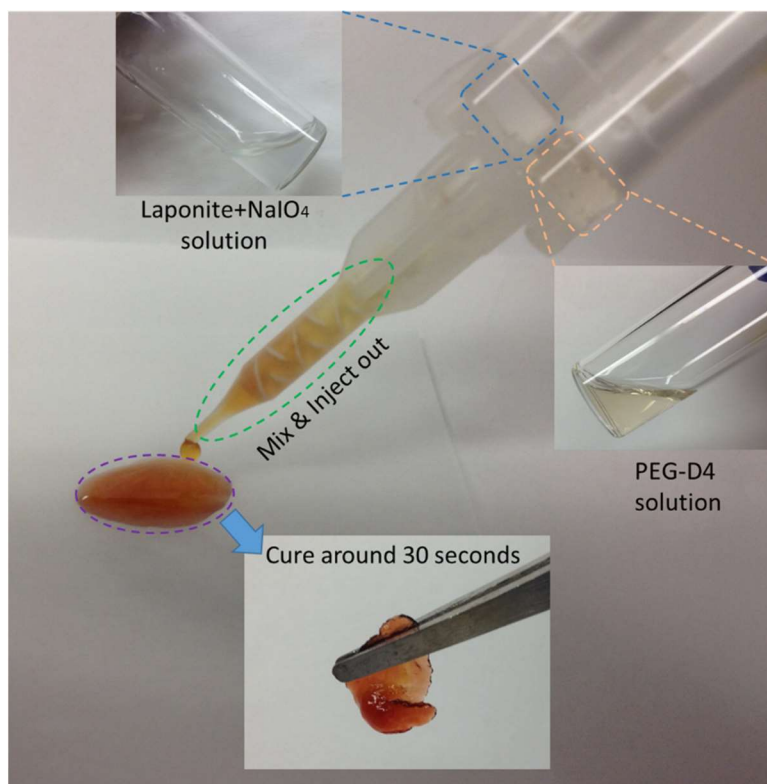
Figure 3.3 Photographs of injecting PEG-D4 nanocomposite hydrogel precursor solutions using a dual-barreled syringe system. The bottom inset showed the cured hydrogel. The final concentration for the nanocomposite hydrogel contains a $NaIO_4$:dopamine molar ratio of 0.5 and 2 wt% Laponite.

The curing time of PEG-D4 hydrogels was strongly dependent on $NaIO_4$ to dopamine molar ratios (**Figure 3.4**). Regardless of Laponite content, the fastest curing time was observed at a $NaIO_4$:dopamine molar ratio of 0.5. Similar trend has been previously reported for DOPA- and dopamine-modified PEG [49, 50]. In periodate-mediated crosslinking, the reduced form of catechol crosslinks with one of the oxidation intermediates of catechol, α,β-dehydrodopamine [179]. As such, a near equal molar concentration of dopamine and $NaIO_4$ was needed to achieve fast curing. Additionally, incorporation of Laponite shortened the curing time for all the stoichiometric ratios of $NaIO_4$ and dopamine tested. For example, at a $NaIO_4$:dopamine

molar ratio of 0.5, the curing time were 1.81±0.12 min , 0.92±0.03 min, and 0.33±0.06 min for samples containing 0, 1, and 2 wt% Laponite, respectively. Strong interfacial binding between dopamine and Laponite resulted in the formation of physical crosslinks within the nanocomposite network, which reduced the number of chemical crosslinks needed for network formation and resulting in reduced cure time. Given a NaIO$_4$:dopamine molar ratio of 0.5 exhibited the optimal curing rate, subsequent tests were performed using samples prepared at this ratio.
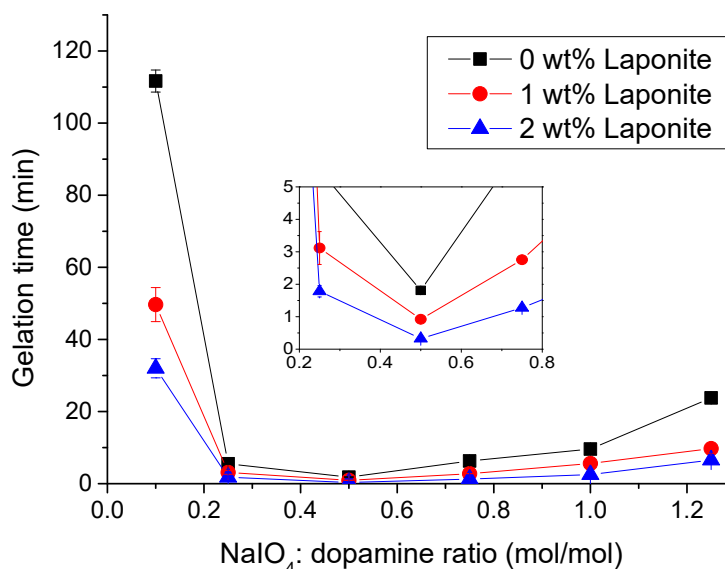

Figure 3.4 Curing time of PEG-D4 hydrogel as a function of NaIO$_4$:dopamine molar ratio with different Laponite concentrations. The inset graph shows the results for NaIO$_4$:dopamine molar ratio between 0.2 and 0.8.

3.4.2 Characterization of nanocomposite hydrogel

FTIR spectra confirmed the incorporation of Laponite into PEG-D4 network (**Figure 3.5**). The spectrum of PEG-D4 showed characteristic peaks for ether bonds (1000-1150 cm^{-1}, -C-O-C-), alkyl groups (2880 cm^{-1}, -CH$_2$-), and carbonyl (1729 cm^{-}

[1], ester bonds) [180] but no Si–O–Si peak (995 cm^{-1}) corresponding to that of Laponite [181]. The Si–O–Si peak was present in the nanocomposite networks (black arrows in **Figure 3.5**), which also increased in intensity with increasing Laponite concentration.
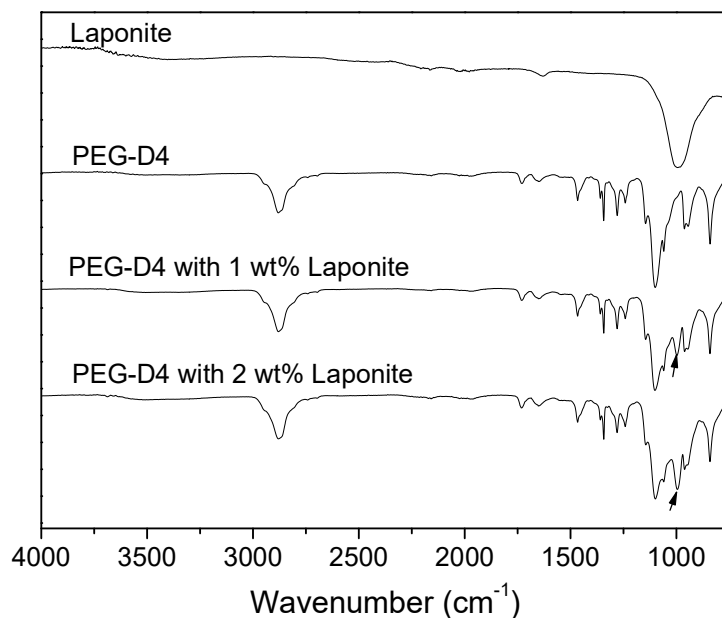

Figure 3.5 FTIR spectra of Laponite, PEG-D4, and PEG-D4 with 1 and 2 wt% Laponite. The arrows indicate the Si-O-Si peak in the nanocomposite hydrogel.

Equilibrium water content (EWC) averaged around 93 wt% for PEG-D4 hydrogels (**Figure 3.6**). Incorporating Laponite into PEG-D4 demonstrated marginal decrease in EWC value (93.3 % ± 0.04 % and 92.8 % ± 0.12 % for 0 and 2 wt% Laponit, respectively). EWC is a measure of the physical properties of a hydrogel network and EWC values are inversely proportional to both the crosslinking density and the mechanical properties of a hydrogel [182, 183]. These results indicated that a relatively small amount of Laponite used in our study did not significantly alter the crosslinking density of the PEG-D4 network.
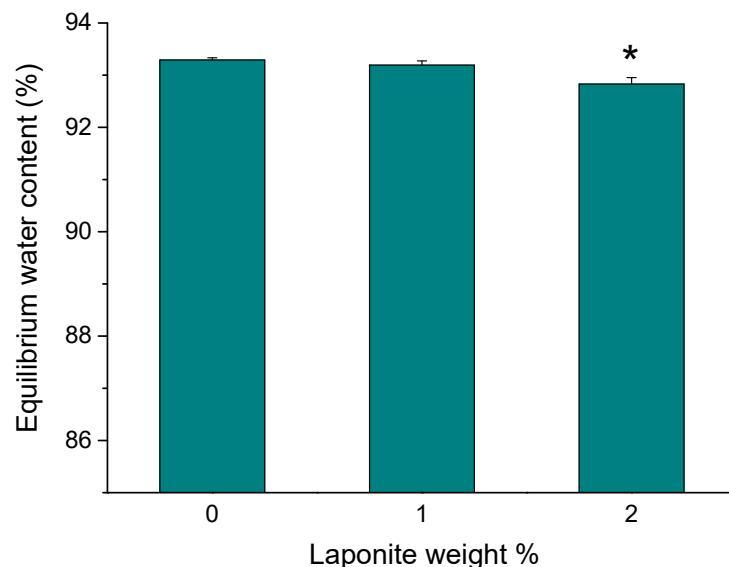
Figure 3.6 Equilibrium water content of PEG-D4 hydrogels cured using a NaIO$_4$:dopamine molar ratio of 0.5 and Laponite content of 0-2 wt%. * p < 0.05 when compared to 0 wt% Laponite.

3.4.3 Mechanical testing of nanocomposite hydrogel

From unconfined compression testing, hydrogels containing Laponite exhibited a significant increase in both the maximum compressive stress, fracture strain, and toughness when compared to Laponite-free samples (**Figure 3.7**). The observed increase in these materials properties was presumably due to the increasing interfacial binding between Laponite and dopamine in the hydrogel. In the presence of external loads, breaking of dopamine-Laponite bonds occurs first while minimizing damage to the chemical crosslinked network, which means higher strength and energy were needed to fracture the more compliant nanocomposite than the Laponite-free hydrogels. Physical interactions between polymer matrix and the embedded nanoparticles have been previously reported to improve the fracture strength of hydrogels via reversible attach-detach processes [184]. However, there was no change in the elastic modulus.

This observation is in agreement with results obtained from EWC analysis, which indicated that the incorporation of 1-2 wt% of Laponite did not drastically change the hydrogel crosslinking density.
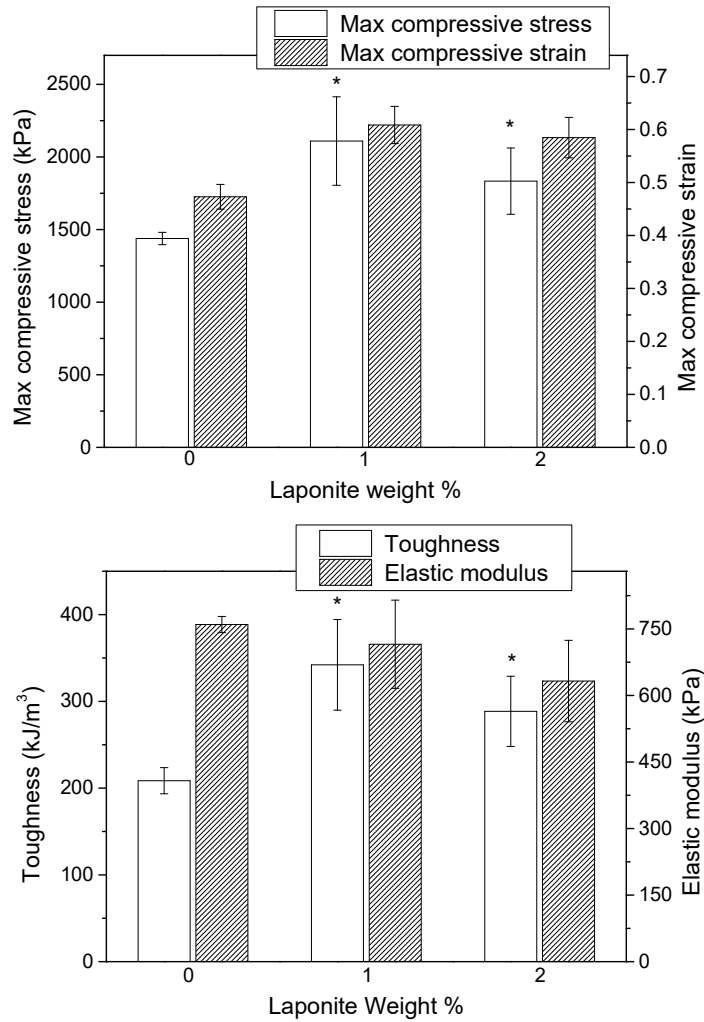

Figure 3.7 Results from compression testing of PEG-D4 hydrogels cured using a $NaIO_4$:dopamine molar ratio of 0.5 and Laponite content of 0-2 wt%. * $p < 0.05$ when compared to 0 wt% Laponite.

The viscoelastic properties of the hydrogel were determined using oscillatory rheometry (**Figure 3.8**). For all the formulations tested, the storage modulus (G') values were greater than the loss moduli (G"), indicating the hydrogels were chemically

crosslinked. For Laponite-containing samples, G' increased with increasing frequency, while G'' reached a plateau at 1 Hz. Similar observations have been reported for hydrogel crosslinked with both covalent and physical bonds [185]. Both measured G' and G'' values for hydrogel containing Laponite were significantly higher than those of Laponite-free samples (~1.5 and ~3 fold increase, respectively, at 1 Hz). An increase in the stiffness of hydrogels implies that the incorporation of Laponite increased the crosslinking density of nanocomposite hydrogel. An increased G'' indicated that these nanocomposites demonstrated elevated viscous dissipation properties due to the presence of reversible bonds in the hydrogel network [184-186]. However, the increase in the measured G' values was marginal when compared to Laponite-free network, suggesting that there may not have been a drastic change in the network structure. There was also no difference between the rheological data for samples containing different amount of Laponite.
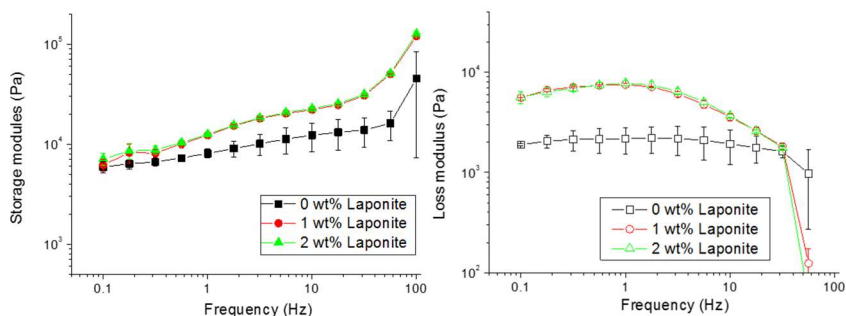

Figure 3.8 Storage (G') and loss (G'') modulus of PEG-D4 hydrogels with NaIO$_4$:dopamine molar ratio of 0.5 containing up to 2 wt% Laponite subjected to oscillatory strain=0.1 at a frequency of 0.1-100 Hz.

From the measured storage modulus (G'), hydrogel with Laponite showed less than 1.5 fold increase when compared to that of Laponite-free hydrogel. Similarly,

EWC data and elastic modulus found from compression testing did not show much difference in values between these formulations. Taken together, we speculate that the crosslinking density of nanocomposite hydrogel was not significantly altered by the addition of 1-2 wt% of Laponite. These observations are potentially due to the location of dopamine as a terminal group in the 4-armed-PEG polymer (**Figure 3.9A**). Previously, we demonstrated that when dopamine is present as a side chain of a polymer network, a small addition of Laponite (1-3 wt%) can increase the crosslinking density (**Figure 3.9B**) and storage modulus of the network by more than an order of magnitude [66]. Additionally, there is competitive crosslinking for dopamine (i.e., covalent crosslinking between dopamine, and non-covalent dopamine-Laponite interaction), which may have also limited the number of dopamine for interacting with Laponite. These observations also suggest that the interaction between PEG chain and Laponite was relatively weak in our sample and this interaction did not sufficiently alter the network architecture. Given that there was a statistical increase in measured toughness and loss moduli in the Laponite-containing networks, strong interfacial physical interaction mainly occurred between terminal dopamine moieties and Laponite as illustrated in **Figure 3.2**.
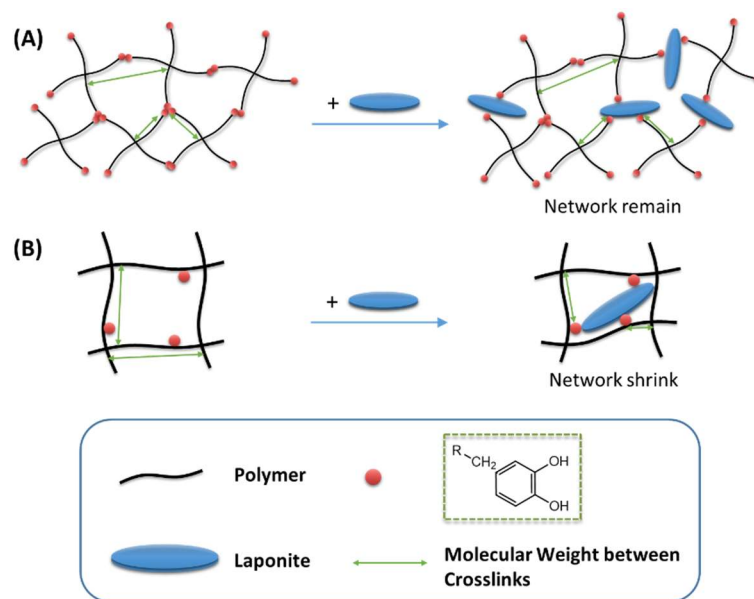
Figure 3.9 Schematic representation of crosslinking density change (in forms of "molecular weight between crosslinks" change) due to the addition of Laponite, dopamine-Laponite bonds happen at polymer end chain (A) and main chain (B).

3.4.4 Lap shear adhesion testing

Incorporation of Laponite significantly enhanced the adhesive properties of the nanocomposite hydrogels (**Figure 3.10**). PEG-D4 containing 2 wt% Laponite exhibited lap shear adhesive strength and work of adhesion values (7.9±1.8 kPa and 16.8±3.5 J/m^2, respectively) that were nearly 2.5 folds higher than those for Laponite free PEG-D4 (3.5±1.2 kPa and 6.7±2.0 J/m^2, respectively). Observed increase in improved adhesive properties is attributed to the strong catechol-Laponite interaction, which required elevated fracture energy to separate the adhesive joint. When compared to mechanical testing results, incorporation of Laponite significantly increased the compressive properties and shear moduli of PEG-D4 hydrogels, indicating that an increased bulk materials properties contributed to improved adhesive performance.

These increases in the bulk materials properties allow the nanocomposite hydrogel to withstand more forces during the lap shear adhesion testing. This observation is consistent with previously published reports where bulk cohesive properties of an adhesive contribute to its adhesive properties [187]. In this work, PEG-D4 adhesive containing up to 2 wt % of Laponite achieved a good balance among the three competitive reactions that dopamine is capable of undergoing (**Figure 3.2**), resulting in enhanced adhesive properties. PEG-D4 with and without Laponite also significantly outperformed CoSeal (Baxter, Inc., 0.6 ± 0.2 kPa and 1.5 ± 0.7 J/m^2, respectively), a commercially available PEG-based adhesive. The lap shear strength values reported here are lower when compared to previously published results for catechol-modified PEG systems with similar architectures, which range around 10-40 kPa [48, 188]. However, it is not possible to compare these values directly due to differences in testing protocols (e.g., preparation of adhesive joint, strain rate, etc.) and substrates used.
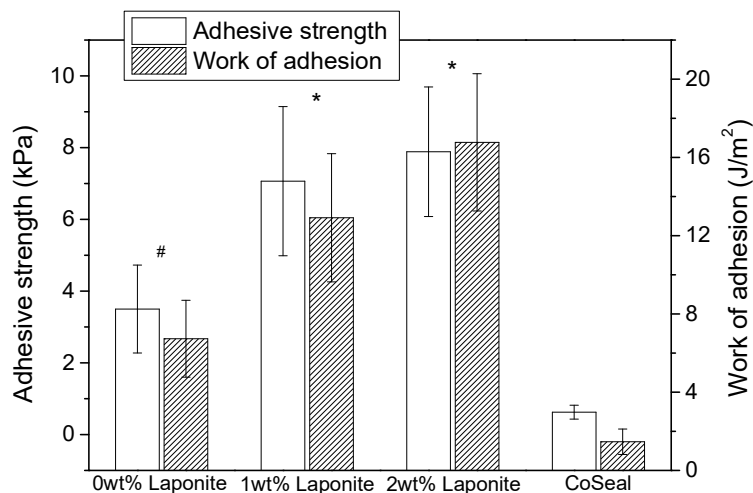

Figure 3.10 Lap shear adhesion test results of PEG-D4 hydrogels with NaIO4:dopamine molar ratio of 0.5 containing up to 2 wt% Laponite. * $p < 0.05$ when compared to 0 wt% Laponite and CoSeal. [#] $p < 0.05$ when compared to CoSeal.

3.4.5 *In vitro* degradation

The effect of Laponite content of the degradation rate of the PEG-D4 was determined by tracking the change in the dry mass of the samples over time (**Figure 3.11**). PEG-D4 lost over 70% of its dry mass over 8 weeks and completely degraded soon after. Incorporation of Laponite did not affect the degradation rate of the hydrogels, indicating that mass loss was driven by the hydrolysis of ester bond between PEG and glutaric acid. FTIR analysis of hydrogel containing 2 wt% of Laponite still show a Si–O–Si peak with reduced intensity after 8 weeks of degradation (**Figure 3.12**), indicating that Laponite is still present in the hydrogel network.
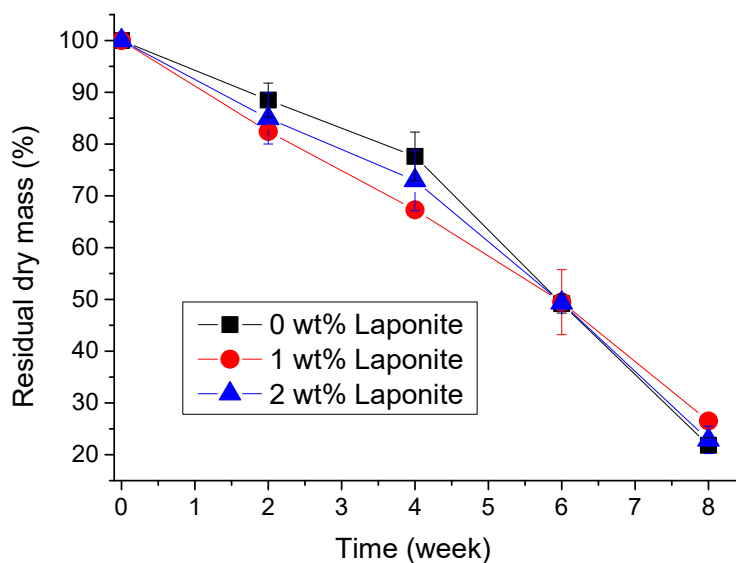

Figure 3.11 *In vitro* degradation of PEG-D4 hydrogels in PBS (pH = 7.4) at 37 °C. The values were normalized to the average dry mass of the hydrogels that did not undergo degradation.
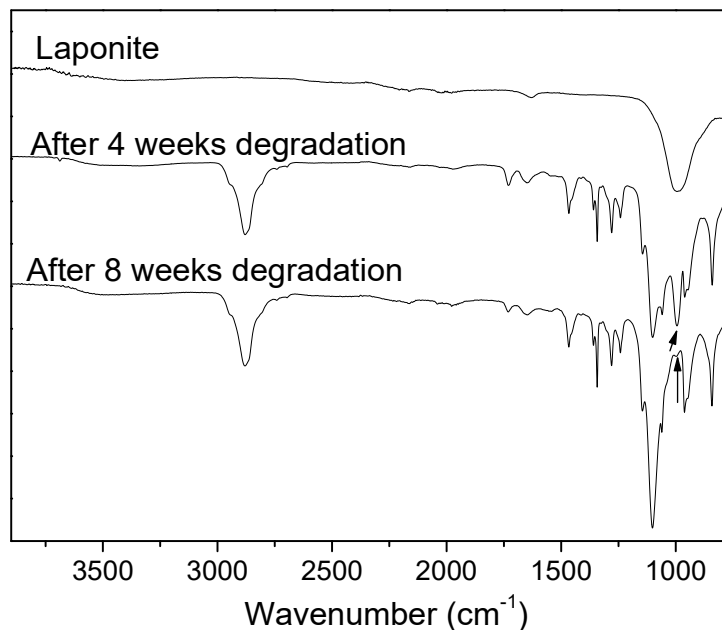
Figure 3.12 FTIR spectra of Laponite, PEG-D4 with 2 wt% Laponite hydrogel after 4 and 8 weeks of degradation. The arrows indicate the Si-O-Si peak in the nanocomposite hydrogel.

3.4.6 MTT assay

A quantitative MTT assay was used to determine the cytocompatibility of PEG-D4 nanocomposites (**Figure 3.13**). Regardless of sterilization methods and hydrogel formulations, hydrogel extracts were found to be non-cytotoxic, with relative cell viability greater than 75%. Other catechol-modified polymeric adhesives have been demonstrated to be non-cytotoxic [50, 162, 188]. As expected, Laponite did not adversely affect the biocompatibility of PEG-D4 formulations as it was previously determine to be biocompatible to various cell types when incorporated into hydrogel [172, 189]. Interestingly, relative cell viability for hydrogel containing 2 wt% Laponite was significantly higher than that of Laponite-free PEG-D4 hydrogel when the hydrogel extracts were sterile filtered. Leachable ions from the degrading Laponite

66

possibly had a proliferative effect on fibroblast. Using ethanol sterilization method, these degradation products were likely removed during soaking in ethanol and repeated washing by PBS, and there were no significant difference in cell viability between formulations.
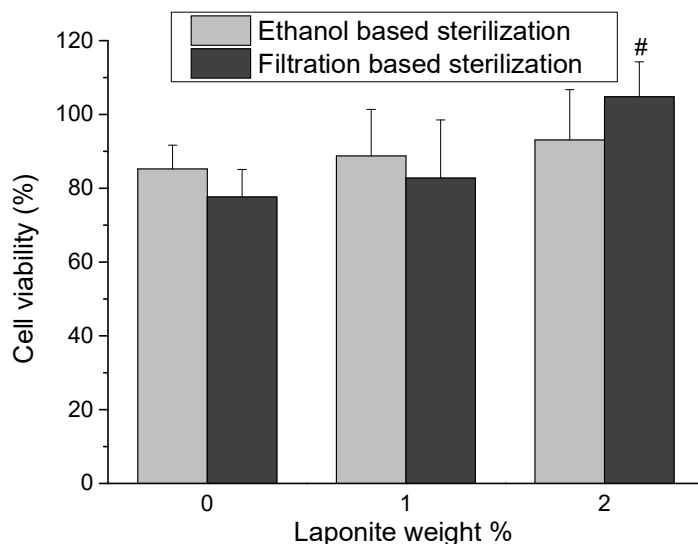

Figure 3.13 Relative cell viability of PEG-D4 hydrogels with up to 2 wt% Laponite (Left-ethanol based sterilization, right-filtration based sterilization). [#] $p < 0.05$ when compared to 0 wt% Laponite normalized to medium control.

3.4.7 Subcutaneous implantation

To further evaluate the biocompatibility of these materials, PEG-D4 with either 0 or 2 wt% Laponite were implanted subcutaneously in rat for 4 and 8 weeks. After 4 weeks of implantation, the histological analysis results revealed the formation of fibrous capsule at the interface between the implant and the subcutaneous tissue as well as a cellular infiltration layer that is rich in fibroblasts (**Figure 3.14**). These observations resembled findings reported by others for degradable implants that promoted cellular infiltration [177, 190, 191]. Thicker fibrous capsules were observed

for Laponite-containing hydrogels (**Table 3.1**), which may be associated with elevated proliferation and activation of fibroblasts, that up-regulated collagen production in the tissues surrounding the hydrogel [177]. Our hydrogel cytotoxicity testing results seem to indicate that leachable ions from Laponite support fibroblast proliferation (**Figure 3.13**). Although there was no difference in the thickness of infiltration layer between samples, there is a significantly higher cellular density for Laponite-containing hydrogels. The infiltration layers of 2 wt% Laponite hydrogels also consisted of a small amount of macrophage while those of 0 wt% Laponite hydrogels were macrophage free (**Figure 3.15**). The release of inorganic ions from Laponite potentially contributed to the increased inflammatory response of the nanocomposite. Both trichrome and immunofluorescent staining indicated that no cells were observed inside the hydrogels.
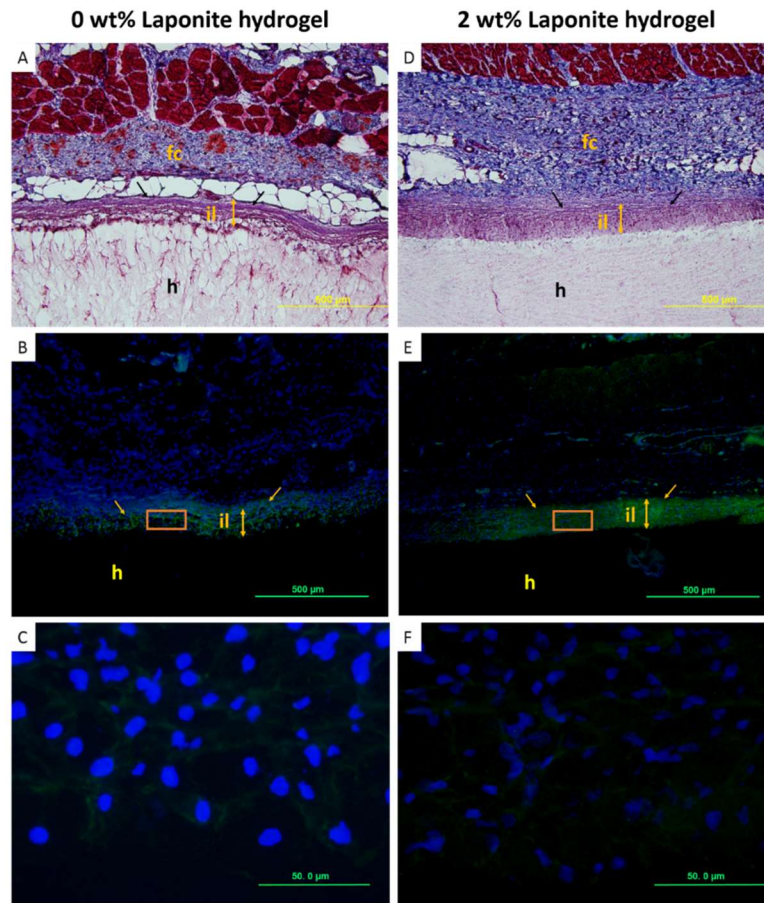
Figure 3.14 Histological characterization of PEG-D4 hydrogels containing 0 and 2 wt% Laponite and surrounding tissues after 4 weeks of subcutaneous implantation. Masson's trichrome staining images for evaluating the overall tissue section morphology and the thickness of the fibrous capsule (fc) (A, D). Immunohistochemical staining images for evaluating the infiltration cell type and density (B, C, E, F). Cell nuclei were stained by DAPI (blue), fibroblasts were stained by marker S100A4 (green). C and F are the enlarged view of the orange boxes in B and E, respectively. "h": hydrogel; "il": infiltration layer; one-sided arrows: interface between hydrogel and tissue; two-sided arrows: the thickness of the infiltration layer.
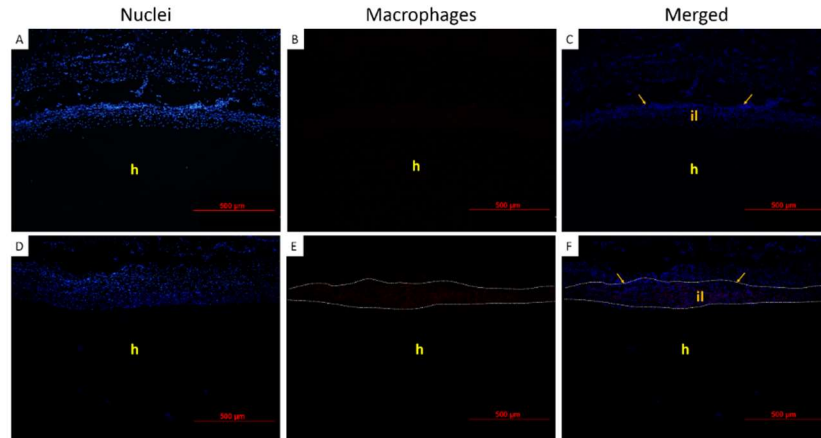
Figure 3.15 Immunohistochemical staining images of PEG-D4 hydrogels with 0wt% (A, B, C) and 2 wt% (D, E, F) Laponite and surrounding tissues after 4 weeks of subcutaneous implantation. Cell nuclei were stained by DAPI (blue), and macrophages were stained by marker CD68 (red). "h": hydrogel; "il": infiltraion layer; arrows: interface between hydrogel and tissue. Panels E and F contain faint red spots enclosed within the white dashed lines, corresponding to the presence of macrophages. No macrophage was detected for Laponite-free samples (B and C).

After 8 weeks, the thickness of fibrous capsule surrounding Laponite-free hydrogels nearly doubled while the fibrous capsule thickness for hydrogels containing 2 wt% Laponite remained the same (**Figure 3.16**, **Table 3.1**). Qualitatively, Laponite-containing samples appeared smaller when explanted when compared to Laponite-free samples by week 8. The resence of macrophages and higher fibroblast cellular density at the earlier time point potentially hasten the degradation of Laponite-containing PEG-D4 network [192]. Therefore, relatively thinner fibrous capsules are attributed to the host resolving the foreign body response for the smaller sized Laponite-containing samples. No macrophages were observed for both hydrogel types (images not shown) and the samples were completely infiltrated with fibroblast, which appeared to be evenly distributed within the whole gel. Additionally, there was a significantly higher

cell density in hydrogels containing 2 wt% Laponite as compared to that of Laponite-free sample.
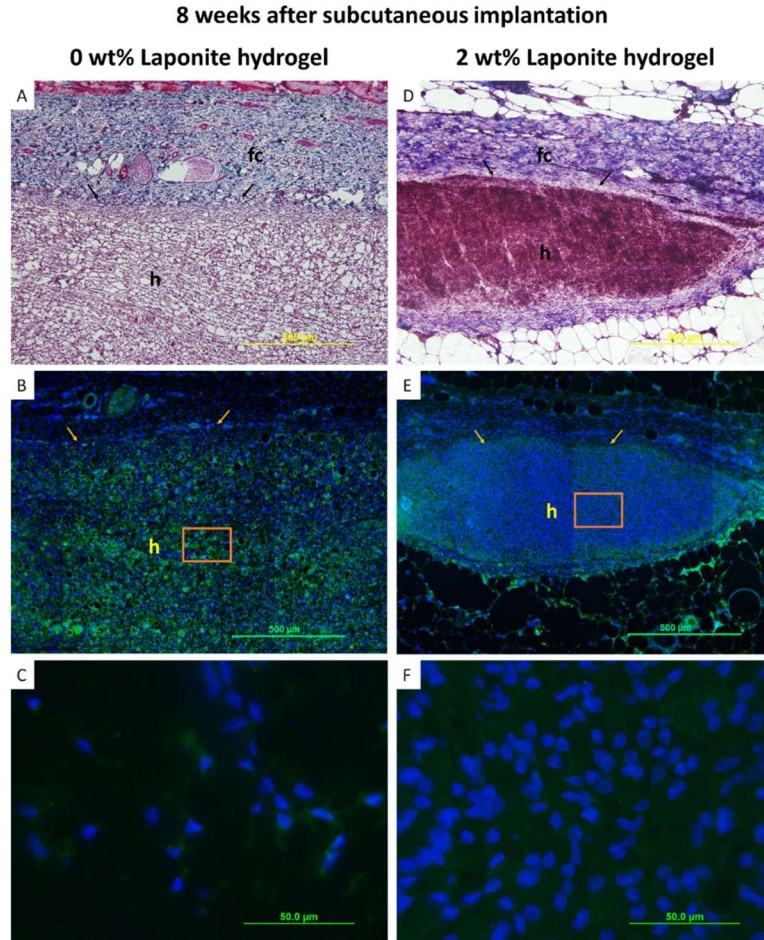
Figure 3.16 Histological characterization of PEG-D4 hydrogels containing 0 and 2 wt% Laponite and surrounding tissues after 8 weeks of subcutaneous implantation. Masson's trichrome staining images for evaluating the overall tissue section morphology and the thickness of the fibrous capsule (fc) (A, D). Immunohistochemical staining images for evaluating the infiltration cell type and density (B, C, E, F). Cell nuclei were stained by DAPI (blue), fibroblasts were stained by marker S100A4 (green). C and F are the enlarged view of the orange boxes in B and E, respectively. "h": hydrogel; arrows: interface between hydrogel and tissue.

Table 3.1 Fibrous capsule thickness, inflammation response, cell infiltration, and infiltrated cell density assessment of the implanted PEG-D4 hydrogels (0 and 2 wt% Laponite) and surrounding tissue retrieved after 4 and 8 weeks subcutaneous implantation.

	4 weeks		8 weeks	
	0 wt% Laponite	2 wt% Laponite	0 wt% Laponite	2 wt% Laponite
Fibrous capsule thickness (μm)	253 ± 18.7	305 ± 41.2	498 ± 60.6	337 ± 77.9
	$p = 0.045$[#]		$p = 0.0002$[#]	
Cell infiltration thickness (μm)	125 ± 15.1	126 ± 4.90	Cellular infiltrated throughout these samples	
	$p = 0.85$[#]			
Inflammatory response[‡]	–	+	–	–
Cell density (cells/mm^2)*	2530 ± 496	4510 ± 711	6860 ± 838	9580 ± 839
	$p = 0.020$[#]		$p = 0.014$[#]	

[#] $p < 0.05$ indicates significant difference (analyzed by t-test).
[‡] "+" and "-" denote positive and negative outcome, respectively.
* Cell density within the infiltration layer and throughout the bulk of the hydrogels for week 4 and 8 samples, respectively.

Subcutaneous implantation results indicated that PEG-D4 nanocomposite is biocompatible. The thickness of fibrous capsule surrounding 2 wt% Laponite hydrogels at 8 weeks post-implantation was significant lower when compared to Laponite-free samples. This indicated that there is a reduced foreign body reaction to the implanted nanocomposite [177, 193]. Additionally, there was no macrophage present after 8 weeks for samples containing either 0 or 2 wt% Laponite, indicating that these hydrogels did not induce prolonged inflammatory response. Other catechol-modified polymeric adhesives have also been demonstrated to elicit minimal inflammatory responses *in vivo* [162, 188]. Additionally, Laponite has been previously shown to be biocompatibile when incorporated into a hydrogel [171, 172, 194] with biocompatible degradation products (Na^+, $Si(OH)_4$, Mg^{2+}, Li^+) [168].

Most interestingly, Laponite incorporated hydrogels displayed an enhanced level of cellular infiltration at both time points. Laponite has been previously reported to provide binding sites for cell attachment and proliferation [171, 172, 194]. The relatively small pore size (mesh size on the order of 70 Å) [50, 195] in the PEG-D4 network provides physical hindrance for cellular ingrowth. However, the presence of dopamine-Laponite physical crosslinks can potentially be broken and displaced by migrating cells. Cellular infiltration into synthetic, physically crosslinked networks have been previously demonstrated [196]. To induce cellular infiltration into inert and synthetic hydrogels, hydrogels are typically modified with cell binding peptides (e.g., RGD) or other bioactive protein [197-199] or designed to be susceptible to matrix metalloproteinase-mediated degradation [188, 200], which required complicated and multi-step chemical synthesis. Compare to these strategies, introducing Laponite into a hydrogel network offered a facile method to simultaneously promote bioactivity and adhesive property of a PEG-based adhesive. The formation of fibrous capsules surrounding PEG-D4 nanocomposite may hinder the molecular exchange between implanted materials and surrounding tissues, indicating that the adhesive may not be appropriate for repairing tissues that are rich in vasculatures [201]. However, Laponite has previously demonstrated to promote osteoblasts proliferation, differentiation, and mineralization [171]. Additionally, Laponite shares much composition similarity to silica that has been previously suggested to serve as a crosslinking agent in connective tissue [202]. Nanocomposite adhesive described here may be a promising biomaterial for bone and connective tissue repair. Additional study is required to evaluate the effect of Laponite incorporation on the performance of adhesive *in vivo*.

73

3.5 Conclusion

We described an injectable nanocomposite tissue adhesive hydrogel based on dopamine-functionalized 4-arm PEG and a synthetic nano-silicate, Laponite. Introduction of Laponite significantly increased the curing rate, bulk mechanical property and adhesive property of the adhesive due to strong interfacial binding between dopamine and Laponite. The addition of Laponite did not alter the degradation rate and biocompatibility of PEG-D4. From subcutaneous implantation in rat, PEG-D4 nanocomposite hydrogels elicited minimal inflammatory response. Additionally, samples containing Laponite exhibited a significantly higher level of cell infiltration than Laponite-free control, indicating that the addition of Laponite is potentially a simple and effective method to simultaneous promote bioactivity and adhesive performance of a bio-inert, synthetic PEG-based adhesive.

3.6 Acknowledgement

Chapter 4 A moldable nanocomposite hydrogel composed of a mussel-inspired polymer and a nanosilicate as a fit-to-shape tissue sealant[4]

4.1 Abstract

The engineering of bioadhesives to bind and conform to the complex contour of tissue surfaces remains a challenge. We have developed a novel moldable nanocomposite hydrogel by combining dopamine-modified poly(ethylene glycol) and the nanosilicate Laponite, without the use of cytotoxic oxidants. The hydrogel transitioned from a reversibly cross-linked network formed by dopamine–Laponite interfacial interactions to a covalently cross-linked network through the slow autoxidation and cross-linking of catechol moieties. Initially, the hydrogel could be remolded to different shapes, could recover from large strain deformation, and could be injected through a syringe to adhere to the convex contour of a tissue surface. With time, the hydrogel solidified to adopt the new shape and sealed defects on the tissue. This fit-to-shape sealant has potential in sealing tissues with non-flat geometries, such as a sutured anastomosis.

4.2 Introduction

Marine mussels secrete adhesive proteins that enable these organisms to attach to various surfaces (rocks, boats, etc.) in a wet, saline environment [19, 158]. The catecholic moiety found in these proteins plays an important role in interfacial binding and intermolecular crosslinking [130, 203]. Catechol-modified synthetic bioadhesives have demonstrated potential in suture-less wound closure [162], fetal membranes sealing [81, 84], Achilles tendon repair [47], and immobilization of therapeutic drugs [72] or cells [80, 163]. However, existing mussel-inspired adhesives are not ideal for sealing tissue surface with a complex and non-flat geometry (i.e., sealing the convex contour of a sutured anastomosis) due to the slow curing rate (~30 s) of the applied liquid precursor solution [163]. A moldable hydrogel that can be processed in the gel form and remolded to fit a desired geometry can potentially address this issue. Although various moldable hydrogels have been reported, these materials are activated by triggers that are potentially unsuitable for biomedical applications (i.e., high pressure [204], high temperature [205], large change in pH [206, 207], and redox reagent [208]). Most importantly, none of these moldable hydrogels has demonstrated adhesive property. Designing a hydrogel which can be remolded under mild physiological conditions and applied as a bioadhesive remains a challenge. Herein, we report a simple approach to construct a moldable nanocomposite hydrogel that can function as a fit-to-shape tissue sealant.

4.3 Experimental section

4.3.1 Materials

4-armed (MW=10 kDa), 6-armed (MW=15 kDa), and 8-armed (MW=20 kDa) poly(ethylene glyco) (PEG, JenKem Technology, Plano, TX) were end-modified sequentially with glutaric acid and dopamine to yield PEG-D4, 6, and 8, respectively following published protocols [209]. Laponite XLG (Laponite) was a gift from Southern Clay Products (Austin, TX). Sodium pyrophosphate decahydrate ($Na_4P_2O_7\cdot10H_2O$) and 4-methylcatechol was obtained from Sigma-Aldrich (St. Louis, MO). 1X phosphate buffer saline (PBS, pH=7.4) was from Fisher Scientific (Pittsburgh, PA). All chemicals were used as received. Bovine pericardium was purchased from Sierra for Medical Science (Whittier, CA). The collagen tubing (collagen-based sausage casing) was from Johnsonville Sausage (Sheboygan Falls, WI). Medical suture (Chromic gut 5-0) was obtained from Ethicon (Somerville, NJ).

4.3.2 Preparation of hydrogel

To prepare D8-15/Lapo-5, PEG-D8 was dissolved in deionized water as 300 mg/ml, and Laponite was dissolved in $Na_4P_2O_7\cdot10H_2O$ as 100 mg/ml while the mass ratio of Laponite to $Na_4P_2O_7\cdot10H_2O$ was always kept at 10. Equal volume of PEG-D8 (30 wt% in deionized water) and Laponite (10 wt% in $Na_4P_2O_7$) solutions were mixed and sonicated for 3 min to obtain the precursor solution. The final concentrations of PEG-D8 and Laponite in precursor solution were half of those in the individual precursor solutions (i.e., 15 and 5 wt% for PEG-D8 and Laponite, respectively). The solution was added to a mold in a sealed environment containing a water bath to keep it moist at room temperature. Similar preparation was used to prepare hydrogels using

different PEG architecture (4-, 6-, and 8-armed) and concentrations of PEG-D and Laponite (10-15 wt% and 2.5-7.5 wt%, respectively). Nanocomposite hydrogel was denoted as Dx-a/Lapo-b, where x, a, and b denoted the arm number of PEG-D, weight percent of PEG-D and Laponite in the hydrogel, respectively.

4.3.3 Catechol oxidation and dimerization studies

At predetermined incubation time points (0-24 h), 5 µl of D4-15/Lapo-5 and PEG-D4 (150 mg/ml in deionized water) was added to 2 ml of deionized water (150 µM dopamine) separately. The UV-Vis spectra (250 to 600 nm; PerkinElmer Lambda35, Waltham, MA) of the solutions were recorded using deionized water as the reference. Recorded values of dopamine quinone ($\lambda_{max} = 392$; $\varepsilon = 1130$ M^{-1} cm^{-1}) [210] were used to identify the oxidation intermediates and calculate their respective concentrations using Beer's law:

$$A = \varepsilon bc \qquad (4.1)$$

where A is the absorbance, ε is the molar absorptivity constant, b is the path length (1 cm), and c is the concentration. 4-methylcatechol was dissolved in deionized water as 120 mM and mixed with 10 wt% Laponite solution, the mixture was incubated at room temperature for 1 day and freeze-dried overnight. Dimethyl sulfoxide-d6 (Sigma-Aldrich) or methanol (Fisher Scientific) was added to the dry 4-methylcatechol/Laponite then the Laponite was removed by centrifugation (5000 rpm for 5 min). 4-methylcatechol incubated with Laponite for 1 day was analyzed on a Varian 400 MHz spectrometer for ^{1}H nuclear magnetic resonance (NMR) spectra and a LCQ Advantage Ion-Trap mass spectrometer (Thermo Finnigan, San Jose, CA) in

negative ion mode with a mobile phase of 95 % methanol and 5 % deionized water for mass spectra (MS).

4.3.4 Remolding and reshaping of hydrogel

For the remolding of hydrogels, the precursor solution was cast into a silicone rubber mold with a rectangular shape (10 by 8 by 0.5 mm). After incubating the hydrogel for 1 day, the gel piece was demolded and fit into a new mold with a shape of an equilateral triangle (length of each side = 8 mm) or a circle (diameter = 8 mm) and allowed to incubated for 3 more days. For the reshaping of hydrogels, the precursor solution was casted into a rectangular silicone rubber mold (30 by 4 by 0.5 mm). After incubating for the predetermined amount of time, the gel strip was demolded and wrapped around a rod made from polytetrafluoroethylene (Teflon® PTFE, diameter = 5 mm, McMaster-Carr, Elmhurst, IL) to generate a helix shape and further incubated so that the total incubation time was 4 days. The incubation was performed in a sealed environment containing a water bath to keep it moist at room temperature. The remolded and reshaped hydrogels were allowed to equilibrate in PBS.

4.3.5 Hydrogel characterization

Hydrogels were equilibrated in deionized water for overnight and then vacuum-dried for at least 2 days to obtain dry gels. Equilibrium water content (EWC) was defined as:

$$EWC = \frac{M_s - M_d}{M_s} \times 100 \text{ \%} \qquad (4.2)$$

where M_s and M_d denote the mass of swollen and dried hydrogels, respectively. Fourier transform *infrared* (FTIR) spectra of the dried samples were obtained using a

PerkinElmer Spectrum One spectrometer. The morphologies of the dried gels were observed using field emission scanning electron microscopy (FE-SEM, Hitachi S-4700).

4.3.6 Rheology studies

The rheological properties of hydrogels were tested using a HR-2 oscillatory rheometer (TA Instruments, New Castile, DE) using a 20 mm parallel-plate geometry at a gap distance of 150 μm. The strain sweep experiment was performed at oscillatory frequency of 1 Hz to determine the linear viscoelastic region (data not shown). The frequency sweep experiment was performed at frequencies ranging from 0.1 to 10 Hz at 1 % strain to determine the storage (G') and loss (G'') moduli. The stress relaxation test was performed by applying a step strain (γ = 10 %) at a frequency of 1 Hz to monitor the relaxation modulus ($G(t)$) over time. The relaxation time (τ) was found by fitting the measured modulus to Kohlrausch's stretched-exponential relaxation model equation [211]:

$$G(t) = G(0)\exp[-(t/\tau)^a], 0 < a < 1 \quad (4.3)$$

The ability for the hydrogel to recover from a large strain deformation was performed in 2 ways. In the first method, the sample was repeatedly subjected to a shear strain of 1 % and 1000 % at a frequency of 1 Hz. In the second method, the sample was subject to increased strain amplitude from 0.1 to 1000 % at an oscillatory frequency of 1 Hz and immediately followed by subjecting the sample at 1 % strain and 1 Hz to monitor the recovery of G'. G' was normalized by its initial value.

4.3.7 Adhesion testing

The burst adhesion testing was performed according to ASTM F2392-04 [116] with minor modifications. A circular piece of bovine pericardium (diameter = 30 mm, hydrated in PBS) with a concentric defect (diameter = 3 mm) was lay over a blue pipet tip to create a curved tissue surface. Hydrogel incubated for different amount of time was applied to seal the defect. The final hydrogel dimension was ~ 10 mm in diameter and ~2 mm in thickness. The hydrogel was further incubated in a sealed environment containing a water bath to keep it moist at room temperature for 1 day prior to testing. A syringe pump (Fisher Scientific) was used to push PBS (2 ml/min) against the hydrogel and the maximum pressure reading was recorded. The burst pressure (P_{burst}) was determined by:

$$P_{\mathbf{burst}} = P_{\mathbf{gauge}}(\frac{d_{\mathbf{pipe}}}{d_{\mathbf{defect}}})^2 \qquad (4.4)$$

where P_{gauge} is the reading of pressure gauge, d_{pipe} and d_{defect} is the diameter of the pressure gauge pipe and concentric defect on tissue, respectively. The failure type was recorded. Cohesive and adhesive failure indicated the failure happened at bulk hydrogel and the interface between hydrogel and tissue, respectively.

4.3.8 Cell attachment

Hydrogel incubated for 4 days (thickness ~ 0.4 mm, diameter ~ 8 mm) were sterilized in 70 % (v/v) ethanol for 45 min and washed three times using sterilized PBS for 30 min each. Human dermal fibroblasts passage 5 (ATCC, Manassas, VA) were seeded onto hydrogel in a 12-well suspension culture plate at a density of 10^4 cells/cm^2. The cells were cultured in Dulbecco's modified eagle medium (DMEM, Life

Technology, Rockville, MD) with 20 % fetal bovine serum (FBS, Atlanta Biologicals, Flowery Branch, GA) and 100 unit/ml catalase (Sigma-Aldrich) at 37 °C and 5 % CO_2 for 48 h. The attached cells on hydrogel were fixed in formalin (Fisher Scientific) for 15 min and blocked in 1 % bovine serum albumin (BSA, Fisher Scientific) for 30 min. The samples were labeled by rhodamine phalloidin (Life Technology) staining (1:400) for 30 min, and followed by 4′, 6-diamidino-2-phenylindole (DAPI, Sigma-Aldrich) nucleus staining (1:1000) for 10 min. Stained samples were imaged using a fluorescent microscope (Olympus BX51, Melville, NY).

4.3.9 Statistical analysis

Statistical analysis was performed on Origin software. Student t-test and One-way analysis of variance (ANOVA) with Tukey HSD analysis were performed for comparing means of two and multiple groups, respectively, using a p-value of 0.05.

4.4   Results and discussion

Herein, we report a simple approach to construct a moldable nanocomposite hydrogel that can function as a fit-to-shape tissue sealant. The hydrogel combines a mussel-inspired polymer, dopamine-modified multi-armed poly(ethylene glycol) (PEG-D) and a synthetic inorganic nano-silicate, Laponite $(Na^{0.7+}(Mg_{5.5}Li_{0.3}Si_8O_{20}(OH)_4)^{0.7-})$ (**Figure 4.1A**). The key to this strategy is the dynamic crosslinking process of PEG-D (**Figure 4.1B**) involving the interfacial interactions between polymer-bound dopamine and Laponite (**Figure 4.1C**) [2, 66].
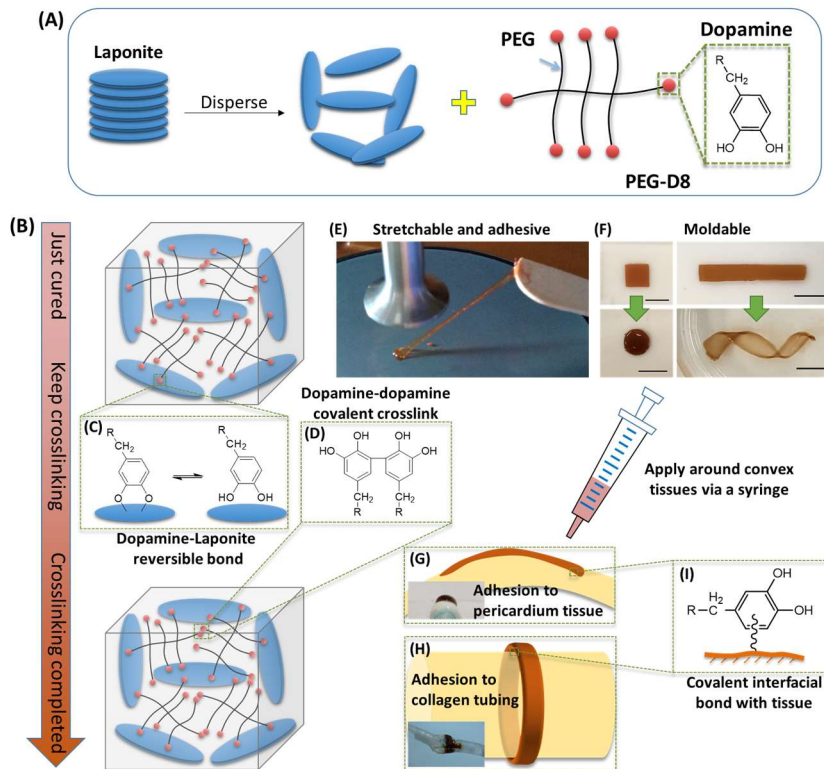
Figure 4.1 Schematic illustration of the preparation of moldable nanocomposite hydrogel. (A) Laponite was combined with PEG-D to prepare the adhesive hydrogel. (B) During the early stage of curing, the hydrogel consists of reversible interaction formed between dopamine and Laponite (C) and is loosely covalent crosslinked (D). Hydrogel was stretchable and adhesive (E), can be remolded to different shapes (F), and can applied around a convex pericardium (G) and collagen tubing (H) via a syringe. As the covalent crosslinking density increased, the hydrogel was shape-fixed and bound to tissue via interfacial covalent bonds (I). Scale bar: 10 mm

A light brown hydrogel was formed from mixing solutions of PEG-D and Laponite. This color change is attributed to the basic nature of Laponite solution [167] leading to the autoxidation of dopamine and the subsequent covalent crosslinking between catechol residues (**Figure 4.1D**) [70]. During the early stage of curing (i.e., incubation time < 24 h), the hydrogel was stretchable and adhesive (**Figure 4.1E**), able to be remolded to different shapes (**Figure 4.1F**), and can be applied around the contour

of a tissue surface (**Figure 4.1 G** and **H**). When the hydrogel was incubated for prolonged periods of time (i.e., > 2 day), it progressively lose its ability to be reshaped (**Figures 4.2A-E**). During which time, the hydrogel transitioned from a light brown color to a dark brown color, resulting from progressive intermolecular crosslinking of the catechol group [70]. As the crosslinking density increased, the hydrogel became shape-fixed and functioned as a fit-to-shape sealant.
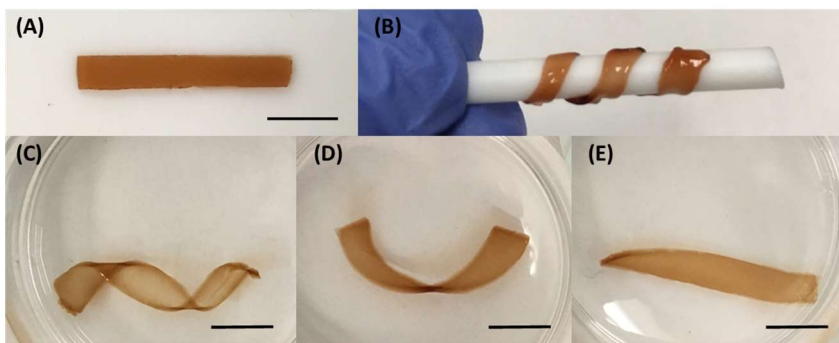

Figure 4.2 The moldable property of nanocomposite hydrogels consisting of 15 wt% PEG-D8 and 5 wt% Laponite (D8-15/Lapo-5). Photographs of hydrogel strip incubated for predetermined time (A) was wrapped around a PTFE rod to generate a helix shape (B) and further incubated to make the total incubation time of 4 days. Hydrogel incubated for 1 day before reshaping maintained the helix shape even when it was submerged in an aqueous solution (C). Whereas hydrogels incubated for 2 (D) and 3 days (E) prior to reshaping cannot maintained the helix shape. Scale bar: 10 mm.

UV-Vis spectra (**Figure 4.3**) revealed the steady increase of oxidation intermediates of dopamine (i.e., dopamine quinone) and dimerized dopamine when incubated with Laponite over time. Model nuclear magnetic resonance (**Figure 4.4**) and mass (**Figure 4.5**) spectrometry studies using reaction product of 4-methylcatechol/Laponite confirmed the formation of dimerized catechol during incubation. Fourier transform infrared spectroscopy spectra confirmed the presence of Laponite in the solidified hydrogel (**Figure 4.6**).
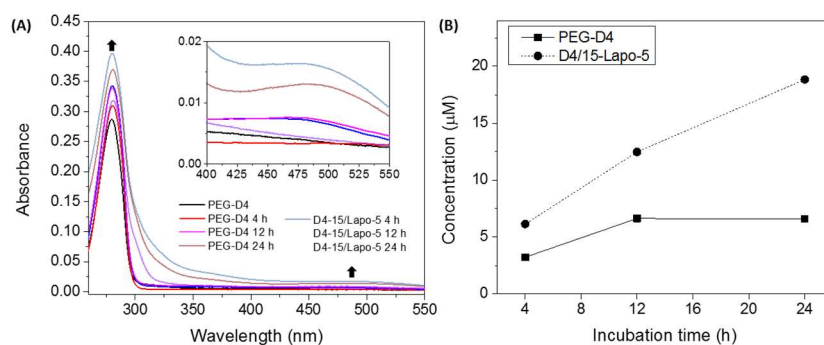
Figure 4.3 (A) UV–vis spectra of solutions containing PEG-D4 and D4-15/Lapo-5 (150 µM dopamine) over 24 h of incubation. The inset enlarge the absorbance between 400 and 550 nm. The new formed broad peak with continuous increasing absorbance at 480 nm and the simultaneously increasing absorbance at 280 nm indicated the formation of dicatechol coupling in D4-15/Lapo-5 [212]. (B) Change in the concentration of dopamine quinone of the solution containing PEG-D4 and D4-15/Lapo-5 (150 µM dopamine) at different incubation time.
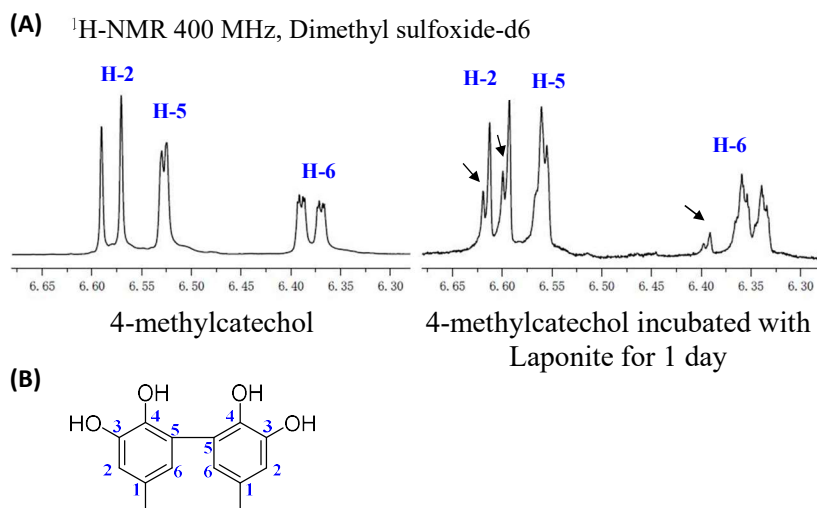

Figure 4.4 (A) ^{1}H NMR spectra of catecholic benzene ring region of 4-methylcatechol and 4-methylcatechol incubated with Laponite for 1 day. The partial peak separations of the ^{1}H linked to C-2 and C-6 (arrows) suggested that the new covalent bonds occurred to C5 [213]. A relative decrease in the peak area for H-5 (from 1.01 to 0.9 when a reference integral value of 1 for H-2 was set) was observed. (B) The proposed structure of dimerized 4-methylcatechol.
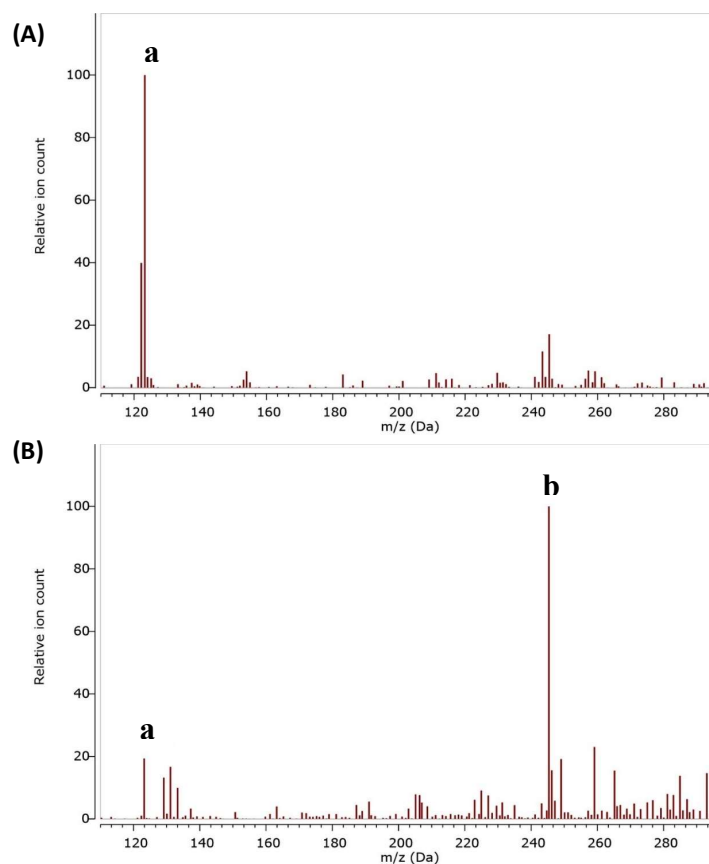
Figure 4.5 Catechol dimerization study by mass spectrometry in negative mode. Mass spectra of 4-methylcatechol (A) and 4-methylcatechol incubated with Laponite for 1 day (B). Peak a: 4-methylcatechol at m/z 123 [M-H]⁻. Peak b: 4-methylcatechol dimer at m/z 245 [M-H]⁻.
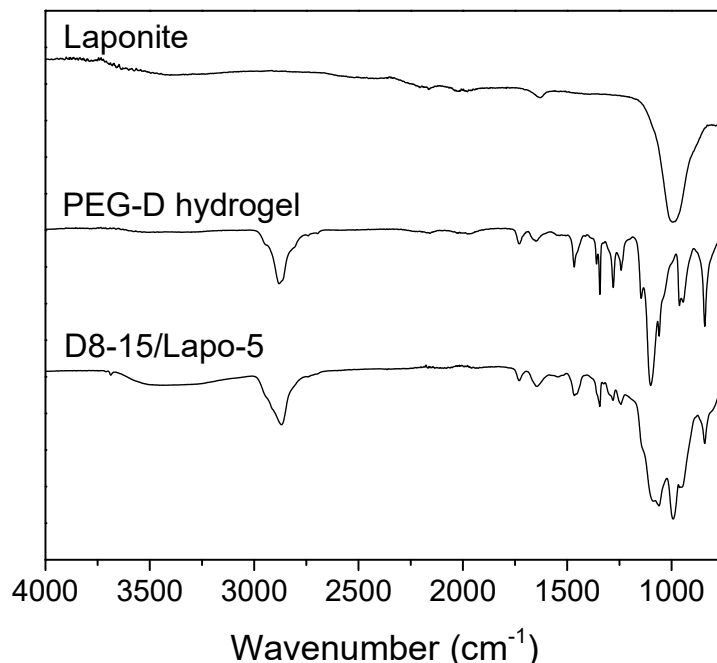
Figure 4.6 FTIR spectra of Laponite, chemically crosslinked PEG-D hydrogel, and nanocomposite hydrogel consisting of 15wt% PEG-D8 and 5 wt% Laponite (D8-15/Lapo-5). D8-15/Lapo-5 exhibited featured peaks of both PEG-D (-C-O-C- at 1000-1150 cm^{-1}, -CH$_2$- at 2880 cm^{-1}, ester bonds at 1729 cm^{-1}) [180] and Laponite (Si–O–Si at 995 cm^{-1}) [181].

To investigate the factors that affect the curing process, PEG architecture (4-, 6-, and 8-armed PEG-D (PEG-D4, 6, and 8, respectively) and the concentrations of PEG-D and Laponite (10-15 wt% and 2.5-7.5 wt%, respectively) were varied. Nanocomposite hydrogel was denoted as Dx-a/Lapo-b, where x, a, and b denoted the arm number of PEG, weight percent of PEG-D and Laponite in the hydrogel, respectively. At all the concentrations tested, PEG-D4 did not cure even after 48 h of incubation (**Table 4.1**). For PEG-D6 and PEG-D8, the concentration of Laponite needed to be 5 wt% or higher to achieve gel formation. For PEG with a reduced number of arms (i.e., 4-armed) or a solution with lower Laponite contents, the polymer chains were unable to connect neighboring Laponite particles to form a network [105]. Both

a higher degree of branching and an elevated content of Laponite provided more physical crosslinking points.

Table 4.1. Curing feasibility of a series of PEG-D/Laponite formulations. "√" marks indicate cure within 24 h, and "x" marks indicate not cure after 48 h.

		PEG-D4 wt%		PEG-D6 wt%		PEG-D8 wt%	
		10	15	10	15	10	15
Laponite wt%	2.5	x	x	x	x	x	x
	5	x	x	√	√	√	√
	7.5	x	x	√	√	√	√

Oscillatory rheology was performed to investigate the hydrogel mechanics during the crosslinking process. For D8-15/Lapo-5, the crossover between the storage G' and G" values (i.e., gel point) occurred after 5 h of incubation (arrow in **Figure 4.7**).
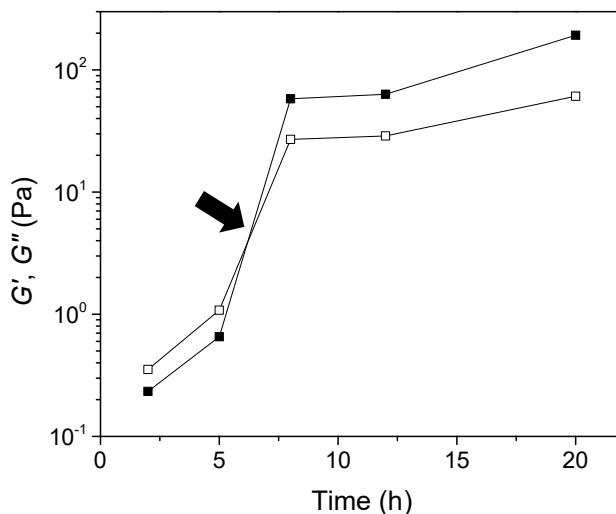

Figure 4.7 Change of storage (G', close symbols) and loss (G", open symbols) modulus as a function of incubation time for hydrogel containing 15wt% PEG-D8 and 5 wt% Laponite (D8-15/Lapo-5) at an oscillatory strain = 1%, frequency =1 Hz. The crossover in the G' and G" values indicated the gel point (arrow).

G' values continued to increase over 4 days, indicating an increased stiffness and crosslinking density over this time period (**Figure 4.8A**). G' values also became

less frequency dependent with time, indicating a more elastic behavior. Similarly, the damping ratio (G"/G') also decreased with inculcation time (**Figure 4.8B**), as the hydrogel transitioned from a predominantly physically crosslinked network to a more chemically crosslinked network. The damping ratio of the fully crosslinked D8-15/Lapo-5 (~0.1 at t = 4 day) is much greater than a purely covalent crosslinked PEG-D8 hydrogel that do not contain nanoparticles (~0.02) [214], and the elevated damping ratio can be attributed to the presence of reversible dopamine-Laponite interactions in the hydrogel. From the stress relaxation experiment, hydrogel incubated for 1 day exhibited rapid stress relaxation (**Figure 4.8C**), indicating that the hydrogel dissipated the strain energy via the disassociation of dopamine-Laponite reversible interactions [105]. Relaxation time increased with incubation time (**Figure 4.8D**), resulting from the formation of permanent chemical crosslinks with the continuous oxidation of dopamine. Both scanning electron microscopy images (**Figure 4.9**) and equilibrium water content values (**Figure 4.10**) confirmed that the crosslinking density of hydrogel increased with incubation time.
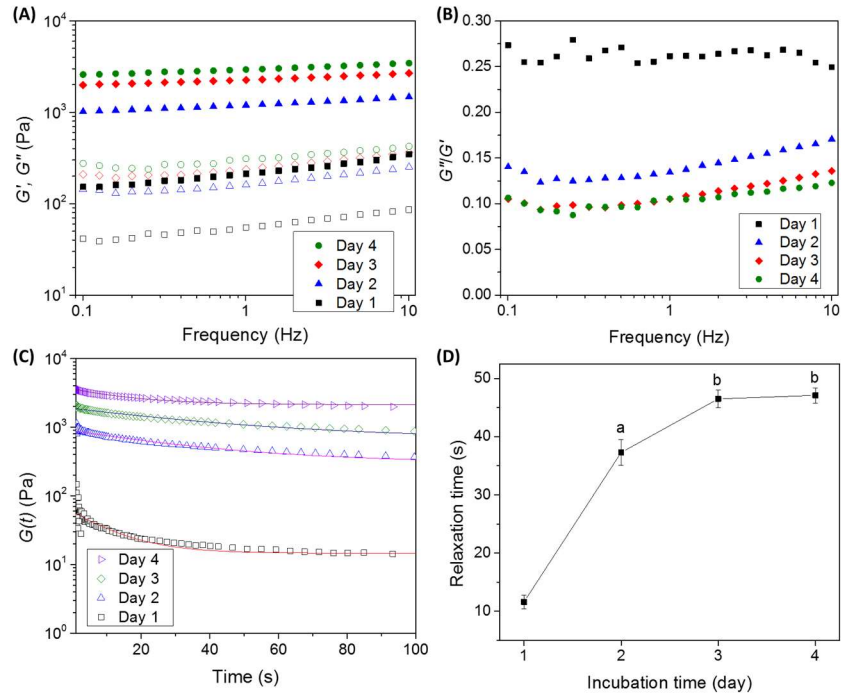
Figure 4.8 Rheological studies of D8-15/Lapo-5 during the crosslinking process of the hydrogel. Frequency dependence of the storage (G', close symbols) and loss (G", open symbols) moduli (A) and damping ratio (G"/G'; B) performed at a strain of 1%. Stress relaxation experiment with fitted relaxation curves (solid lines; C) and the calculated relaxation time (D) for an applied step strain of 10 %. Data were presented as mean ± SD (n = 3). [a] $p <$ 0.05 when compared to day 1. [b] $p < 0.05$ when compared to day 2.
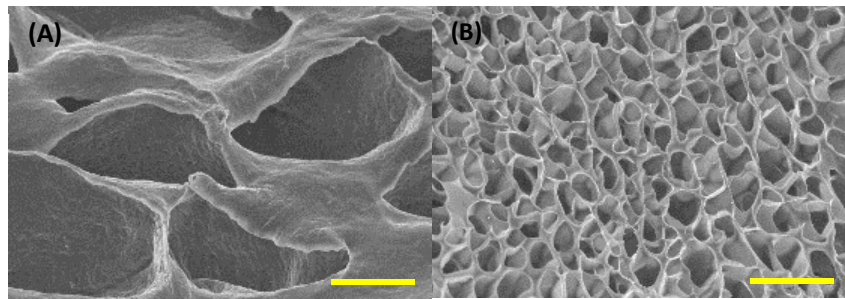

Figure 4.9 SEM images of dried nanocomposite hydrogels consisting of 15wt% PEG-D8 and 5 wt% Laponite (D8-15/Lapo-5) incubated for 1 (average pore size 25 ± 4.0 µm; A) and 4 days (average pore size 4.8 ± 0.72 µm; B). Pore size decreased with time. Scale bar: 10 µm.
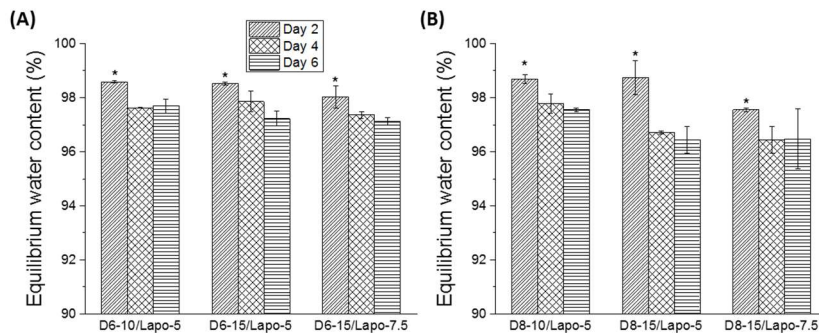
Figure 4.10 Equilibrium water content (EWC) of hydrogels consisting of PEG-D6 (A) and PEG-D8 (B) with different polymer and Laponite concentrations incubated for 2, 4, and 6 days. EWC values decreased with incubation time, which indicated the increased crosslinking density over time. * $p < 0.05$ when compared to results of day 4 and day 6.

The time dependent recovery properties of the hydrogel were assessed after applying a large oscillatory shear strain. Hydrogel incubated for 1 day repeatedly recovered its initial G' value immediately after failure caused by 1000% shear strain (**Figure 4.11A** and **B**). This mechanical reversibility suggested that the hydrogel is loosely chemically crosslinked and able to re-establish its network via strong dopamine-Laponite interactions. In contrast, the hydrogel incubated for 4 days did not fully recover its initial G' value (**Figure 4.11B**), potentially due to irreversible breakage of covalent bonds. The rheological experiments collectively demonstrated that the hydrogel exhibited reduced ability to rearrange its structure with the formation of covalent crosslinks over time.
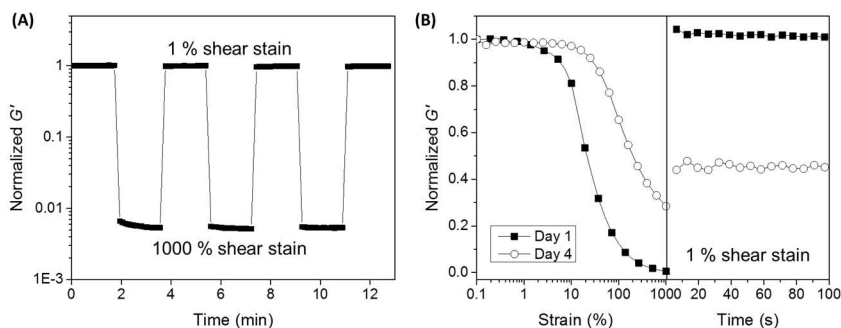
Figure 4.11 Rheological studies of D8-15/Lapo-5 during the crosslinking process of the hydrogel. Normalized *G'* values of D8-15/Lapo-5 (incubated for 1 day) subjected to repeated cycles of 1% and 1000% shear strain with 10 s resting time in between (A). Normalized *G'* values of D8-15/Lapo-5 (incubated for 1 and 4 days) subjected to increasing applied strain (0.1 - 1000% at 1 Hz) followed by a reduced applied strain of 1% at 1 Hz (B).

The adhesive property of the nanocomposite hydrogel was evaluated using burst adhesion testing (**Figure 4.12A**). The pericardium tissue with a central concentric defect was placed over a pipette tip to simulate the application of the hydrogel on a convex surface (**Figure 4.12B** and **C**). D8-15/Lapo-7.5 exhibited the highest burst pressure (320 ± 22 mmHg) among all the formulations tested, which was superior than the reported values for sealing renal vein [215] and intestinal anastomosis [216]. The hydrogel formulated with a reduced concentration of Laponite (D8-15/Lapo-5) or PEG with reduced branching (D6-15/Lapo-5) demonstrated a significantly reduced burst pressure (**Figure 4.12D**). The effect of hydrogel formulation on burst pressure coincided with the corresponding hydrogel bulk property in rheological testing (**Figure 4.13**), which confirmed that an increased bulk materials property contributed to improved adhesive performance [3]. For all the formulations tested, the hydrogels failed cohesively (i.e., at the bulk of the hydrogel), indicating strong interfacial binding between the hydrogel and the pericardium tissue. The adhesive is tightly bound to the

pericardium tissue and resisted the externally applied tension and torsion forces (**Figure 4.14**). However, when the hydrogel was incubated for a longer period of time (30 h) prior to application, it demonstrated a remarkable decrease in the measured burst pressure and the adhesive failed at the interface (**Figure 4.12E**). Tissue adhesion of catechol-containing adhesives involves the formation of interfacial bonds between the oxidized quinone with the reactive functional groups present on the tissue surface (i.e., $-NH_2$ and $-SH$ of lysine and cysteine, respectively; **Figure 4.1I**) [130, 203]. As the incubation time increased, more dopamine-dopamine covalent bonds were formed while reducing the number of available quinone for tissue adhesion, leading to the adhesive failure at the hydrogel-tissue interface.
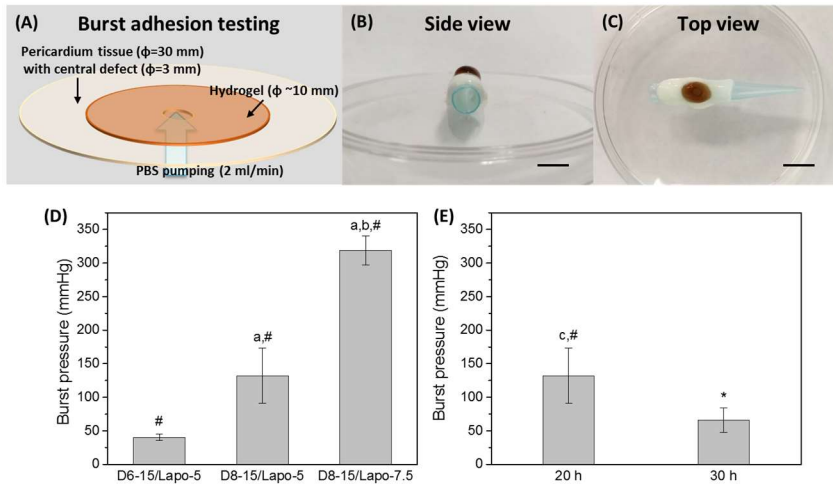

Figure 4.12 (A) Schematic illustration of the burst adhesion testing set up. PBS was pumped against the hydrogel until failure. (B) Side and (C) top view of hydrogel sealing a convex pericardium with a central concentric defect. Scale bar: 10 mm. (D) The effect of hydrogel formulation and (E) incubation time prior to application on the max burst pressure. Data were presented as mean $\pm$ SD (n = 4). [a] $p < 0.05$ when compared to D6-15/Lapo-5. [b] $p < 0.05$ when compared to D8-15/Lapo-5. [c] $p < 0.05$ when compared to 30 h incubation time. [#] Cohesive failure at max burst pressure. * Adhesive failure at max burst pressure.
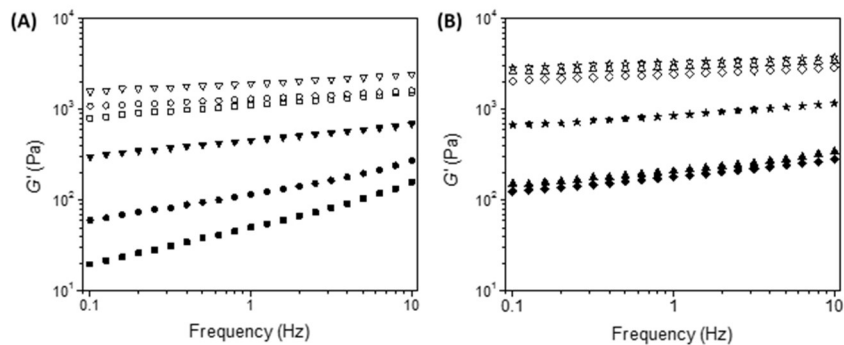
Figure 4.13 Storage modulus (G') of hydrogels consisting of PEG-D6 and PEG-D8 with different polymer and Laponite concentrations performed at a strain of 1 %. (A) G' of D6-10/Lapo-5 (■,□), D6-15/Lapo-5 (●,○), and D6-15/Lapo-7.5 (▼,▽). (B) G' of D8-10/Lapo-5 (◆,◇), D8-15/Lapo-5 (▲,△), and D8-15/Lapo-7.5 (★,☆). The close and open symbols indicated that the samples were tested after 1 and 4 days of incubation time, respectively. Higher concentration of polymer and Laponite in precursor solution and more branched structure of PEG-D8 than PEG-D6 contributed to the elevated level of storage modulus. For all formulations tested, G' values increased with time, indicating increased stiffness due to increased dopamine-dopamine crosslinking.
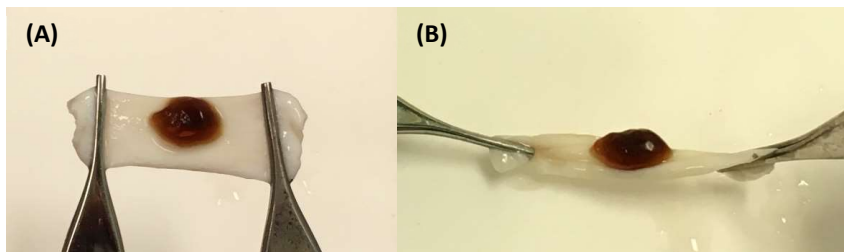
Figure 4.14 Photographs of hydrogel consisting of 15 wt% PEG-D8 and 5wt% Laponite (D8-15/Lapo-5) adhered to pericardium tissue subjected to tension (A), and torsion and tension (B).

We further examined the feasibility of sealing the sutured anastomosis performed on a collagen tubing using the nanocomposite hydrogel (**Figure 4.1H**). D8-15/Lapo-5 incubated for 20 h was applied via a syringe around the contour of the tubing over the suture line and demonstrated no leakage when phosphate buffered saline (PBS)

was pumped through the tubing. For comparison, PEG-D8 was applied via a double-barreled syringe using sodium periodate ($NaIO_4$) to initiate the curing. The liquid adhesive noticeably dripped below the tubing when applied and cannot seal the anastomosis during the pumping of PBS, which confirmed the disadvantage of using a slow curing liquid sealant on a non-flat surface.

Inducing the oxidation of the catechol adhesive moiety is the critical first step for initiating the curing and interfacial crosslinking for catechol-contatining bioadhesives [49, 50, 217, 218]. However, the application of cytotoxic chemical oxidant such as the oft-used $NaIO_4$ may not be desirable for many biomedical applications [219]. Additionally, *in situ* activation using an oxidizing reagent requires mixing of two precursor solutions during application. Ion-induced slow, oxidative crosslinking of catechol have been recently reported to form hydrogels that transitioned from a physically crosslinked network into a predominantly covalently crosslinked network [217, 220]. Our nanocomposite hydrogel exhibited similar transition without the addition of oxidizing reagents. This unique dynamic crosslinking process enabled the stretching, remolding, and adhesion of the hydrogel onto a tissue surface with convex contour. The hydrogel then adapted to a new shape with the formation of intermolecular covalent crosslinks. Additionally, incorporation of Laponite into the highly biocompatible yet bioinert PEG-based material supported human dermal fibroblast attachment (**Figure 4.15**), which is needed for rapid tissue repair and regeneration [214, 221].
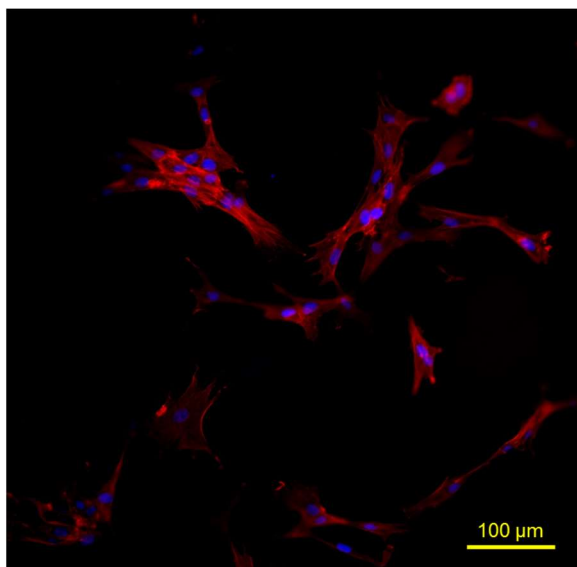
**Figure 4.15** Immunofluorescent staining of human dermal fibroblasts attached to the surface of hydrogel consisting of 15 wt% PEG-D8 and 5wt% Laponite (D8-15/Lapo-5) after 48 h of culture. Blue: cell nuclei stained by DAPI, Red: filamentous actin stained by rhodamine phalloidin.

4.5 Conclusion

In summary, a nanocomposite hydrogel was constructed through the simple combination of PEG-D and Laponite. The hydrogel transitioned from a reversibly cross-linked network formed by dopamine–Laponite interfacial interactions to a more covalently and densely cross-linked network through the gradual autoxidation and cross-linking of catechol moieties. The hydrogel initially exhibited the ability to be remolded and adhered to the convex contour of a tissue surface. With time, the hydrogel became fixed in its new shape and functioned as a fit-to-shape sealant. This novel strategy overcomes existing challenges associated with sealants that are curable *in situ*. Previously described sealants of this type were unable to seal tissue with a non-flat geometry, required a cytotoxic oxidizing reagent, and required a mixing tip for mixing

precursor solutions. The incubation time prior to application of the nanocomposite hydrogel described herein is crucial for optimal adhesion. For clinical applications, there is a need to better control the cross-linking process (i.e., the temperature [222] or oxygen content [223] during incubation), so that the hydrogel can be adapted to different clinical situations.

4.6 Acknowledgement

Chapter 5 Summary and future research

5.1 Enable the recovery of DN hydrogel by incorporating catechol-Laponite interactions

In Chapter 3, Laponite was introduced into DN hydrogel that contained network-bound catechol. This nanocomposite DN hydrogel exhibited enhanced mechanical properties when compared to the control DN that do not contain catechol-Laponite reversible bonds. The reversible bonds were broken under compressive loading, which dissipated fracture energy. When the nanocomposite DN were allowed to recover, catechol-Laponite bonds reformed and the hydrogel recovered over 82% of energy dissipated during successive loading cycles. Conversely, DN do not contained this reversible bonds cannot recover its original mechanical property under identical condition. Additionally, minimal changes to the architecture and stiffness of the nanocomposite DN network after compression were demonstrated in both the equilibrium volume and oscillatory rheological results

5.2 Improve the materials property, adhesive property and bioactivity of injectable mussel-inspired tissue adhesive hydrogel

In Chapter 3, Laponite was incorporated into an injectable adhesive hydrogel that constructed by oxidative catalyst-induced crosslinking of catechol-functionalized 4-arm PEG. The catechol-Laponite interfacial interactions significantly increased the curing rate, bulk mechanical property and adhesive property of the adhesive. Serendipitously, the addition of Laponite was found to serve dual roles-enhance both adhesive performance and bioactivity of nanocomposite hydrogel. Subcutaneous

implantation in rat demonstrated that nanocomposite hydrogels elicited minimal inflammatory response and samples containing Laponite exhibited a significantly higher level of cell infiltration than Laponite-free control, indicating that the addition of Laponite is potentially a simple and effective method to promote bioactivity of a bio-inert, synthetic PEG-based adhesive.

5.3 Construct moldable mussel-inspired hydrogel as fit-to-shape tissue sealant

On the basis of Chapter 3, a hydrogel was prepared by combining higher concentration of Laponite with adhesive polymer, 6- and 8-armed catechol functionalized PEG without introducing any additional oxidative catalyst. The nanocomposite hydrogel was loosely chemical crosslinked and contained large amount of catechol-Laponite interactions. Strikingly, this hydrogel underwent dynamic transition from soft, moldable, recoverable (the stiffness healed immediately after strain-induced failure) to firm, shape-fixed, unrecoverable (the stiffness permanently reduced after strain-induced failure), and eventually a densely chemical crosslinked hydrogel was achieved. This unique transition made this hydrogel a good candidate to seal the contoured surface of biological tissue, providing a potential solution to seal the tissue in various geometry.

5.4 Future research

Efforts have been made to tune the mechanical performance of hydrogel via structurally control inspired by catechol chemistry [105, 106, 224, 225]. We demonstrated the structure-property relation of mussel-inspired materials by

investigating the contribution of catechol-Laponite reversible chemistry to hydrogel mechanics. For the tissue adhesive application specifically, how to exploit the controllability of the hydrogel crosslinking process via tuning the reversible and irreversible catechol interactions for adapting to different clinical situation requires advanced investigation.

Reference

1. Liu, Y., et al., *Biomimetic Adhesives and Coatings Based on Mussel Adhesive Proteins*, in *Biological Adhesives*. 2016, Springer. p. 345-378.
2. Liu, Y. and B.P. Lee, *Recovery property of double-network hydrogel containing a mussel-inspired adhesive moiety and nano-silicate.* Journal of Materials Chemistry B, 2016. **4**(40): p. 6534-6540.
3. Liu, Y., et al., *Injectable Dopamine-Modified Poly(ethylene glycol) Nanocomposite Hydrogel with Enhanced Adhesive Property and Bioactivity.* Acs Applied Materials & Interfaces, 2014. **6**(19): p. 16982-16992.
4. Liu, Y., et al., *A Moldable Nanocomposite Hydrogel Composed of a Mussel-Inspired Polymer and a Nanosilicate as a Fit-to-Shape Tissue Sealant.* Angewandte Chemie International Edition, 2017: p. n/a-n/a.
5. Waite, J.H., *Mussel beards : A coming of Age.* Chemistry and Industry, 1991. **2 September**: p. 607-611.
6. Warner, S.C. and J.H. Waite, *Expression of multiple forms of an adhesive plaque protein in an individual mussel, Mytilus edulis.* Marine Biology, 1999. **134**(4): p. 729-734.
7. Rzepecki, L.M., K.M. Hansen, and J.H. Waite, *Characterization of a cystine-rich polyphenolic protein family from the blue mussel Mytilus edulis.* Biol Bull, 1992. **183**(1): p. 123-37.
8. Zhao, H. and J.H. Waite, *Linking adhesive and structural proteins in the attachment plaque of Mytilus californianus.* Journal of Biological Chemistry, 2006. **281**(36): p. 26150-26158.
9. Waite, J.H., et al., *Mussell Adhesion: Finding the Tricks Worth Mimicking.* Journal of Adhesion, 2005. **81**: p. 1-21.
10. Waite, J.H. and X. Qin, *Polyphosphoprotein from the Adhesive Pads of Mytilus edulis.* Biochemistry, 2001. **40**(9): p. 2887-93.
11. Papov, V.V., et al., *Hydroxyarginine-containing polyphenolic proteins in the adhesive plaques of the marine mussel Mytilus edulis.* J Biol Chem, 1995. **270**(34): p. 20183-92.
12. Long, J.R., et al., *A peptide that inhibits hydroxyapatite growth is in an extended conformation on the crystal surface.* Proceedings of the National Academy of Sciences of the United States of America, 1998. **95**(21): p. 12083-12087.
13. Meisel, H. and C. Olieman, *Estimation of calcium-binding constants of casein phosphopeptides by capillary zone electrophoresis.* Anal. Chim. Acta, 1998. **372**(1-2): p. 291-297.
14. Baty, A.M., et al., *Adsorption of Adhesive Proteins from the Marine Mussel, Mytilus edulis, on Polymer Films in the Hydrated State Using Angle Dependent X-ray Photoelectron Spectroscopy and Atomic Force Microscopy.* Langmuir, 1997. **13**(21): p. 5702-5710.
15. Deacon, M.P., et al., *Structure and Mucoadhesion of Mussel Glue Protein in Dilute Solution.* Biochemistry, 1998. **37**(40): p. 14108-14112.

16.   Huang, K., et al., *Synthesis and Characterization of Self-Assembling Block Copolymers Containing Bioadhesive End Groups.* Biomacromolecules, 2002. **3**(2): p. 397-406.

17.   Schnurrer, J. and C.-M. Lehr, *Mucoadhesive properties of the mussel adhesive protein.* International Journal of Pharmaceutics, 1996. **141**(1,2): p. 251-256.

18.   Chirdon, W.M., W.J. O'Brien, and R.E. Robertson, *Adsorption of catechol and comparative solutes on hydroxyapatite.* Journal of Biomedical Materials Research, Part B: Applied Biomaterials, 2003. **66B**(2): p. 532-538.

19.   Waite, J.H., *Nature's underwater adhesive specialist.* International Journal of Adhesion and Adhesives, 1987. **7**(1): p. 9-14.

20.   Martin, S.T., et al., *Surface Structures of 4-chlorocatechol adsorbed on titanium dioxide.* Environ. Sci. Technol., 1996. **30**: p. 8.

21.   Rodriguez, R., M.A. Blesa, and A.E. Regazzoni, *Surface Complexation at the TiO2 (anatase) /Aqueous Solution Interface: Chemisorption of Catechol.* J. Colloid Interface Sci., 1996. **177**.

22.   Sever, M.J. and J.J. Wilker, *Visible absorption spectra of metal-catecholate and metal-tironate complexes.* Dalton Trans, 2004(7): p. 1061-72.

23.   Taylor, S.W., et al., *Ferric Ion Complexes of a DOPA-Containing Adhesive Protein from Mytilus edulis.* Inorg. Chem., 1996. **35**: p. 6.

24.   Holten-Andersen, N., et al., *Metals and the integrity of a biological coating: the cuticle of mussel byssus.* Langmuir, 2009. **25**(6): p. 3323-6.

25.   Sun, C. and J.H. Waite, *Mapping chemical gradients within and along a fibrous structural tissue, mussel byssal threads.* J Biol Chem, 2005. **280**(47): p. 39332-6.

26.   Pizer, R. and L. Babcock, *Mechanism of Complexation of Boron Acids with Catechol and Substituted Catechols.* Inorganic Chemistry, 1977. **16**(7): p. 1677-1681.

27.   Fang, H., G. Kaur, and B.H. Wang, *Progress in boronic acid-based fluorescent glucose sensors.* Journal of Fluorescence, 2004. **14**(5): p. 481-489.

28.   Lee, H., B.P. Lee, and P.B. Messersmith, *A reversible wet/dry adhesive inspired by mussels and geckos.* Nature, 2007. **448**(7151): p. 338-341.

29.   Kummert, R. and W. Stumm, *The surface complexation of organic acids on hydrous g-alumina.* Journal of Colloid and Interface Science, 1980. **75**(2): p. 373-85.

30.   Soriaga, M.P. and A.T. Hubbard, *Determination of the orientation of aromatic molecules adsorbed on platinum electrodes. The effect of solute concentration.* Journal of American Chemical Society, 1982. **104**(14): p. 3937-45.

31.   Hansen, D.C., S.C. Dexter, and J.H. Waite, *The inhibition of corrosion of S30403 stainless steel by a naturally occurring catecholic polymer.* Corrosion Science, 1995. **37**(9): p. 1423-41.

32.   Lee, B.P., et al., *Rapid Photocurable of Amphiphilic Block Copolymers Hydrogels with High DOPA Contents.* Maclomolecules, 2006. **39**: p. 1740-48.

33. Araujo, P.Z., P.J. Morando, and M.A. Blesa, *Interaction of catechol and gallic acid with titanium dioxide in aqueous suspensions. 1. Equilibrium studies.* Langmuir, 2005. **21**(8): p. 3470-4.

34. Creutz, C. and M.H. Chou, *Binding of catechols to mononuclear titanium(IV) and to 1- and 5-nm TiO2 nanoparticles.* Inorg Chem, 2008. **47**(9): p. 3509-14.

35. Dalsin, J.L., et al., *Mussel Adhesive Protein Mimetic Polymers for the Preparation of Nonfouling Surfaces.* J Am Chem Soc, 2003. **125**: p. 6.

36. Kawabata, T., et al., *Iron coordination by catechol derivative antioxidants.* Biochem Pharmacol, 1996. **51**(11): p. 1569-77.

37. Anderson, T.H., et al., *The Contribution of DOPA to Substrate-Peptide Adhesion and Internal Cohesion of Mussel-Inspired Synthetic Peptide Films.* Adv Funct Mater, 2010. **20**(23): p. 4196-4205.

38. Wei, Y.F., et al., *Polydopamine-assisted decoration of ZnO nanorods with Ag nanoparticles: an improved photoelectrochemical anode.* Journal of Materials Chemistry A, 2013. **1**(16): p. 5045-5052.

39. Amstad, E., et al., *Ultrastable iron oxide nanoparticle colloidal suspensions using dispersants with catechol-derived anchor groups.* Nano Lett, 2009. **9**(12): p. 4042-8.

40. Dalsin, J.L., et al., *Protein Resistance of Titanium Oxide Surfaces Modified by Biologically Inspired mPEG-DOPA.* Langmuir, 2005. **21**(2): p. 640-646.

41. Lee, H., N.F. Scherer, and P.B. Messersmith, *Single-molecule mechanics of mussel adhesion.* Proceedings of the National Academy of Sciences, 2006. **103**(35): p. 12999-13003.

42. Yamamoto, H. and H. Tatehata, *Oxidation of synthetic precursors of adhesive proteins from mytilid bivalves using tyrosinase.* J. Mar. Biotechnol., 1995. **2**(2): p. 95-100.

43. Lee, B.P., J.L. Dalsin, and P.B. Messersmith, *Enzymatic and Non-enzymatic Pathways to Formation of DOPA-Modifled PEG Hydrogels.* Polymer Preprint, 2001. **42**: p. 151-152.

44. Burzio, L.A. and J.H. Waite, *Cross-linking in adhesive quinoproteins: studies with model decapeptides.* Biochemistry, 2000. **39**(36): p. 11147-53.

45. Herlinger, E., R.F. Jameson, and W. Linert, *Spontaneous Autoxidation of Dopamine.* Journal of the Chemical Society-Perkin Transactions 2, 1995(2): p. 259-263.

46. Yu, M., J. Hwang, and T.J. Deming, *Role of L-3, 4-dihydroxyphenylalanine in mussel adhesive proteins.* Journal of the American Chemical Society, 1999. **121**(24): p. 5825-5826.

47. Brodie, M., et al., *Biomechanical properties of Achilles tendon repair augmented with a bioadhesive-coated scaffold.* Biomedical Materials, 2011. **6**(1): p. 015014.

48. Burke, S.A., et al., *Thermal gelation and tissue adhesion of biomimetic hydrogels.* Biomedical Materials, 2007. **2**(4): p. 203.

49. Lee, B.P., J.L. Dalsin, and P.B. Messersmith, *Synthesis and gelation of DOPA-modified poly (ethylene glycol) hydrogels.* Biomacromolecules, 2002. **3**(5): p. 1038-1047.

50.   Cencer, M.M., et al., *Effect of pH on the rate of curing and bioadhesive properties of dopamine functionalized poly(ethylene glycol) hydrogels.* Biomacromolecules, 2014. **15**(8): p. 2861–2869.

51.   Li, J. and B.M. Christensen, *Effect of pH on the oxidation pathway of dopamine and dopa.* Journal of Electroanalytical Chemistry, 1994. **375**(1–2): p. 219-231.

52.   Ohman, H. and A. Vahlquist, *In vivo studies concerning a pH gradient in human stratum corneum and upper epidermis.* Acta Dermato-Venereologica, 1994. **74**(5): p. 375-379.

53.   Soller, B.R., et al., *Feasibility of non-invasive measurement of tissue pH using near-infrared reflectance spectroscopy.* Journal of Clinical Monitoring, 1996. **12**(5): p. 387-395.

54.   Soller, B.R., et al., *Investigation of muscle pH as an indicator of liver pH and injury from hemorrhagic shock.* Journal of Surgical Research, 2003. **114**(2): p. 195-201.

55.   Kuang, J., J.L. Guo, and P.B. Messersmith, *High ionic strength formation of DOPA-melanin coating for loading and release of cationic antimicrobial compounds.* Adv Mater Interfaces, 2014. **1**(6).

56.   Deming, T.J., *Facile synthesis of block copolypeptides of defined architecture.* Nature, 1997. **390**(6658): p. 386-9.

57.   Yu, M. and T.J. Deming, *Synthetic polypeptide mimics of marine adhesives.* Macromolecules, 1998. **31**(15): p. 4739-45.

58.   Westwood, G., T.N. Horton, and J.J. Wilker, *Simplified polymer mimics of cross-linking adhesive proteins.* Macromolecules, 2007. **40**(11): p. 3960-3964.

59.   Matos-Pérez, C.R., J.D. White, and J.J. Wilker, *Polymer composition and substrate influences on the adhesive bonding of a biomimetic, cross-linking polymer.* Journal of the American Chemical Society, 2012. **134**(22): p. 9498-9505.

60.   Meredith, H.J., C.L. Jenkins, and J.J. Wilker, *Enhancing the Adhesion of a Biomimetic Polymer Yields Performance Rivaling Commercial Glues.* Advanced Functional Materials, 2014. **24**(21): p. 3259-3267.

61.   White, J.D. and J.J. Wilker, *Underwater bonding with charged polymer mimics of marine mussel adhesive proteins.* Macromolecules, 2011. **44**(13): p. 5085-5088.

62.   Lee, K., et al., *Stabilized calcium phosphate nano-aggregates using a dopa-chitosan conjugate for gene delivery.* International Journal of Pharmaceutics, 2013. **445**(1-2): p. 196-202.

63.   You, I., et al., *Enhancement of Blood Compatibility of Poly(urethane) Substrates by Mussel-Inspired Adhesive Heparin Coating.* Bioconjugate Chemistry, 2011. **22**(7): p. 1264-1269.

64.   Matos-Perez, C.R. and J.J. Wilker, *Ambivalent Adhesives: Combining Biomimetic Cross-Linking with Antiadhesive Oligo(ethylene glycol).* Macromolecules, 2012. **45**(16): p. 6634-6639.

65. Zhang, Y.C., et al., *pH- and Voltage-Responsive Chitosan Hydrogel through Covalent Cross-Linking with Catechol.* Journal of Physical Chemistry B, 2012. **116**(5): p. 1579-1585.

66. Skelton, S., et al., *Biomimetic adhesive containing nanocomposite hydrogel with enhanced materials properties.* Soft Matter, 2013. **9**(14): p. 3825-3833.

67. Ryu, J.H., et al., *Catechol-Functionalized Chitosan/Pluronic Hydrogels for Tissue Adhesives and Hemostatic Materials.* Biomacromolecules, 2011. **12**(7): p. 2653-2659.

68. Lee, Y., et al., *Thermo-sensitive, injectable, and tissue adhesive sol-gel transition hyaluronic acid/pluronic composite hydrogels prepared from bio-inspired catechol-thiol reaction.* Soft Matter, 2010. **6**(5): p. 977-983.

69. Ding, X.C., et al., *Nitro-Group Functionalization of Dopamine and its Contribution to the Viscoelastic Properties of Catechol-Containing Nanocomposite Hydrogels.* Macromolecular Chemistry and Physics, 2015. **216**(10): p. 1109-1119.

70. Hong, S.H., et al., *STAPLE: stable alginate gel prepared by linkage exchange from ionic to covalent bonds.* Advanced healthcare materials, 2016. **5**(1): p. 75-79.

71. Lee, C., et al., *Bioinspired, Calcium-Free Alginate Hydrogels with Tunable Physical and Mechanical Properties and Improved Biocompatibility.* Biomacromolecules, 2013. **14**(6): p. 2004-2013.

72. Kastrup, C.J., et al., *Painting blood vessels and atherosclerotic plaques with an adhesive drug depot.* Proceedings of the National Academy of Sciences, 2012. **109**(52): p. 21444-21449.

73. Kim, E., et al., *Biomimetic Approach to Confer Redox Activity to Thin Chitosan Films.* Advanced Functional Materials, 2010. **20**(16): p. 2683-2694.

74. Kim, K., et al., *Bio-inspired catechol conjugation converts water-insoluble chitosan into a highly water-soluble, adhesive chitosan derivative for hydrogels and LbL assembly.* Biomaterials Science, 2013. **1**(7): p. 783-790.

75. Shazly, T.M., et al., *Augmentation of postswelling surgical sealant potential of adhesive hydrogels.* Journal of Biomedical Materials Research Part A, 2010. **95A**(4): p. 1159-1169.

76. Park, J.Y., et al., *Cell-repellant Dextran Coatings of Porous Titania Using Mussel Adhesion Chemistry.* Macromolecular Bioscience, 2013. **13**(11): p. 1511-1519.

77. Choi, Y.C., et al., *Human gelatin tissue-adhesive hydrogels prepared by enzyme-mediated biosynthesis of DOPA and Fe3+ ion crosslinking.* Journal of Materials Chemistry B, 2014. **2**(2): p. 201-209.

78. Yang, X., et al., *Mussel-inspired human gelatin nanocoating for creating biologically adhesive surfaces.* International Journal of Nanomedicine, 2014. **9**: p. 2753-2765.

79. Neto, A.I., et al., *Nanostructured Polymeric Coatings Based on Chitosan and Dopamine-Modified Hyaluronic Acid for Biomedical Applications.* Small, 2014. **10**(12): p. 2459-2469.

80. Hong, S., et al., *Hyaluronic Acid Catechol: A Biopolymer Exhibiting a pH‐Dependent Adhesive or Cohesive Property for Human Neural Stem Cell Engineering.* Advanced Functional Materials, 2013. **23**(14): p. 1774-1780.

81. Bilic, G., et al., *Injectable candidate sealants for fetal membrane repair: bonding and toxicity in vitro.* American Journal of Obstetrics and Gynecology, 2010. **202**: p. 85.e1-9.

82. Harris, J.M., et al., *New polyethylene glycols for biomedical applications*, in *Water-Soluble Polymer*. 1991. p. 418-429.

83. Catron, N.D., H. Lee, and P.B. Messersmith, *Enhancement of poly (ethylene glycol) mucoadsorption by biomimetic end group functionalization.* Biointerphases, 2006. **1**(4): p. 134-141.

84. Haller, C.M., et al., *Mussel-mimetic tissue adhesive for fetal membrane repair: an ex vivo evaluation.* Acta biomaterialia, 2012. **8**(12): p. 4365-70.

85. Dalsin, J.L., et al., *Multi-armed Catechol Compound Blends*. 2012: US.

86. Messersmith, P.B., et al., *DOPA-Functionalized, Branched, Poly(aklylene oxide) Adhesives*. 2014: US.

87. Lee, B.P., J.L. Murphy, and S. Silvary, *Multibranched Bioadhesive Compounds and Synthetic Methods Therefor*. 2010.

88. Lee, B.P., et al., *Bioadhesive Construct*. 2010: US20100137902.

89. Lee, B.P., et al., *Bioadhesive Construct sith Polymer Blends*. 2012: US20120003888.

90. Murphy, J.L., et al., *Adhesive performance of biomimetic adhesive-coated biologic scaffolds.* Biomacromolecules, 2010. **11**(11): p. 2976-2984.

91. Lee, B.P., et al., *Synthesis of 3,4-Dihydroxyphenylalanine (DOPA) Containing Monomers and Their Copolymerization with PEG-Diacrylate to Form Hydrogels.* Journal of Biomaterials Science, Polymer Edition, 2004. **15**(4): p. 449-64.

92. Anderson, J., et al., *Wireless magnetoelastic sensors for tracking degradation profiles of nitrodopamine-modified poly(ethylene glycol).* ScienceJet, 2015. **4**: p. 80.

93. Liu, Y., et al. *Marine adhesive containing nanocomposite hydrogel with enhanced materials and bioadhesive properties*. in *MRS Proceedings*. 2013. Cambridge Univ Press.

94. Gracias, D.H., *Stimuli responsive self-folding using thin polymer films.* Current Opinion in Chemical Engineering, 2013. **2**(1): p. 112-119.

95. Lim, H.L., et al., *Smart hydrogels as functional biomimetic systems.* Biomaterials Science, 2014. **2**(5): p. 603-618.

96. Ionov, L., *Biomimetic Hydrogel-Based Actuating Systems.* Advanced Functional Materials, 2013. **23**(36): p. 4555-4570.

97. Lee, B.P. and S. Konst, *Novel hydrogel actuator inspired by reversible mussel adhesive protein chemistry.* Advanced Materials, 2014. **26**(21): p. 3415-3419.

98. Lee, B.P., et al., *Modulating the Movement of Hydrogel Actuator based on Catechol-Iron Ion Coordination Chemistry.* Sensors and Actuators B: Chemical, 2015. **206**: p. 456–462.

99. Lee, B.P., Y. Liu, and S. Konst, *Novel Hydrogel Actuator Based on Biomimetic Chemistry.* MRS Proceedings, 2014. **1710**: p. mrss14-1710-XX08-01.

100. Lee, B.P., A. Narkar, and R. Wilharm, *Effect of metal ion type on the movement of hydrogel actuator based on catechol-metal ion coordination chemistry.* Sensors and Actuators B: Chemical, 2016. **227**: p. 248-254.

101. Holten-Andersen, N., et al., *Metal-coordination: using one of nature's tricks to control soft material mechanics.* Journal of Materials Chemistry B, 2014. **2**(17): p. 2467-2472.

102. Krogsgaard, M., M.R. Hansen, and H. Birkedal, *Metals & polymers in the mix: fine-tuning the mechanical properties & color of self-healing mussel-inspired hydrogels.* Journal of Materials Chemistry B, 2014. **2**(47): p. 8292-8297.

103. Wang, W.N., et al., *Zinc induced polyelectrolyte coacervate bioadhesive and its transition to a self-healing hydrogel.* Rsc Advances, 2015. **5**(82): p. 66871-66878.

104. Holten-Andersen, N., et al., *pH-induced metal-ligand cross-links inspired by mussel yield self-healing polymer networks with near-covalent elastic moduli.* Proceedings of the National Academy of Sciences of the United States of America, 2011. **108**(7): p. 2651-2655.

105. Li, Q., et al., *Controlling Hydrogel Mechanics via Bio-Inspired Polymer–Nanoparticle Bond Dynamics.* ACS nano, 2016. **10**(1): p. 1317-1324.

106. Grindy, S.C., et al., *Control of hierarchical polymer mechanics with bioinspired metal-coordination dynamics.* Nature Materials, 2015. **14**(12): p. 1210-1216.

107. He, L.H., et al., *pH responsive self-healing hydrogels formed by boronate-catechol complexation.* Chemical Communications, 2011. **47**(26): p. 7497-7499.

108. Zhang, M., et al., *Preparation and characterization of a novel magnetic biochar for arsenic removal.* Bioresource Technology, 2013. **130**: p. 457-462.

109. Ahn, B.K., et al., *Surface-initiated self-healing of polymers in aqueous media.* Nature Materials, 2014. **13**(9): p. 867-872.

110. Drury, J.L. and D.J. Mooney, *Hydrogels for tissue engineering: scaffold design variables and applications.* Biomaterials, 2003. **24**(24): p. 4337-4351.

111. Lee, K.Y. and D.J. Mooney, *Hydrogels for tissue engineering.* Chemical Reviews, 2001. **101**(7): p. 1869-1879.

112. Liu, W.G., et al., *Collagen-phosphorylcholine interpenetrating network hydrogels as corneal substitutes.* Biomaterials, 2009. **30**(8): p. 1551-1559.

113. Torres-Rendon, J.G., et al., *Bioactive Gyroid Scaffolds Formed by Sacrificial Templating of Nanocellulose and Nanochitin Hydrogels as Instructive Platforms for Biomimetic Tissue Engineering.* Advanced Materials, 2015. **27**(19): p. 2989-2995.

114. Liu, X.J., et al., *Highly stretchable and tough pH-sensitive hydrogels with reversible swelling and recoverable deformation.* Rsc Advances, 2016. **6**(6): p. 4850-4857.

115. Hong, S.M., et al., *3D Printing of Highly Stretchable and Tough Hydrogels into Complex, Cellularized Structures.* Advanced Materials, 2015. **27**(27): p. 4035-4040.

116. Zhai, D.Y., et al., *Highly Sensitive Glucose Sensor Based on Pt Nanoparticle/Polyaniline Hydrogel Heterostructures.* Acs Nano, 2013. **7**(4): p. 3540-3546.

117. Zheng, W.J., et al., *Tough Al-alginate/Poly(N-isopropylacrylamide) Hydrogel with Tunable LCST for Soft Robotics.* Acs Applied Materials & Interfaces, 2015. **7**(3): p. 1758-1764.

118. Bodugoz-Senturk, H., et al., *Poly(vinyl alcohol)-acrylamide hydrogels as load-bearing cartilage substitute.* Biomaterials, 2009. **30**(4): p. 589-596.

119. Stella, J.A., et al., *On the biomechanical function of scaffolds for engineering load-bearing soft tissues.* Acta Biomaterialia, 2010. **6**(7): p. 2365-2381.

120. Gong, J.P., et al., *Double-network hydrogels with extremely high mechanical strength.* Advanced Materials, 2003. **15**(14): p. 1155-1158.

121. Tanaka, Y., et al., *Determination of fracture energy of high strength double network hydrogels.* The Journal of Physical Chemistry B, 2005. **109**(23): p. 11559-11562.

122. Hagiwara, Y., et al., *Ligament-like tough double-network hydrogel based on bacterial cellulose.* Cellulose, 2010. **17**: p. 93-101.

123. Na, Y.H., et al., *Necking phenomenon of double-network gels.* Macromolecules, 2006. **39**(14): p. 4641-4645.

124. Sun, J.-Y., et al., *Highly stretchable and tough hydrogels.* Nature, 2012. **489**(7414): p. 133-136.

125. Chen, Q., et al., *A Robust, One‑Pot Synthesis of Highly Mechanical and Recoverable Double Network Hydrogels Using Thermoreversible Sol‑Gel Polysaccharide.* Advanced Materials, 2013. **25**(30): p. 4171-4176.

126. Bakarich, S.E., et al., *Recovery from applied strain in interpenetrating polymer network hydrogels with ionic and covalent cross-links.* Soft Matter, 2012. **8**(39): p. 9985-9988.

127. Stevens, L., et al., *Ionic-covalent entanglement hydrogels from gellan gum, carrageenan and an epoxy-amine.* Soft Matter, 2013. **9**(11): p. 3009-3012.

128. Harrass, K., et al., *Mechanically strong hydrogels with reversible behaviour under cyclic compression with MPa loading.* Soft Matter, 2013. **9**(10): p. 2869-2877.

129. Yamamoto, H., *Marine adhesive proteins and some biotechnological applications.* Biotechnology and Genetic Engineering Reviews, Vol 13, 1996. **13**: p. 133-165.

130. Lee, B.P., et al., *Mussel-inspired adhesives and coatings.* Annual review of materials research, 2011. **41**: p. 99.

131. Hou, S. and P.X. Ma, *Stimuli-Responsive Supramolecular Hydrogels with High Extensibility and Fast Self-Healing via Precoordinated Mussel-Inspired Chemistry.* Chemistry of Materials, 2015. **27**(22): p. 7627-7635.

132. Myung, D., et al., *Biomimetic strain hardening in interpenetrating polymer network hydrogels.* Polymer, 2007. **48**(18): p. 5376-5387.

133. Bicerano, J., *Prediction of polymer properties*. 2002: CRC Press.

134. Cummins, H.Z., *Liquid, glass, gel: The phases of colloidal Laponite.* Journal of Non-Crystalline Solids, 2007. **353**(41-43): p. 3891-3905.

135. Yu, J., et al., *Adhesion of Mussel Foot Protein-3 to TiO2 Surfaces: the Effect of pH.* Biomacromolecules, 2013. **14**(4): p. 1072-1077.

136. Li, P., et al., *Swelling behavior of polyacrylamide/laponite clay nanocomposite hydrogels: pH-sensitive property.* Composites Part B-Engineering, 2009. **40**(4): p. 275-283.

137. Li, P., et al., *Novel PAAm/Laponite clay nanocomposite hydrogels with improved cationic dye adsorption behavior.* Composites Part B-Engineering, 2008. **39**(5): p. 756-763.

138. Waiter, J.H., *Reverse engineering of bioadhesion in marine mussels.* Annals of the New York Academy of Sciences, 1999. **875**(1): p. 301-309.

139. Brown, H.R., *A model of the fracture of double network gels.* Macromolecules, 2007. **40**(10): p. 3815-3818.

140. Xin, H., et al., *Effect of First network topology on the toughness of double network hydrogels.* Macromolecules, 2013. **46**(16): p. 6613-6620.

141. Gong, J.P., *Why are double network hydrogels so tough?* Soft Matter, 2010. **6**(12): p. 2583-2590.

142. Pettignano, A., et al., *Self-healing alginate–gelatin biohydrogels based on dynamic covalent chemistry: elucidation of key parameters.* Materials Chemistry Frontiers, 2017.

143. Mukherjee, S., M.R. Hill, and B.S. Sumerlin, *Self-healing hydrogels containing reversible oxime crosslinks.* Soft matter, 2015. **11**(30): p. 6152-6161.

144. Webber, R.E., et al., *Large strain hysteresis and mullins effect of tough double-network hydrogels.* Macromolecules, 2007. **40**(8): p. 2919-2927.

145. Mian, S.A., et al., *Density Functional Theory Study of Catechol Adhesion on Silica Surfaces.* Journal of Physical Chemistry C, 2010. **114**(48): p. 20793-20800.

146. Berg, J.M., J.L. Tymoczko, and L. Stryer, *Biochemistry, Fifth Edition*. 2002: W.H. Freeman.

147. Ikada, Y., *Tissue adhesives*, in *Wound Closure Biomaterials and Devices*, C.C. Chu, J.A. von Fraunhofer, and H.P. Greisler, Editors. 1997, CRC Press, Inc.: Boca Raton, Florida. p. 317-346.

148. Mehdizadeh, M. and J. Yang, *Design Strategies and Applications of Tissue Bioadhesives.* Macromolecular Bioscience, 2013. **13**(3): p. 271-288.

149. Spotnitz, W.D., *History of tissue adhesive*, in *Surgical Adhesives and Sealants: Current Technology and Applications*, D.H. Sierra and R. Saltz, Editors. 1996, Technomic Publishing Co. Inc.: Lancaster, Pennsylvania. p. 3-11.

150. Eriksen, J.R., et al., *Laparoscopic intraperitoneal mesh fixation with fibrin sealant (Tisseel) vs. titanium tacks: a randomised controlled experimental study in pigs.* Hernia, 2008. **12**: p. 483-491.

151. Olivier ten Hallers, E.J., Jansen, J.A., Marres, H.A.M., Rakhorst, G., Verkerke, G.J., *Histological assessment of titanium and polypropylene fiber mesh implantation with and without fibrin tissue glue.* Journal of Biomedical Materials Research Part A, 2006: p. 372-380.

152. Saltz, R., et al., *Experimental and clinical applications of fibrin glue.* Plast Reconstr Surg, 1991. **88**(6): p. 1005-15; discussion 1016-7.

153. Refojo, M.F., C.H. Dohlman, and J. Koliopoulos, *Adhesives in ophthalmology: a review.* Surv. Ophthamol., 1971. **15**(4): p. 217-36.

154. Fortelny, R.H., et al., *Cyanoacrylate tissue sealant impairs tissue integration of macroporous mesh in experimental hernia repair* Surgical Endoscopy, 2007. **21**(10): p. 1781-1785.

155. Blackburn, S.L. and M.D. Smyth, *Hydrogel-induced cervicomedullary compression after posterior fossa decompression for Chiari malformation - Case report.* Journal of Neurosurgery, 2007. **106**(4): p. 302-304.

156. Mulder, M., J. Crosier, and R. Dunn, *Cauda Equina Compression by Hydrogel Dural Sealant After a Laminotomy and Discectomy Case Report.* Spine, 2009. **34**(4): p. E144-E148.

157. West, J.L. and J.A. Hubbell, *Separation of the arterial wall from blood contact using hydrogel barriers reduces intimal thickening after balloon injury in the rat: The roles of medial and luminal factors in arterial healing.* Proceedings of the National Academy of Sciences, 1996. **93**(23): p. 13188-13193.

158. Waite, J.H., *Adhesion a la moule.* Integrative and Comparative Biology, 2002. **42**(6): p. 1172-1180.

159. Rzepecki, L.M., K.M. Hansen, and J.H. Waite, *Bioadhesives: dopa and phenolic proteins as component of organic composite materials*, in *Principles of Cell Adhesion*. 1995, CRC Press. p. 107-142.

160. Sugumaran, M., *Unified mechanism for sclerotization of insect cuticles.* Advances in Insect Physiology, 1998. **27**: p. 230-334.

161. Guvendiren, M., et al., *Adhesion of DOPA-functionalized model membranes to hard and soft surfaces.* Journal of Adhesion, 2009. **86**: p. 631-645.

162. Mehdizadeh, M., et al., *Injectable citrate-based mussel-inspired tissue bioadhesives with high wet strength for sutureless wound closure.* Biomaterials, 2012. **33**(32): p. 7972-83.

163. Brubaker, C.E., et al., *Biological performance of mussel-inspired adhesive in extrahepatic islet transplantation.* Biomaterials, 2010. **31**(3): p. 420-427.

164. Hoppe, A., N.S. Güldal, and A.R. Boccaccini, *A review of the biological response to ionic dissolution products from bioactive glasses and glass-ceramics.* Biomaterials, 2011. **32**(11): p. 2757-2774.

165. Hench, L.L., *Genetic design of bioactive glass.* Journal of the European Ceramic Society, 2009. **29**(7): p. 1257-1265.

166. Hench, L.L. and H.A. Paschall, *Direct chemical bond of bioactive glass-ceramic materials to bone and muscle.* Journal of Biomedical Materials Research, 1973. **7**(3): p. 25-42.

167. Thompson, D.W. and J.T. Butterworth, *The nature of laponite and its aqueous dispersions.* Journal of Colloid and Interface Science, 1992. **151**(1): p. 236-243.

168. Carlisle, E.M., *Silicon: A Possible Factor in Bone Calcification.* Science, 1970. **167**(3916): p. 279-280.

169. Reffitt, D.M., et al., *Orthosilicic acid stimulates collagen type 1 synthesis and osteoblastic differentiation in human osteoblast-like cells in vitro.* Bone, 2003. **32**(2): p. 127-135.

170. Zreiqat, H., et al., *Mechanisms of magnesium-stimulated adhesion of osteoblastic cells to commonly used orthopaedic implants.* Journal of Biomedical Materials Research, 2002. **62**(2): p. 175-184.

171. Gaharwar, A.K., et al., *Assessment of using Laponite® cross-linked poly(ethylene oxide) for controlled cell adhesion and mineralization.* Acta biomaterialia, 2011. **7**(2): p. 568-577.

172. Gaharwar, A.K., et al., *Transparent, elastomeric and tough hydrogels from poly(ethylene glycol) and silicate nanoparticles.* Acta biomaterialia, 2011. **7**(12): p. 4139-48.

173. ASTM F2255-05 (2010), S.T.M.f.S.P.o.T.A.i.L.-S.b.T.L., " ASTM International, West Conshohocken, PA, 2010, DOI: 10.1520/F2255-05R10, www.astm.org.

174. *ISO 10993-5: Biological evaluation of medical devices*, in *Part 5: Tests for cytotoxicity: in vitro methods*. 2012, International Organization for Standardization.

175. Huebsch, N., M. Gilbert, and K.E. Healy, *Analysis of sterilization protocols for peptide-modified hydrogels.* Journal of Biomedical Materials Research Part B: Applied Biomaterials, 2005. **74B**(1): p. 440-447.

176. Kerby, R.E., et al., *Evaluation of tertiary amine co-initiators using differential scanning photocalorimetry.* Journal of Macromolecular Science, Pure and Applied Chemistry, 1999. **A36**(9): p. 1227-1239.

177. Rujitanaroj, P.O., et al., *Controlling fibrous capsule formation through long-term down-regulation of collagen type I (COL1A1) expression by nanofiber-mediated siRNA gene silencing.* Acta Biomaterialia, 2013. **9**(1): p. 4513-4524.

178. Knop, K., et al., *Poly (ethylene glycol) in drug delivery: pros and cons as well as potential alternatives.* Angewandte Chemie International Edition, 2010. **49**(36): p. 6288-6308.

179. Sugumaran, M., et al., *Evidence for the formation of a quinone methide during the oxidation of the insect cuticular sclerotizing precursor 1,2-dehydro-N-acetyldopamine.* Journal of Biological Chemistry, 1992. **267**(15): p. 10355-61.

180. Kolhe, P. and R.M. Kannan, *Improvement in ductility of chitosan through blending and copolymerization with PEG: FTIR investigation of molecular interactions.* Biomacromolecules, 2003. **4**(1): p. 173-180.

181. Li, P., et al., *Improved mechanical and swelling behavior of the composite hydrogels prepared by ionic monomer and acid-activated Laponite.* Applied Clay Science, 2009. **46**(4): p. 414-417.

182. Anseth, K.S., C.N. Bowman, and L. Brannon-Peppas, *Mechanical properties of hydrogels and their experimental determination.* Biomaterials, 1996. **17**(17): p. 1647-57.

183. Peppas, N.A., et al., *Hydrogels in pharmaceutical formulations.* European Journal of Pharmaceutics & Biopharmaceutics, 2000. **50**(1): p. 27-46.

184. Yang, J., et al., *Cellulose Nanocrystals Mechanical Reinforcement in Composite Hydrogels with Multiple Cross-Links: Correlations between Dissipation Properties and Deformation Mechanisms.* Macromolecules, 2014.

185. Narita, T., et al., *Viscoelastic Properties of Poly (vinyl alcohol) Hydrogels Having Permanent and Transient Cross-Links Studied by Microrheology, Classical Rheometry, and Dynamic Light Scattering.* Macromolecules, 2013. **46**(10): p. 4174-4183.

186. Rose, S.v., et al., *Dynamics of Hybrid Polyacrylamide Hydrogels Containing Silica Nanoparticles Studied by Dynamic Light Scattering.* Macromolecules, 2013. **46**(11): p. 4567-4574.

187. da Silva, L.F.M., et al., *Effect of Adhesive Type and Thickness on the Lap Shear Strength* Journal of Adhesion, 2006. **82**: p. 1091-1115.

188. Brubaker, C.E. and P.B. Messersmith, *Enzymatically Degradable Mussel-Inspired Adhesive Hydrogel.* Biomacromolecules, 2011. **12**(12): p. 4326-4334.

189. Gaharwar, A.K., et al., *Highly extensible, tough, and elastomeric nanocomposite hydrogels from poly(ethylene glycol) and hydroxyapatite nanoparticles.* Biomacromolecules, 2011. **12**(5): p. 1641-50.

190. Cao, H., et al., *The topographical effect of electrospun nanofibrous scaffolds on the in vivo and in vitro foreign body reaction.* Journal of Biomedical Materials Research Part A, 2010. **93A**(3): p. 1151-1159.

191. Ferreira, L., et al., *Biocompatibility of chemoenzymatically derived dextran-acrylate hydrogels.* Journal of Biomedical Materials Research Part A, 2004. **68A**(3): p. 584-596.

192. Pan, H., H. Jiang, and W. Chen, *The biodegradability of electrospun Dextran/PLGA scaffold in a fibroblast/macrophage co-culture.* Biomaterials, 2008. **29**(11): p. 1583-1592.

193. Azab, A.K., et al., *Biocompatibility evaluation of crosslinked chitosan hydrogels after subcutaneous and intraperitoneal implantation in the rat.* Journal of Biomedical Materials Research Part A, 2007. **83A**(2): p. 414-422.

194. Schexnailder, P.J., et al., *Tuning Cell Adhesion by Incorporation of Charged Silicate Nanoparticles as Cross-Linkers to Polyethylene Oxide.* Macromolecular Bioscience, 2010. **10**(12): p. 1416-1423.

195. Cruise, G.M., D.S. Scharp, and J.A. Hubbell, *Characterization of permeability and network structure of interfacially photopolymerized poly(ethylene glycol) diacrylate hydrogels* Biomacromolecules, 1998. **19**(14): p. 1287-1294.

196. Zhang, J., et al., *Physically Associated Synthetic Hydrogels with Long-Term Covalent Stabilization for Cell Culture and Stem Cell Transplantation.* Advanced Materials, 2011. **23**(43): p. 5098-5103.

197. Slaughter, B.V., et al., *Hydrogels in regenerative medicine.* Adv Mater, 2009. **21**(32-33): p. 3307-29.

198. Seal, B.L., T.C. Otero, and A. Panitch, *Polymeric biomaterials for tissue and organ regeneration.* Materials Science & Engineering R-Reports, 2001. **34**(4-5): p. 147-230.

199. Seliktar, D., *Designing cell-compatible hydrogels for biomedical applications.* Science, 2012. **336**(6085): p. 1124-8.

200. Lutolf, M.P., et al., *Synthetic matrix metalloproteinase-sensitive hydrogels for the conduction of tissue regeneration: Engineering cell-invasion characteristics.* Proceedings of the National Academy of Sciences, 2003. **100**(9): p. 5413-5418.

201. Ravin, A.G., et al., *Long- and short-term effects of biological hydrogels on capsule microvascular density around implants in rats.* Journal of Biomedical Materials Research, 2001. **58**(3): p. 313-318.

202. Schwarz, K., *A bound form of silicon in glycosaminoglycans and polyuronides.* Proc Natl Acad Sci U S A, 1973. **70**(5): p. 1608-12.

203. Forooshani, P.K. and B.P. Lee, *Recent approaches in designing bioadhesive materials inspired by mussel adhesive protein.* Journal of Polymer Science Part a-Polymer Chemistry, 2017. **55**(1): p. 9-33.

204. Lei, Z.Q., et al., *Room-Temperature Self-Healable and Remoldable Cross-linked Polymer Based on the Dynamic Exchange of Disulfide Bonds.* Chemistry of Materials, 2014. **26**(6): p. 2038-2046.

205. Dai, X.Y., et al., *A Mechanically Strong, Highly Stable, Thermoplastic, and Self-Healable Supramolecular Polymer Hydrogel.* Advanced Materials, 2015. **27**(23): p. 3566-3571.

206. Hu, Y.W., et al., *A Shape-Memory DNA-Based Hydrogel Exhibiting Two Internal Memories.* Angewandte Chemie-International Edition, 2016. **55**(13): p. 4210-4214.

207. Phadke, A., et al., *Rapid self-healing hydrogels.* Proceedings of the National Academy of Sciences, 2012. **109**(12): p. 4383-4388.

208. Nakahata, M., et al., *Redox-responsive self-healing materials formed from host–guest polymers.* Nature Communications, 2011. **2**: p. 511.

209. Dalsin, J.L., et al., *Multi-armed catechol compound blends*. 2014, US Patent 8,916,652.

210. Rzepecki, L.M. and J.H. Waite, *A Chromogenic Assay for Catecholoxidases Based on the Addition of L-Proline to Quinones.* Analytical Biochemistry, 1989. **179**(2): p. 375-381.

211. Palmer, R.G., et al., *Models of hierarchically constrained dynamics for glassy relaxation.* Physical Review Letters, 1984. **53**(10): p. 958.

212. Andersen, S.O., et al., *Phenoloxidase catalyzed coupling of catechols. Identification of novel coupling products.* Biochimica et Biophysica Acta

(BBA) - Protein Structure and Molecular Enzymology, 1992. **1118**(2): p. 134-138.

213. Hong, S., et al., *Non‑covalent self‑assembly and covalent polymerization co‑contribute to polydopamine formation.* Advanced Functional Materials, 2012. **22**(22): p. 4711-4717.

214. Li, Y., et al., *Gelatin Microgel Incorporated Poly (Ethylene Glycol)-based Bioadhesive with Enhanced Adhesive Property and Bioactivity.* ACS applied materials & interfaces, 2016. **8**(19): p. 11980-11989.

215. Landman, J., et al., *Evaluation of a Vessel Sealing System, Bipolar Electrosurgery, Harmonic Scalpel, Titanium Clips, Endoscopic Gastrointestinal Anastomosis Vascular Staples and Sutures for Arterial and Venous Ligation in a Porcine Model.* The Journal of Urology, 2003. **169**(2): p. 697-700.

216. Hendriks, T. and W.J. Mastboom, *Healing of experimental intestinal anastomoses.* Diseases of the colon & rectum, 1990. **33**(10): p. 891-901.

217. Shin, M., et al., *Complete prevention of blood loss with self-sealing haemostatic needles.* Nature Materials, 2017. **16**(1): p. 147-152.

218. Ryu, J.H., et al., *Chitosan-g-hematin: Enzyme-mimicking polymeric catalyst for adhesive hydrogels.* Acta Biomaterialia, 2014. **10**(1): p. 224-233.

219. Meng, H., Y. Liu, and B.P. Lee, *Model polymer system for investigating the generation of hydrogen peroxide and its biological responses during the crosslinking of mussel adhesive moiety.* Acta Biomaterialia, 2017. **48**: p. 144-56.

220. Fullenkamp, D.E., et al., *pH-dependent cross-linking of catechols through oxidation via Fe3+ and potential implications for mussel adhesion.* RSC Advances, 2014. **4**(48): p. 25127-25134.

221. Shin, H., et al., *In vivo bone and soft tissue response to injectable, biodegradable oligo (poly (ethylene glycol) fumarate) hydrogels.* Biomaterials, 2003. **24**(19): p. 3201-3211.

222. Winder, F. and J.M. Denneny, *Metal-catalysed auto-oxidation of isoniazid.* Biochemical Journal, 1959. **73**(3): p. 500.

223. Haemers, S., G.J.M. Koper, and G. Frens, *Effect of oxidation rate on cross-linking of mussel adhesive proteins.* Biomacromolecules, 2003. **4**(3): p. 632-640.

224. Ghadban, A., et al., *Bioinspired pH and magnetic responsive catechol-functionalized chitosan hydrogels with tunable elastic properties.* Chemical Communications, 2016. **52**(4): p. 697-700.

225. Lee, J., et al., *Phase Controllable Hyaluronic Acid Hydrogel with Iron (III) Ion–Catechol Induced Dual Cross-Linking by Utilizing the Gap of Gelation Kinetics.* Macromolecules, 2016. **49**(19): p. 7450-7459.

Appendix

Permission license for the content in Chapter 1

Permission for the content in Chapter 2

As the first author, I have the right to reproduce material contained in this article in my dissertation without requesting for permission.

Recovery property of double-network hydrogel containing a mussel-inspired adhesive moiety and nano-silicate

If you are not the author of this article and you wish to reproduce material from it in a third party non-RSC publication you must formally request permission using RightsLink. Go to our Instructions for using RightsLink page for details.

Authors contributing to RSC publications (journal articles, books or book chapters) do not need to formally request permission to reproduce material contained in this article provided that the correct acknowledgement is given with the reproduced material.

Reproduced material should be attributed as follows:

- For reproduction of material from NJC:
  Reproduced from Ref. XX with permission from the Centre National de la Recherche Scientifique (CNRS) and The Royal Society of Chemistry.
- For reproduction of material from PCCP:
  Reproduced from Ref. XX with permission from the PCCP Owner Societies.
- For reproduction of material from PPS:
  Reproduced from Ref. XX with permission from the European Society for Photobiology, the European Photochemistry Association, and The Royal Society of Chemistry.
- For reproduction of material from all other RSC journals and books:
  Reproduced from Ref. XX with permission from The Royal Society of Chemistry.

If the material has been adapted instead of reproduced from the original RSC publication "Reproduced from" can be substituted with "Adapted from".

In all cases the Ref. XX is the XXth reference in the list of references.

If you are the author of this article you do not need to formally request permission to reproduce figures, diagrams etc. contained in this article in third party publications or in a thesis or dissertation provided that the correct acknowledgement is given with the reproduced material.

Reproduced material should be attributed as follows:

- For reproduction of material from NJC:
  [Original citation] - Reproduced by permission of The Royal Society of Chemistry (RSC) on behalf of the Centre National de la Recherche Scientifique (CNRS) and the RSC
- For reproduction of material from PCCP:
  [Original citation] - Reproduced by permission of the PCCP Owner Societies
- For reproduction of material from PPS:
  [Original citation] - Reproduced by permission of The Royal Society of Chemistry (RSC) on behalf of the European Society for Photobiology, the European Photochemistry Association, and RSC
- For reproduction of material from all other RSC journals:
  [Original citation] - Reproduced by permission of The Royal Society of Chemistry

http://pubs.rsc.org/en/content/requestpermission?msid=c6tb01828a   1/2

If you are the author of this article you still need to obtain permission to reproduce the whole article in a third party publication with the exception of reproduction of the whole article in a thesis or dissertation.

Information about reproducing material from RSC articles with different licences is available on our Permission Requests page.

Permission for the content in Chapter 3

Permission license for the content in Chapter 4